INSTITUTO TECNOLÓGICO DE TOLUCA

“CONSTRUCCIÓN TEÓRICA DE UN CÁTODO A BASE DE GRAFINO EN UNA BATERÍA LITIO-AIRE POR MEDIO DE CÁLCULOS DFT”

QUE PARA OBTENER EL GRADO DE DOCTOR EN CIENCIAS AMBIENTALES

PRESENTA:

ARMANDO VERA GARCÍA

No. CONTROL:

DD21281383

DIRECTOR DE TESIS:

DR. JUAN HORACIO PACHECO SÁNCHEZ

METEPEC, ESTADO DE MÉXICO, SEPTIEMBRE DE 2025

Educación
Secretaría de Educación Pública

TECNOLÓGICO NACIONAL DE MÉXICO

Instituto Tecnológico de Toluca
División de Estudios de Posgrado e Investigación

Metepec, Edo. de México, 19/Agosto/2025
DEPI-3200-461/2025

ARMANDO VERA GARCÍA
CANDIDATO AL GRADO DE DOCTOR
EN CIENCIAS AMBIENTALES

PRESENTE

De acuerdo con los Lineamientos para la Operación de los Estudios de Posgrado en el Tecnológico Nacional de México y las disposiciones en este Instituto, habiendo cumplido con todas las indicaciones que la Comisión Revisora realizó con respecto a su Trabajo de Tesis titulado **"Construcción Teórica de un Cátodo a Base de Grafino en una Bateria Litio-Aire por Medio de Cálculos DFT"**, la División de Estudios de Posgrado e Investigación de este Instituto, concede la Autorización para que proceda al envío del trabajo final vía correo Institucional.

Sin más por el momento, quedo de usted.

A T E N T A M E N T E
Excelencia en Educación Tecnológica®
"Educación, integridad y ciencia"

Educación
Secretaría de Educación Pública | TECNOLÓGICO NACIONAL DE MÉXICO

INSTITUTO TECNOLÓGICO DE TOLUCA

DIVISIÓN DE ESTUDIOS DE POSGRADO E INVESTIGACIÓN

JORGE SÁNCHEZ JAIME
ENCARGADO DE LA JEFATURA DE LA DIVISIÓN
DE ESTUDIOS DE POSGRADO E INVESTIGACIÓN

ccp. Archivo
JSJ/mccl

2025 Año de La Mujer Indígena

Educación
Secretaría de Educación Pública

TECNOLÓGICO NACIONAL DE MÉXICO

Instituto Tecnológico de Toluca
Comunicación y Difusión

Metepec, Edo. de México, 15/Agosto/2025
DEPI-3200-434/2025

DR. JORGE SÁNCHEZ JAIME
JEFE DE LA DIVISIÓN DE ESTUDIOS
DE POSGRADO E INVESTIGACIÓN
P R E S E N T E

Por este medio comunicamos a usted que la comisión Revisora designada para analizar la tesis denominada **"Construcción Teórica de un Cátodo a Base de Grafino en una Bateria Litio-Aire por Medio de Cálculos DFT"**, que como parte de los requisitos para obtener el grado académico de **Doctor en Ciencias Ambientales** presenta el **C. Armando Vera García** con número de control **D21281383** para sustentar el acto de Recepción Profesional, ha dictaminado que dicho trabajo reúne las características de contenido y calidad para proceder a la impresión del mismo.

A T E N T A M E N T E

DR. JUAN HORACIO PACHECO SÁNCHEZ
DIRECTOR DE TESIS

DR. FRANK JHONATAN ISIDRO ORTEGA
CODIRECTOR DE TESIS

DR. FRANCISCO JAVIER ILLESCAS MARTÍNEZ
REVISOR DE TESIS

DR. CELSO HERNÁNDEZ TENORIO
REVISOR DE TESIS

DR. LUIS ALBERTO DESALES GUZMÁN
REVISOR DE TESIS

DRA. NAYELY TORRES GÓMEZ
REVISORA DE TESIS

ccp. Archivo
JSJ/mccl

2025 Año de La Mujer Indígena

Av. Tecnológico S/N, Col. Agrícola Bellavista, Metepec, Edo. de México,
C.P. 52149, Tels. Dirección: 7222087205, Conmut.: 7222087200
e-mail: info@toluca.tecnm.mx tecnm.mx | toluca.tecnm.mx

Agradecimientos

Agradezco, en primer lugar, a Dios, por haberme permitido culminar esta etapa profesional, así como por todos los conocimientos adquiridos y los momentos memorables vividos durante este proceso.

Expreso mi sincero agradecimiento al SECIHTI (anteriormente CONACyT) por el apoyo económico y la provisión de recursos que hicieron posible el desarrollo de esta investigación.

Al programa de Doctorado en Ciencias Ambientales y al Instituto Tecnológico de Toluca, por facilitarme el acceso a las instalaciones y al centro de cómputo del área de Posgrado e Investigación.

De manera muy especial, y con profunda admiración, agradezco al Dr. Horacio Pacheco Sánchez y al Dr. Frank Isidro Ortega, por el valioso tiempo dedicado a la dirección de este trabajo, su paciencia, orientación y consejos invaluables, que fueron fundamentales para la culminación de esta tesis.

Asimismo, extiendo mi agradecimiento al Dr. Celso Hernández Tenorio, Dr. Luis Alberto Desales Guzmán, Dr. Francisco Javier Illescas Martínez y a la Dra. Nayely Torres Gómez, por su revisión, orientación y recomendaciones que enriquecieron este trabajo.

A mi familia: a mis padres, abuelos y hermana, por su amor, apoyo incondicional y por ser siempre un pilar en mi vida.

Y, con especial cariño, a mi amada esposa Karla Esteban Valdés y a mis hijos, Armando y Gabriela, quienes son mi mayor fortaleza y alegría, y a quienes agradezco profundamente por su amor, comprensión y constante apoyo.

Resumen

Hoy en día, las baterías de litio-aire (Li-O_2) se consideran uno de los candidatos a dispositivos de almacenamiento y conversión de energía más prometedores para su uso en futuras aplicaciones de movilidad, como los vehículos eléctricos, debido a su densidad de energía teórica ultra alta (hasta ~3600 Wh kg^{-1}). El objetivo principal de este trabajo fue estudiar un modelo catalítico electroquímico de un cátodo para baterías de Li-O_2 con el fin de simular el proceso de descarga, se realizaron cálculos de Teoría Funcional de la Densidad (DFT) para investigar el γ-Grafino y el N-γ-Grafino como posibles catalizadores catódicos para las baterías de Li-O_2. Tanto las superficies de γ-Grafino como las de N-γ-Grafino exhiben una alta estabilidad según los cálculos, la superficie prístina exhibe una pequeña mejora en la energía de formación de Li_xO_2, además la superficie funcionalizada (N-γ-Grafino) puede reducir significativamente la energía de formación de Li_xO_2 en la reacción de oxido reducción (ORR). Los cálculos explican el mecanismo catalítico e identifican los sitios activos para realizar el dopado con N en γ-Grafino prístino. Este estudio demostró un enfoque factible para lograr el diseño de γ-Grafino y N-γ-Grafino como catalizador para baterías de Li-aire, lo que promete una reducción de costos en la producción masiva de baterías de Li-aire.

Abstract

Nowadays lithium-air batteries (Li-O_2) are considered one of the most promising energy storage and conversion device candidates for use in future mobility applications, such as electric vehicles due to their ultrahigh theorical energy density (up to ~3600 Wh kg^{-1}). The main goal in this work is to study an electrochemical catalytic model for a cathode for Li-O_2 batteries to simulate the oxygen reduction reaction ORR during discharging process. Herein Density Functional Theory (DFT) calculations were performed to investigate γ-Graphyne and N-γ-Graphyne as the potential cathode catalyst for Li-O_2 batteries. Both γ-Graphyne and N-γ-Graphyne surfaces exhibit high stability according to calculations, pristine surface exhibits a small improvement in the formation energy of Li_xO_2, moreover the functionalized surface (N-γ-Graphyne) can reduce significant formation energy of Li_xO_2 in the ORR. Calculations explain the catalytic mechanism and identify the actives sites to perform N-doped on pristine γ-Graphyne. This study demonstrates a feasible approach to achieve designed γ-Graphyne and N-γ-Graphyne as cathodes catalyst for Li air batteries, promising cost reduction in mass production of Li-air batteries.

Contenido

1. Introducción

1.1 Fundamentos

Actualmente, se ha estimado que el consumo mundial de energía se encuentra en la asombrosa cifra de 19 (TW), y las proyecciones indican que esta cifra experimente un incremento del triple para el año 2050 [1]. En la actualidad, la mayor parte de esta creciente demanda se satisface predominantemente a través de la utilización de diversos combustibles fósiles. En otros términos, los combustibles fósiles han servido como fuente de energía convencional durante el siglo pasado, apuntalando gran parte de la infraestructura energética mundial. Es ampliamente reconocido dentro de la comunidad científica que los combustibles fósiles, que incluyen sustancias como el carbón, el petróleo y el gas natural, han sido responsables de importantes problemas ambientales que incluyen, entre otros, la deforestación severa, la contaminación atmosférica y el alarmante fenómeno del calentamiento global [2]. Además, considerando la naturaleza no renovable de los combustibles fósiles, las desventajas inherentes asociadas a su uso han catalizado esfuerzos sustanciales encaminados a investigar e identificar fuentes de energía alternativas y respetuosas con el medio ambiente. En consecuencia, existe una demanda urgente y apremiante de investigación científica e innovaciones tecnológicas que puedan conducir al desarrollo de sistemas avanzados de almacenamiento de energía caracterizados por una alta eficiencia y emisiones mínimas o nulas de carbono [1, 3]. En este contexto, en las últimas décadas, se han propuesto diversos dispositivos de almacenamiento de energía electroquímica como soluciones viables para satisfacer las crecientes demandas de energía en una multitud de aplicaciones, que incluyen almacenamiento de energía renovable, dispositivos electrónicos portátiles y vehículos eléctricos [4]. Los dispositivos electroquímicos, como pilas de combustible y baterías han demostrado un potencial excepcional para facilitar aplicaciones de almacenamiento y conversión de energía limpia a gran escala. En el ámbito de la conversión de energía limpia, las celdas de combustible son capaces de convertir directamente la energía química almacenada en los combustibles en electricidad con notable eficiencia y emisiones mínimas, mientras que, en el dominio del almacenamiento de energía limpia,

las baterías sirven como dispositivos de almacenamiento típicos que exhiben una alta densidad de energía junto con una reversibilidad y durabilidad encomiables [5]. Las baterías se destacan como una tecnología ejemplar para el almacenamiento de energía que es particularmente adecuada para la integración de recursos de energía renovable. Su tamaño compacto hace que las baterías sean altamente apropiadas para su implementación en ubicaciones distribuidas, lo que les permite entregar un control de frecuencia que puede reducir efectivamente las fluctuaciones en la producción solar local y mitigar las variaciones en la producción de energía de fuentes como parques eólicos y solares. En consecuencia, en los últimos años, se ha dado un impulso concertado hacia el desarrollo de baterías que no solo sean más sostenibles sino también respetuosas con el medio ambiente [6]. Entre las diversas opciones disponibles, las baterías de iones de litio (Li-ion) han surgido como la opción más favorecida para el almacenamiento de energía en dispositivos electrónicos portátiles, ya que estas baterías de iones de litio ofrecen una de las relaciones energía-peso más favorables disponibles, aunado a una baja tasa de autodescarga cuando no están en uso activo [7, 8]. Actualmente, las baterías de iones de litio están alcanzando con éxito el importante y ambicioso objetivo de facilitar la electrificación de los sistemas de transporte, lo que implica fundamentalmente la sustitución integral de motores tradicionales de gasolina en diversos tipos de automóviles con configuraciones avanzadas de paquetes de baterías secundarias. No obstante, la limitación inherente asociada a la densidad de energía gravimétrica que se encuentra en las baterías de iones de litio disponibles comercialmente, que es de aproximadamente ~200 Wh kg^{-1}, impide significativamente su aplicación efectiva para facilitar capacidades de conducción de largo alcance, particularmente en el contexto de vehículos de servicio medio a pesado, como se señala en referencias académicas [9].

1.2 Baterías litio aire

Por otro lado, las baterías Li-O_2 presentan una densidad de capacidad teórica, que puede alcanzar hasta aproximadamente 3600 Wh kg^{-1}, cifra que es atribuible a los pesos moleculares bajos tanto del oxígeno como del litio, posicionando con ello a estas baterías como candidatas prometedoras para soluciones de almacenamiento de energía recargable de próxima generación, como se destaca en las referencias [10] y [11]. La composición estructural de las baterías Li-O_2 se caracteriza por la presencia de un ánodo de metal de litio, un medio electrolítico adecuado, y un cátodo basado en oxígeno, en donde los procesos reversibles de carga y descarga se facilitan a través de la reacción de reducción de oxígeno (ORR) que implica las interacciones entre litio y oxígeno, así como la reacción de evolución de oxígeno (OER) que pertenece a la descomposición del peróxido de litio [10]. No obstante, se reconoce que aún se requieren extensos esfuerzos de investigación debido a la brecha sustancial que existe entre las capacidades teóricas que se han postulado para las baterías de Li-O_2 y las capacidades prácticas reales que se han logrado en aplicaciones del mundo real.

1.2.1 Clasificación de baterías litio aire

Es ampliamente reconocido dentro de la comunidad académica que las baterías de Li-O_2 pueden ser categorizadas en función del tipo de electrolito utilizado:

I). Sistemas aquosos

II). Sistemas apróticos

III). Configuraciones de estado sólido

IV). Sistemas híbridos acuosos/aporticos

Cada categoría exhibe reacciones electroquímicas únicas y diferentes voltajes de circuito abierto asociados con los respectivos tipos de baterías Li-O_2. No obstante, mayoría de los esfuerzos de investigación dentro de este campo se han concentrado en su mayoría en la investigación de baterías apróticas Li-O_2, como lo demuestran los trabajos referenciados en [12-15]. Una ventaja significativa que presenta la utilización de electrolitos aporticos es la formación espontánea de una barrera protectora que se desarrolla entre el ánodo de metal de litio y el electrolito, que protege al metal litio de sufrir reacciones adicionales no deseadas con el medio electrolítico. En el contexto de un electrolito aprótico, los productos de descarga, que pueden manifestarse como óxido de litio o peróxido de litio, se generan en el cátodo, siguiendo las reacciones electroquímicas netas que son representativas de la formación ya sea de peróxido de litio o de óxido de litio [16]. En la presente investigación, la reacción electroquímica se ve facilitada por un electrolito aprótico, el cual es un componente fundamental en el sistema general.

1.3 Retos para la implementación de baterías litio aire

La producción industrial a gran escala de baterías Li-O_2 depende de la resolución exitosa de numerosos problemas y desafíos importantes que deben abordarse antes de su plena adopción comercial y su utilización generalizada en diversas aplicaciones. Es ampliamente reconocido dentro de la comunidad científica que una multitud de cuestiones críticas están influyendo en el rendimiento de las baterías de Li-O_2, una de las cuales incluye los avances y mejoras necesarios al ánodo de litio, tal como se revisan exhaustivamente en las referencias [17] y [18]. Además, la atmósfera operativa [19] , la elección de los materiales aglutinantes [20, 21], los disolventes utilizados [22, 23] y las diversas sales de litio empleadas [24, 25] son factores que contribuirían de manera significativa a la mejora del rendimiento general del sistema de baterías, abordando particularmente desafíos como la ciclabilidad subóptima y la eficiencia energética insuficiente. Se ha identificado que el factor predominante que contribuye al desempeño de estos sistemas es la inadecuada eficacia operativa del cátodo de aire [26], que sigue siendo un elemento crucial en la ecuación de desempeño. Se han llevado a cabo numerosos esfuerzos concertados para mejorar la eficiencia y la funcionalidad general de las baterías de Li-O_2. La investigación del lado del cátodo gira predominantemente en torno a la evaluación del desempeño de diversos catalizadores con ORR y OER; el cátodo ideal diseñado para baterías Li-O_2 abarca varias características esenciales, incluyendo pero no limitándose a: la presencia de sitios activos catalíticos altamente eficientes, una abundancia de poros interconectados que faciliten la transferencia de electrones, masa y especies que contienen oxígeno, además de poseer un estabilidad y durabilidad robustas para soportar las demandas operacionales [27]. Los materiales basados en platino son actualmente reconocidos como los electrocatalizadores más efectivos para la reacción de reducción de oxígeno (ORR), exhibiendo una eficiencia catalítica sin igual que los ha convertido en el estándar en este campo de estudio. Sin embargo, la limitada disponibilidad de platino, combinada con su alto costo, impone limitaciones significativas a su potencial de utilización comercial generalizada, lo que requiere la exploración de soluciones alternativas [28]. En consecuencia, se ha vuelto importante acelerar el desarrollo de electrocatalizadores ORR más económicamente

viables que puedan facilitar un acceso e implementación más amplios en diversas aplicaciones. En la investigación contemporánea, una amplia gama de materiales, incluidos metales no nobles y diversos compuestos basados en carbono, ha sido el foco de una extensa investigación, lo que refleja el creciente interés en encontrar sustitutos adecuados para los catalizadores tradicionales [29-31]. Entre estos materiales, los materiales basados en carbono han despertado considerable atención, principalmente debido a su bajo costo, sus características respetuosas con el medio ambiente y su abundante disponibilidad lo cual aumenta su atractivo para posibles aplicaciones. No obstante, a pesar de estas ventajas, la actividad catalítica asociada a la reacción de reducción de oxígeno en materiales basados en carbono sigue estando, en gran medida debajo de los niveles deseados; así, se han propuesto diversas estrategias, incluyendo la incorporación de heteroátomos metálicos o no metálicos mediante técnicas de dopaje, así como la introducción de vacantes intrínsecas dentro de la matriz de carbono, las cuales se han reportado para potenciar la formación de sitios activos y reducir las barreras energéticas asociadas al proceso ORR [32-34]. En el ámbito de las tecnologías avanzadas de almacenamiento de energía, se ha documentado meticulosamente una selección de investigaciones centradas en mejorar la eficacia de los catalizadores empleados dentro de los cátodos de las baterías de metal-aire.

1.3.1 Investigaciones relacionadas

En su trabajo pionero, Ziraki *et al.,* [31] realizaron un examen extenso de cómo la incorporación de dopantes de sodio (Na) e itrio (Y), influye en las características de desempeño electroquímico de un material cátodo específico; este análisis se ejecutó mediante métodos computacionales utilizando la teoría funcional de densidad (DFT). Sus hallazgos explican que un determinante primario que influye en la integridad estructural y estabilidad del material catódico durante el proceso crítico de des-litiación es efectivamente la naturaleza de los dopantes empleados, corroborando con ello el profundo impacto que tiene el dopaje en la mitigación de la velocidad a la que se libera oxígeno durante las reacciones electroquímicas [31].

En un estudio complementario, Wu *et al.,* [10] emprendieron el desarrollo innovador de una monocapa bidimensional (2D) de di boruro de titanio (Ti_2B), que se propone servir como catalizador catódico para baterías de Li-O_2 y sodio-oxígeno (Na-O_2), con su investigación fundamentada en el marco computacional proporcionado por los cálculos de la teoría funcional de densidad (DFT). Los resultados de su investigación revelan que este novedoso material 2D presenta una alternativa prometedora para catalizadores catódicos específicamente diseñados para baterías Li-O_2 y Na-O_2, al tiempo que proporciona nuevas perspectivas sobre el diseño de catalizadores a través de la modificación estratégica de las propiedades superficiales [10].

Además, Cheng *et al.,* [28] introdujeron una sofisticada metodología dirigida a la síntesis de sitios activos coordinados boro-nitrógeno (B-N) controlables que están anclados sobre sustratos de carbono, que funcionan eficientemente como electrocatalizadores para ORR, esto también fue apoyado por cálculos integrales de DFT. El notable desempeño exhibido por estos electrocatalizadores en la ORR se atribuye a la actividad catalítica inherentemente elevada asociada a los sitios activos coordinados B-N, conclusión que se fundamenta mediante un análisis meticuloso del área superficial activa electroquímica (ECSA) [28].

Además, Yin *et al.,* [35] se embarcaron en el desarrollo de un compuesto de iones de sodio sustituido litio-níquel-cobre, específicamente $Na_{0.67}Li_{0.1}(Mn_{0.7}Ni_{0.2}Cu_{0.1})_{0.9}O_2$

(NLMNC), y realizaron cálculos DFT para determinar los mecanismos de reacción pertinentes a NLMNC. Sus hallazgos de DFT indican que la reacción redox aniónica ocurre predominantemente cerca de los iones manganeso (Mn), mientras que al mismo tiempo demuestra la estabilidad de los iones níquel (Ni); los conocimientos obtenidos de su investigación allanan el camino para la aplicación práctica de materiales de óxido en capas en el contexto de las baterías de iones de sodio por sus siglas en inglés (SIB).

Wang *et al.,* [36] realizaron una serie de cálculos de primeros principios diseñados destinados a explorar las diversas propiedades de WN MXenes, enfocándose específicamente tanto en las estructuras prístinas denotadas como $W_{n+1}N_n$ como en las variantes funcionalizadas con oxígeno identificadas como $W_{n+1}N_nO_2$ (n=1,2, and 3), donde n puede tomar los valores de 1, 2, o 3, con la intención de evaluar su viabilidad como catalizadores potenciales en el contexto de litio-aire tecnología de batería; sus análisis computacionales exhaustivos indicaron que tanto $W_{n+1}N_n$ como $W_{n+1}N_nO_2$ demuestran que podrían facilitar un mejor desempeño electroquímico. Además, el W_2NO_2 MXene terminado en O no solo exhibe un impresionante nivel de conductividad eléctrica, sino que también muestra potenciales notablemente bajos para ORR, OER y la caída de voltaje total medida a 0.12, 0.17 y 0.29 volts, respectivamente, lo que subraya su promesa significativa como un catalizador catódico eficaz dentro de los sistemas de baterías de litio y oxígeno [36]. En una investigación separada, Peng *et al.,* [37] desarrollaron con éxito una batería de litio-aire reversible y de alta tasa empleando un electrodo de oro nanoporoso (NPG) como componente catódico, al tiempo que utilizaba dimetilsulfóxido (DMSO) como medio electrolítico, lo que colectivamente permitió alcanzar una impresionante tasa de retención de capacidad del 95% incluso después de someterse a 100 ciclos completos de carga-descarga. Adicionalmente, Chen *et al.,* [34] introdujeron una innovadora metodología de oxidación en dos pasos, que implica un tratamiento inicial de oxidación débil utilizando peróxido de hidrógeno (H_2O_2) seguido de un ajuste cuidadoso y selectivo de la relación entre compuestos de fenol y carbonilo/quinona; los hallazgos de su investigación sugirieron fuertemente que los defectos topológicos resultantes de la eliminación estratégica de fenol y carbonilo/quinona son cruciales para mejorar la actividad de la reacción de reducción de oxígeno (ORR) observada en múltiples paredes nanotubos de carbono (MWCNT).

Por último, Kim *et al.,* [38] revelaron que la capacidad de descarga del cátodo de carbono podría mejorarse significativamente como resultado de un aumento en la porosidad y mejoras realizadas a la textura general del material de carbono utilizado en el sistema de batería. En este trabajo, se desarrolló un modelo catalítico específicamente diseñado para la configuración de un cátodo utilizado en baterías de litio-oxígeno (Li-O_2), el cual tiene como objetivo simular de manera efectiva los mecanismos asociados a la reacción de reducción de oxígeno (ORR) y la reacción de evolución de oxígeno (OER) que se producen durante los procesos de descarga y carga de estos sistemas de almacenamiento de energía. Los procesos electrocatalíticos asociados a una capa singular de γ-Grafino junto con sus diversos derivados funcionalizados, enfocándonos así únicamente en las características y propiedades inherentes del electrocatalizador.

1.4 Simulaciones moleculares

La simulación molecular se ha convertido en una herramienta fundamental y cada vez más importante en varias disciplinas científicas, lo que demuestra su profunda influencia y aplicabilidad en una multitud de contextos de investigación. Su utilización abarca un amplio espectro de aplicaciones que van desde el examen de las propiedades termodinámicas a las diferentes formas de la materia hasta el diseño innovador de materiales novedosos y la síntesis de nuevos productos farmacéuticos [39]. La razón de su importancia se basa en la notable capacidad de la simulación para servir como una alternativa altamente eficaz a los métodos experimentales tradicionales, particularmente en escenarios en los que las condiciones específicas de interés son extremadamente desafiantes o incluso imposibles de reproducir, como en los casos en los que se producen temperaturas y presiones extremas. Mediante el proceso de simulación, los investigadores tienen la oportunidad de conceptualizar y explorar sistemas fisicoquímicos hipotéticos, cuyas propiedades pueden proporcionar una amplia gama de información, particularmente en el contexto especializado de materiales y estructuras de carbono recientemente desarrollados que están intrínsecamente vinculados a los fenómenos de adsorción.

En el contexto de este esfuerzo de investigación en particular, se empleó el sofisticado y avanzado software BIOVIA Material Studio, que utilizó el módulo especializado DMol^3, que se basa fundamentalmente en la estimada teoría de los funcionales de densidad y los principios de la dinámica molecular, respectivamente, lo que garantiza un enfoque integral de la investigación en cuestión [40].

1.4.1 Teoría de funcionales de la densidad

La teoría funcional de la densidad, por sus siglas en inglés (DFT), representa una metodología variacional que sirve como alternativa a la resolución independiente del tiempo de la ecuación de Schrödinger, en la que el funcional relacionado con la energía electrónica se optimiza en relación con la densidad electrónica [39]. Este enfoque se considera alternativo únicamente porque no pretende calcular la función de onda molecular, sino que se centra en calcular la densidad de probabilidad de los electrones moleculares para determinar la energía molecular.

Los enfoques convencionales de los marcos teóricos sobre la estructura electrónica de la materia permiten una caracterización precisa de la dinámica de los sistemas diminutos; sin embargo, su eficacia en la resolución de problemas se ve limitada por la excesiva complejidad de las ecuaciones, lo que las hace intratables tanto numérica como analíticamente.

La teoría funcional de la densidad reformula el problema para trabajar con el funcional de la densidad electrónica en vez de la función de onda. Una ventaja significativa radica en el hecho de que la densidad constituye una función más sencilla en comparación con la función de onda, lo que facilita los cálculos en sistemas complejos; por ejemplo, la función de onda de un sistema de electrones depende de múltiples variables, mientras que la densidad electrónica se basa únicamente en tres variables, lo que evita las complejidades asociadas a la función de onda, que aumenta exponencialmente con el incremento del recuento de electrones [41].

$$\psi(x_1, y_1, z_{1,} x_2, y_2, z_{2,}, \dots\ x_n, y_n, z_{n,})\rho(x, y, z) \qquad \textit{Ecuación 1.4.1.1}$$

La Teoría de Funcionales de la Densidad postula que la densidad de estados electrónicos, tanto para el núcleo, como para los electrones se encuentra relacionada con el número total de electrones N, a partir de la normalización de la función de densidad electrónica:

$$\int (r)\, dr = N \qquad \textit{Ecuación 1.4.1.2}$$

Ante esto se propone escribir la energía como una suma de funciones que depende de $\rho(r)$,

$$\mathrm{E}[\rho] = \mathrm{T}[\rho] + \mathrm{Vne}[\rho] + \mathrm{Vee}[\rho] \qquad \textit{Ecuación 1.4.1.3}$$

donde $T[\rho]$ es la energía cinética, $Vne[\rho]$ es la interacción núcleo-electrón y $Vee[\rho]$ es la interacción electrón-electrón, que se puede separar a su vez en una contribución de Coulomb $J[p]$ y otra de intercambio $K[\rho]$.

1.4.2 Ecuación de Schrödinger independiente del tiempo

Para poder entender los beneficios y el uso de la Teoría de Funcional de la Densidad tenemos que partir de la ecuación de Schrödinger independiente del tiempo [42].

$$-\frac{\hbar^2}{2m}\frac{d^2\Psi(x)}{dx^2} + V(x)\Psi(x) = E\Psi(x) \qquad \textit{Ecuación 1.4.2.1}$$

Para simplificar se escribe:

$$\hat{\mathrm{H}}\Psi = E\Psi \qquad \textit{Ecuación 1.4.2.2}$$

donde $\hat{\mathrm{H}}$ es el operador Hamiltoniano

$$\hat{\mathrm{H}} = -\frac{\hbar^2}{2m}\frac{\partial^2}{\partial x^2} + V(x) \qquad \textit{Ecuación 1.4.2.3}$$

Este operador $\hat{\mathrm{H}}$ incluye una serie de operaciones matemáticas que aplicadas a la función de una onda del sistema Ψ nos devuelve los valores propios de la energía de dicho sistema.

El Hamiltoniano de una molécula que contiene N núcleos y n electrones es:

$$\hat{H} = -\sum_{\propto=1}^{N} \frac{\hbar^2}{2M_{\propto}} \nabla_i^2 - \sum_{i=1}^{n} \frac{\hbar^2}{2m} \nabla_i^2 - \sum_{\propto=1}^{N} \sum_{i=1}^{n} \frac{Z_{\alpha} e^2}{r_{i\propto}} + \sum_{i=1}^{n} \sum_{j>i}^{n} \frac{e^2}{r_{ij}} + \sum_{\propto=1}^{N} \sum_{\beta>\propto}^{N} \frac{Z_{\alpha} Z_{\beta} e^2}{R_{\propto\beta}}$$

Ecuación 1.4.2.4

donde $\boldsymbol{M}\propto$ es la masa del núcleo α, $\boldsymbol{m}$ es la masa del electrón, $Z\boldsymbol{\alpha}$ es la carga del núcleo α, e es la carga del electrón, $R\propto\boldsymbol{\beta}$ es la distancia entre los núcleos α y β, $ri\propto$ es la distancia entre el núcleo α y el electrón i y rij es distancia entre los electrones i y j [43].

El primer término de la ecuación 1.4.2.4 corresponde a la energía cinética nuclear, el segundo a la energía cinética electrónica, el tercero a la energía de repulsión nuclear, el cuarto a la energía de atracción electrón-núcleo y el último a la energía de repulsión electrónica. La ecuación de Schrödinger independiente del tiempo solo se puede resolver de forma exacta en el caso de sistemas simples. En caso de sistemas más complejos como las moléculas es necesario el empleo de aproximaciones.

1.4.3 Aproximación de Born-Oppenheimer

En una molécula los núcleos son mucho más pesados que los electrones. Los electrones se mueven mucho más rápido y recorren muchos “ciclos” de movimiento durante el tiempo en que los núcleos recorren una distancia muy corta y reajustan sus movimientos muy rápidamente al cambio de las coordenadas de los núcleos [41].

La aproximación de Born-Oppenheimer considera que, para describir el movimiento de los electrones, los núcleos se pueden considerar prácticamente “parados” o estacionarios en unas coordenadas determinadas, y puede describirse el movimiento electrónico en medio del campo eléctrico que crean los núcleos situados en unas coordenadas fijas [39]. Esta aproximación equivale a separar el movimiento electrónico del nuclear despreciando la energía cinética de los núcleos.

Expresando el Hamiltoniano de la ecuación de Schrödinger de la siguiente manera:

$$\hat{\mathrm{H}}\Psi(r,R) = E\Psi(r,R) \qquad \textit{Ecuación 1.4.3.1}$$

$$\hat{\mathrm{H}} = E_{CN}(R) + E_{CE}(r) + V_{NN}(R) + V_{EE}(r) + V_{NE}(r,R) \qquad \textit{Ecuación 1.4.3.2}$$

donde:

E_{CN} = Energía cinética del núcleo

E_{CE} = Energía cinética del electrón

V_{NN} = Energía repulsiva núcleo - núcleo

V_{EE} = Energía repulsiva núcleo - electrón

V_{NE} = Energía atractiva electrón-electrón

Con la propuesta de Born-Oppenheimer se omite el primer término y el tercero, quedando la ecuación 1.4.3.3 de la siguiente forma:

$$\hat{H} = E_{CE}(r) + V_{EE}(r) + V_{NE}(r, R) \qquad \textit{Ecuación 1.4.3.3}$$

Reescribiendo la ecuación 1.4.3.3 en la ecuación 1.4.3.4 queda expresada como:

$$\hat{H} = -\sum_{i=1}^{N} \frac{\hbar^2}{2m} \nabla_i^2 - \sum_{\propto=1}^{N} \sum_{i=1}^{n} \frac{Z_\alpha e^2}{r_{i\propto}} + \sum_{i=1}^{n} \sum_{j>i}^{n} \frac{e^2}{r_{ij}} \qquad \textit{Ecuación 1.4.3.4}$$

La ecuación 1.4.3.4 describe el movimiento de los electrones, cuando los núcleos están en posiciones fijas con coordenadas r y R respectivamente.

1.4.4 Teoría de Hartree-Fock

La aproximación de Hartree-Fock o del campo auto consistente, es un procedimiento iterativo para calcular la solución a la ecuación de Schrödinger, independiente del tiempo, aplicable a moléculas aisladas tanto en estado fundamental como excitado, tras haber aplicado la aproximación de Born-Oppenheimer.

La base de la teoría de Hartree-Fock es suponer que la función de onda de muchos cuerpos es un determinante de Slater de orbitales de una partícula, ecuación 1.4.4.1. Para un sistema de n electrones es:

$$\psi(r_1, r_2) = \frac{1}{\sqrt{n}} \begin{bmatrix} x_1(r_1) & x_2(r_2) & \dots & \dots & x_N(r_1) \\ . & . & & & . \\ . & . & & & . \\ . & . & & & . \\ x_1(r_N) & x_2(r_N) & \dots & \dots & x_N(r_N) \end{bmatrix}$$

Ecuación 1.4.4.1

Esto garantiza la antisimetría de la función de onda y considera la energía de intercambio. Sin embargo, no considera efectos de correlación que no son despreciables [44]. La correlación electrónica es la interacción entre los electrones en la estructura electrónica de un sistema cuántico, a partir de esta suposición, se puede aplicar el principio variacional de mecánica cuántica.

El punto de partida para el cálculo Hartree-Fock es un conjunto de orbitales aproximados. Para un cálculo atómico, estos son típicamente los orbitales de un átomo hidrogenoide: un átomo con una carga nuclear cualquiera, pero con un sólo electrón. Para cálculos moleculares o cristalinos, las funciones de ondas iníciales son típicamente una combinación lineal de orbitales atómicos.

1.4.5 Teoría de Tomas-Fermi-Dirac

Las primeras nociones de DFT fueron desarrolladas por Thomas y Fermi en los años 1920. Calcularon la energía de un átomo en una caja con la ecuación de Schrodinger, representando su energía cinética como función de su densidad electrónica, y combinando esto con las expresiones clásicas de las interacciones núcleo-electrón y electrón-electrón (que también se pueden representar en términos de densidad electrónica) [45].

El modelo fue mejorado por Dirac, que añadió un funcional de energía de intercambio en 1928, donde la expresión de la energía de un átomo (considerando el núcleo del átomo con carga positiva Z y una densidad electrónica $\rho(r)$) donde r es la distancia al núcleo, y se expresa [39]:

$$E_{TF}[\rho(r)] = T_{TF}[\rho(r)] - Z\int \frac{\rho(r)}{r}dr + \frac{1}{2}\iint \frac{\rho(r_1)\rho(r_2)}{r_{12}}dr_1 dr_2 \qquad \textit{Ecuación 1.4.5.1}$$

donde:

$$T_{TF}[\rho(r)] = \frac{3}{10}(3\pi^2)^{2/3}\int \rho^{5/3}(r)\,dr \qquad \textit{Ecuación 1.4.5.2}$$

Sin embargo, la teoría de Thomas-Fermi-Dirac era imprecisa para la mayoría de las aplicaciones, por la mala representación de la energía cinética como función de la densidad.

1.4.6 Teoría de Hohenberg y Kohn

En 1964 el método de DFT fue sometido a un tratamiento por Hohenberg y Kohn, lo cual puso en bases sólidas las ideas propuestas por Tomas-Fermi. Hohenberg y Kohn mostraron que la energía es un funcional de la densidad y que además la densidad del sistema minimiza este funcional [46]. Demostraron que, para el estado fundamental, existe una relación uno a uno entre la densidad electrónica y el potencial externo, $v(r)$.

Mostraron que la energía es un funcional de la densidad a través de la relación

$$E[\rho] = T[\rho] + V_{NE}[\rho] + V_{EE}[\rho] \qquad \textit{Ecuación 1.4.6.1}$$

$$E[\rho] = T[\rho] + V_{EE}[\rho] + \int \rho(r)\, v(r) dr \qquad \textit{Ecuación 1.4.6.2}$$

$$E[\rho] = F_{HK}[\rho] + \int \rho(r)\, v(r) dr \qquad \textit{Ecuación 1.4.6.3}$$

Donde $F_{HK}[\rho]$ es el funcional de Hohenberg y Kohn, independiente del potencial externo, que contiene la energía cinética $T[\rho]$ y la interacción electrón-electrón $Vee[\rho]$. El potencial externo $v(r)$ es un funcional único de la densidad $\rho(r)$ más una constante aditiva. El potencial externo $v(r)$ es el que distingue un sistema determinado de N partículas de otros sistemas distintos con el mismo número de partículas. Por tanto, sistemas físicos diferentes con el mismo número de electrones, pero con potenciales externos, tienen diferentes densidades de carga electrónicas en sus estados fundamentales.

Para toda densidad de prueba $\tilde{\rho}(r)$ tal que $\tilde{\rho}(r) \geq 0$ y $\int \tilde{\rho}(r) dr = N$ se cumple que.

$$E0 \leq Ev[\rho(r)] \qquad \textit{Ecuación 1.4.6.4}$$

El problema con el teorema de Hohenberg y Kohn es que los funcionales de energía cinética y de intercambio y correlación, son desconocidos, por lo que deben ser aproximados.

1.4.7 Teoría de Kohn y Sham

Kohn y Sham presentaron una forma de aproximar la parte cinética, recurriendo a un sistema ficticio constituido por un sistema de electrones no interactuantes.

$$Ts[\rho] = \sum \langle \phi_i \left| -\frac{1}{2}\nabla^2 \right| \phi_i \rangle \qquad \textit{Ecuación 1.4.7.1}$$

Esto significa que tal sistema puede estar representado por un determinante (determinante de Slater) cuyos elementos son funciones que representan a cada uno de los electrones del sistema (orbitales). Introduciendo los orbitales $\phi(r, s)$ expresando la densidad de la siguiente manera:

$$\rho(r) = \sum_{i}^{N} \sum_{S} |\phi_i(r,s)|^2 \qquad \textit{Ecuación 1.4.7.2}$$

Con este punto de partida la energía cinética corresponde a una suma de energías cinéticas individuales y la densidad electrónica a la suma de densidades orbitales.

Un elemento adicional en el modelo de Kohn y Sham es la aproximación a la interacción electrón-electrón ya que proponen como parte principal de ésta a la interacción de Coulomb y con esto el funcional universal es escrito como:

$$F[\rho(r)] = T_s[\rho(r)] + J[\rho(r)] + E_{xc}[\rho(r)] \qquad \textit{Ecuación 1.4.7.3}$$

donde el funcional de intercambio y correlación, se define como:

$$E_{xc}[\rho(r)] = T[\rho(r)] - T_s[\rho(r)] + V_{EE}[\rho(r)] - J[\rho(r)] \qquad \textit{Ecuación 1.4.7.4}$$

De esta manera el funcional de la energía queda como:

$$F[\rho(r)] = \int \rho(r)v(r)dr + \sum \langle \phi_i \left| -\frac{1}{2}\nabla^2 \right| \phi_i \rangle + V_{EE}[\rho(r)] - J[\rho(r)] \qquad \textit{Ecuación 1.4.7.5}$$

Aunque las ecuaciones de Kohn-Sham se resuelven iterativamente y son muy similares al método de Hartree-Fock, el significado físico de ambos métodos es diferente ya que tienen asociados potenciales efectivos diferentes [47].

1.5 Optimización geométrica y pozo de potencial.

La optimización geométrica constituye una metodología iterativa destinada a identificar un mínimo en la superficie de la energía potencial por sus siglas en inglés (PES), variando sistemáticamente las longitudes y ángulos de los enlaces hasta alcanzar un estado en el que las estructuras moleculares alcancen el equilibrio o la estabilidad. Un PES puede caracterizar eficazmente una molécula o un conjunto de moléculas con una composición atómica constante o, alternativamente, abarcar un sistema en el que se produce una reacción química. Una representación precisa de un PES requiere la existencia de una superficie multidimensional, cuya dimensionalidad aumenta de acuerdo con el número de variables independientes [47]. Dado que cada átomo abarca tres variables independientes (específicamente, las coordenadas x, y, z), la visualización de un PES para un modelo multiatómico resulta inviable. Esta limitación se soluciona generalizando el problema y considerando solo dos variables independientes para cada átomo.

Los puntos críticos de una PES son:

1.- Mínimo global: Es la energía más baja y nos indica la conformación más estable. Solo existe un mínimo global para cada molécula.

2.-Mínimo local: Mínimos distintos del anterior, que constituyen regiones donde un cambio en la geometría en cualquier dirección nos da una geometría de mayor energía.

3.-Punto de silla: es el punto entre dos energías extremas. El punto silla se define como un punto en la PES en el cual hay un incremento de energía en todas las direcciones excepto una, y para el cual la pendiente de la superficie es cero.

La optimización geométrica se refiere al cálculo de la función de onda y la energía derivada de la geometría inicial, reconociendo que la geometría constituye una disposición espacial de los átomos dentro de la molécula. Posteriormente, el esfuerzo se dirige a identificar una geometría de menor energía, en la que se determinen la distancia de equilibrio del TIR en esa coyuntura (mínimo local) y la energía potencial correspondiente [47]. El proceso de optimización se considera exitoso o finalizado cuando se logra la convergencia, específicamente cuando las fuerzas netas que actúan sobre los átomos son iguales a cero, dependiendo de la geometría inicial, la función de energía potencial empleada y las condiciones estipuladas para lograr un gradiente mínimo aceptable entre etapas iterativas. A medida que los átomos y las moléculas se acercan entre sí, las fuerzas intermoleculares comienzan a manifestarse. Estas fuerzas muestran características repulsivas a distancias extremadamente cortas; sin embargo, a medida que aumenta la separación espacial, se transforman en fuerzas de atracción.

Estas fuerzas generan un pozo de potencial asimétrico parecido al de Lennard-Jones [47], el cual muestra la posición del mínimo de energía potencial, es decir, la distancia de equilibrio a la que se encuentra el pozo de potencial y la magnitud de la fuerza de enlace, como muestra la figura siguiente:

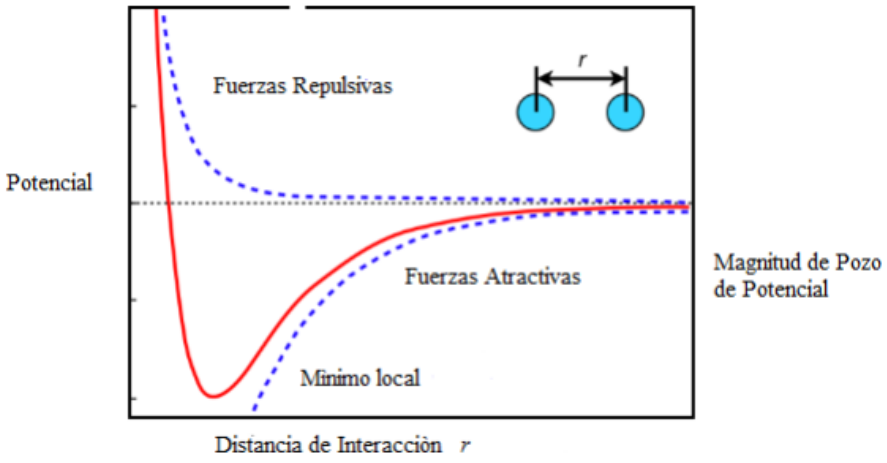

Fig. 1.5.1 Pozo de potencial.

2. Metodología

Para los primeros cálculos se utilizó un procedimiento variacional en donde el funcional de la energía electrónica es minimizado con respecto a la densidad electrónica de acuerdo con DMol^3 de BIOVIA Materials Studio [40], con una metodología basada en la Teoría de funcionales de densidad, utilizando un funcional de correlación propuesto por Perdew-Burke-Ernzerhof (PBE) [44, 48].

Los procedimientos computacionales implementados en esta investigación también incorporan el método de corrección de dispersión Grimme, el cual es esencial para capturar interacciones de Van der Waals que puedan influir en la estabilidad de los sistemas modelados. Es importante señalar que las configuraciones de electrones de valencia para litio (Li) consisten en el orbital 2s, mientras que las de carbono (C) y nitrógeno (N) incluyen tanto los orbitales 2s como 2p, que son integrales para comprender las características de enlace dentro de los materiales estudiados. A lo largo de esta investigación, todas las estructuras modeladas se someten a un proceso de relajación integral hasta que las fuerzas que actúan sobre los átomos se minimizan a un rango dentro de ±0.02 eV/Å, asegurando que las geometrías estén completamente optimizadas para obtener resultados precisos. Las estructuras de peróxido de litio (Li_2O_2) en la disposición Föppl y óxido de litio (Li_2O) en la configuración anti-fluorita empleadas en esta investigación son representativas de las estructuras estándar frecuentemente reportadas en la literatura referente a estudios de baterías de litio-aire, proporcionando así un marco confiable para la comparación. Las energías libres asociadas a todas las estructuras investigadas se calculan con cuidadosa consideración de las contribuciones fonónicas a la entropía, asegurando que las frecuencias vibracionales se incluyan adecuadamente en el análisis termodinámico. Para evaluar la viabilidad y practicidad de las estrategias de funcionalización superficial, se calculan las energías de formación correspondientes a cada grupo funcional específico, proporcionando conocimientos críticos sobre las posibles modificaciones que podrían mejorar el rendimiento del cátodo de γ-Grafino en aplicaciones de baterías.

3. Resultados

Para realizar una investigación teórica exhaustiva sobre los catalizadores que se utilizan en las baterías de litio-oxígeno (Li-O_2), es imperativo reconocer la influencia significativa que los productos que se generan en el cátodo durante los ciclos de carga-descarga tienen en el rendimiento y eficiencia general de un sistema de baterías Li-aire. El producto de descarga predominante que se genera en el cátodo durante estas reacciones se identifica como peróxido de litio (Li_2O_2), que se presenta junto a una cantidad relativamente menor de óxido de litio (Li_2O). Las reacciones químicas que caracterizan los procesos de descarga de las baterías Li-aire, particularmente cuando el peróxido de litio (Li_2O_2) sirve como producto primario, pueden representarse sistemáticamente a través del siguiente conjunto de ecuaciones.

$$Li \leftrightarrow Li^+ + e^- \quad \text{(Oxidación del ánodo)}$$

$$O_2 + 2Li^+ + 2e^- \leftrightarrow Li_2O_2 \quad \text{(Reducción del cátodo)} \qquad \textit{Ecuación 3.0.1}$$

$$2Li + O_2 \leftrightarrow Li_2O_2 \quad \text{(Reacción en toda la batería)}$$

Las reacciones de descarga asociadas al óxido de litio, específicamente Li_2O, pueden articularse de manera integral a través de la formulación de la reacción global, la cual puede ser delineada de la siguiente manera.

$$4Li + O_2 \leftrightarrow 2Li_2O \qquad \textit{Ecuación 3.0.2}$$

Si Li_2O constituye el resultado. Parece que la reacción 3.0.2 no es óptima debido a su reversibilidad limitada, ya que no se puede restaurar completamente a Li y O_2 [49], por lo que la eficacia de una batería de Li-aire está significativamente influenciada por los productos específicos producidos en el cátodo a lo largo de los mecanismos de carga-descarga.

3.1 Curvas de energía potencial

Referente al objetivo de simular computacionalmente, la actividad electrocatalítica que existe entre el cátodo de grafino en aplicaciones de baterías Li-O_2. Se construyen superficies de energía potencial (PES). Las curvas de energía potencial en dos dimensiones surgen de la proyección de las superficies de energía potencial en un plano [50] utilizando DFT. Además, se comparan con datos reportados experimentalmente. Para ello se calculan las curvas de energía potencial en sistemas pequeños. Primero se realizó la interacción de un átomo de Litio y un átomo de oxígeno (Li-O) y posteriormente se realizó la interacción entre un átomo de Litio y una molécula de oxígeno (Li-O_2). La metodología para realizar las curvas de energía potencial para las interacciones Li-O y Li-O_2, fue primero obtener la optimización geométrica de cada interacción, la cual proporciona el mínimo de la energía y distancia, correspondiente al punto de equilibrio. Posteriormente oscilar (aumentar y disminuir) la distancia alrededor del mínimo, para ir calculando las energías punto a punto en cálculos “single point”, con el fin de reunir datos de energía y distancia necesarios para poder graficar la distancia contra la energía, a este resultado se le llama gráfica de energía potencial. Es importante destacar que el equilibrio está en el mínimo de la curva de energía potencial, esto implica que en este punto la fuerza es cero. Para las interacciones Li-O y Li-O_2, se fija el átomo y molécula de oxígeno respectivamente y se mueve el átomo metálico (Li), este átomo metálico comenzará a sentir una fuerza atractiva. Mientras se aleja el átomo metálico, la tendencia es separar el sistema y obtener productos que en este caso son los mismos que los reactivos. Las curvas de energía potencial son construidas y se muestran en la figura 3.1.1 y 3.1.2 para el sistema Li-O y Li-O_2 Respectivamente. Las curvas de energía potencial son calculadas con 7 funcionales diferentes como se muestra en la Figura 3.1.1. Para el caso de la interacción Li-O, la distancia y la energía de equilibrio utilizando el funcional GGA RPBE es -86.109 kcal/mol y 1.721 Å respectivamente. La energía de equilibrio calculada se compara con datos experimentales de (energía de disociación) el cual es -81.4 ± 1.5 kcal/mol. [51]. La energía de equilibro calculada representa una sobreestimación del 5% con respecto al dato teórico obtenido. El cálculo de energías potenciales para la interacción Li-O con 7 funcionales diferentes, nos permite saber cuál funcional se adecua más a datos experimentales. Para el caso de los funcionales LDA,

BLYP Y m-GGA los datos calculados superan el 10% de sobreestimación al dato teórico (-81.4 ± 1.5 kcal/mol), por loque los últimos 3 funcionales son descartados para la interacción Li-O.

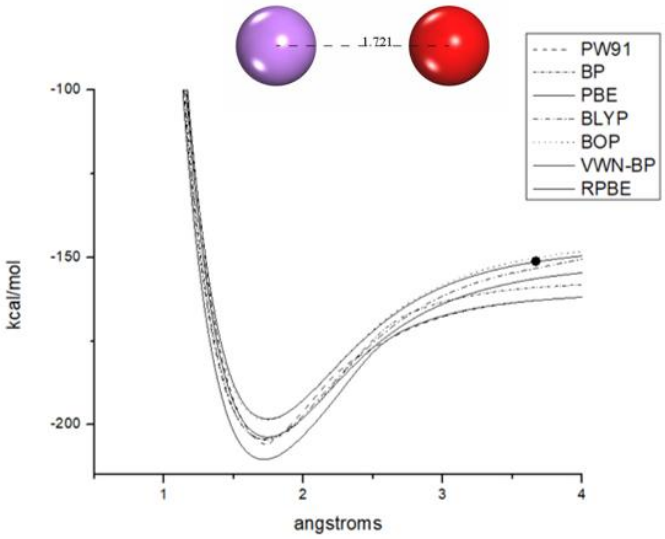

Figura 3.1.1 Pozo de potencial para la interacción Li-O

Para el caso de la interacción Li-O_2, la distancia y la energía de equilibrio promedio es -61.065 kcal/mol y 1.669 Å respectivamente. La energía de equilibrio calculada se compara con datos experimentales (energía de disociación). Para el caso experimental de la energía de disociación de la interacción Li-O_2 es 70.7 kcal/mol reportado por B. de B. Darwent [51]. La energía de equilibro calculada representa una subestimación del 16 y 13% con respecto a los datos teórico calculado.

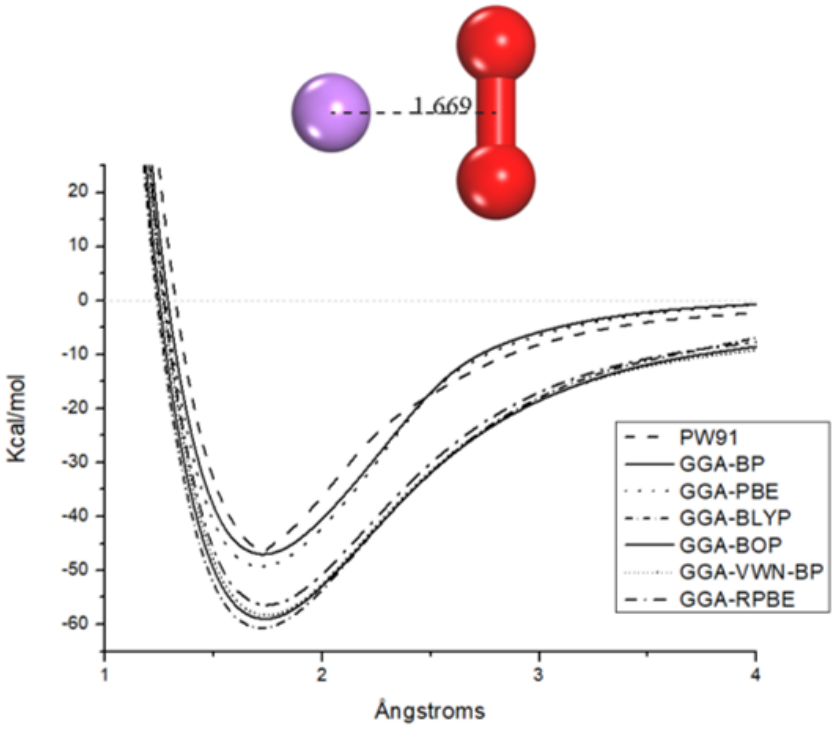

Fig. 3.1. Pozo de potencial para la interacción LiO_2

Las Interacciones Li-O y Li-O_2 son la base para conocer el proceso catalítico de la carga y descarga de una batería Li-aire. El siguiente paso por seguir es la construcción del cátodo a base de carbono. Para ello tomaremos como base el γ–Graphyne ya que es una estructura 2D con propiedades eléctricas, magnéticas únicas. Además de que posee una gran área superficial (788.05 m^2 g^{-1}) [52].

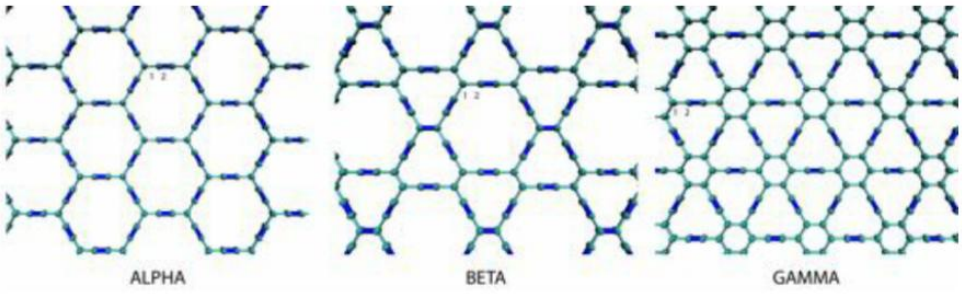

Fig. 3.1.3 Tipos de Grafino

Como se muestra en la imagen 3.1.4, tanto el carburo de calcio (CaC_2) como el hexabromobenceno ($PhBr_6$) se emplearon como precursores y se implementó ball milling como fuerza motriz de la reacción de acoplamiento cruzado. Se encontró que la composición y la constante de red de la muestra preparada se atribuyen bien al γ-Grafino.

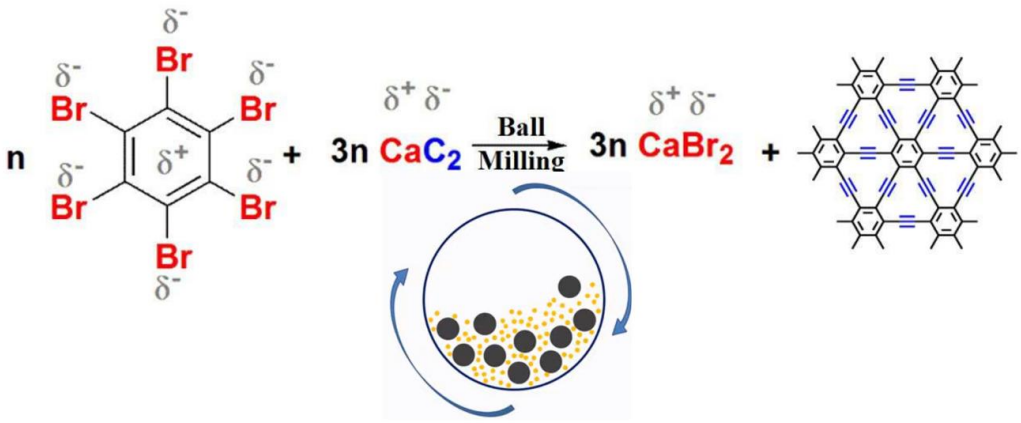

Fig. 3.1.4 síntesis del γ-Grafino

Para las siguientes etapas se tomará de base el funcional GGA-PBE el cual arroja los resultados más cercanos a lo reportado experimentalmente y además ha sido estudiado para diferentes casos usando LiO y LiO_2 [53].

3.2 Elaboración de estructuras cristalinas

Metal de litio a granel y óxidos de litio. Las constantes de red son calculadas, así como las energías de formación para $Li_{(s)}$, $Li_2O_{2(s)}$, y $Li_2O_{(s)}$. Para $Li_{(s)}$, la configuración cúbica centrada en el cuerpo, por sus siglas en inglés (BCC) es la más estable a temperatura ambiente [54].

a) b) c)

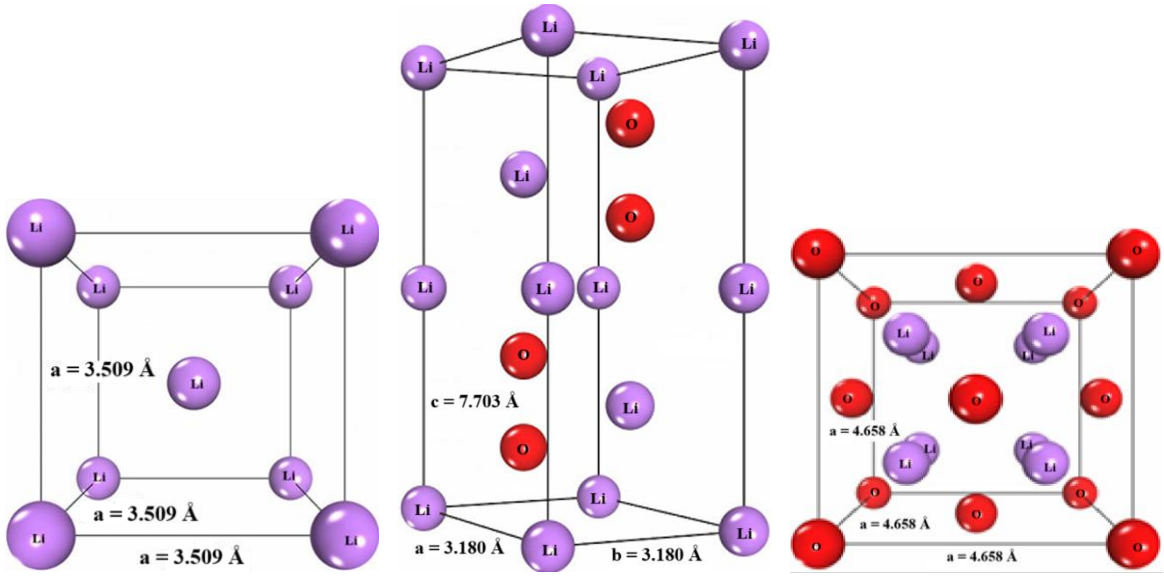

Fig. 3.2.1 Estructuras de: a) bulk Li (s) bcc; b) Li_2O_2 (s); c) Li_2O (s). Las esferas azules y rojas representan átomos de Li and O átomos respectivamente.

El parámetro cristalino para el metal de litio macroscópico, configuración Li2O2 Föppl (grupo espacial $P\bar{6}$) [55], y configuración anti-fluorita Li_2O ($Fm\underline{3}m$) [56] se presentan en la Tabla 3.2.1. Las constantes de red para Li_2O_2 y Li_2O se calculan para ser a=b=3.180, c=7.703 Å y 4.658 Å respectivamente; los valores calculados exhiben concordancia con los valores experimentales de a=b=3.142, c=7.65 Å y 4.619. La figura 3.2.1 muestra configuraciones para Li(s), Li_2O_2(s), y Li_2O(s).

Las energías se obtienen para calcular las energías libres estándar de la formación para óxidos de litio macroscópicos utilizando la ecuación subsiguiente [57]:

$$\Delta G_f^0 = G^0_{Li_xO_y(S)} - xG^0_{Li_x} - \frac{y}{2}G^0_{O_2(g)} \qquad \textit{Ecuación 3.2.1}$$

Los G_f^0 teóricos abarcan contribuciones fonónicas a la entropía: $G = E + E^{ZPE} + \Delta U(T) - TS(T)$, donde E representa la energía total de DFT, y ΔU significa la variación en la energía interna de 0 K a T. $E^{ZPE}, \Delta U\ y\ S$ se calculan con las frecuencias vibracionales correlacionadas con los modos normales de las entidades adsorbidas calculadas en la aproximación armónica. Los resultados se presentan en la Tabla 3.2.1.

Tabla 3.2.1. Simetría, Constantes de red, energías de formación y Frecuencias vibracionales para Li (s) metal y Li_2O_2 (s) y Li_2O (s) óxidos

	Simetría	Constantes de Red (Å)		Energías de formación (eV)		Frecuencias Vibracionales	
		Experimental	Calculado	Experimental	Calculado	Experimental	Calculado
Li (s)	Bcc (IM-3M)	3.49 [49]	3.509 Å	1.63 [58]	-1.537	----	----
Li_2O_2 (s)	Foppl (P63)	a=b=3.142, c=7.65 [55]	a=b=3.180, c=7.703	-5.918 [59]	-5.586	795 [57]	767.17
$(Li_2O_2)_2$ (s)	Foppl (P63)	a=b=3.142, c=7.65	a=b=3.180, c=7.703	----	-11.159	----	767.17
Li_2O (s)	Antifluorite (FM-3M)	4.619 [60]	4.658	-5.826 [59]	-5.406	523 [57]	547.05
$(Li_2O)_2$ (s)	Antifluorite (FM-3M)	4.619 [60]	4.658	----	-11.045	----	547.05

Numerosas investigaciones indican que los funcionales de GGA exageran la entalpía del enlace O-O en O_2 [57, 61]. Por esta razón, las energías acumuladas de H_2O ($\Delta H^0_{f,H_2O} = -241.83\ kJ/mol$), documentadas en la referencia [59], y H_2 calculadas utilizando la metodología DFT se amalgaman de la siguiente manera:

$$G_{O_2} = 2E_{H_2O} - 2E_{H_2} - 2\Delta H^0_{f,H_2O} \qquad \textit{Ecuación 3.2.2}$$

Los valores calculados de las energías de formación derivadas en este estudio son 1.537, -5.586, y -5.406 eV para las estructuras de Li, Li_2O_2 y Li_2O, respectivamente. Estas cifras exhiben una concordancia sustancial con los hallazgos documentados en la Ref. [58] y Ref. [59] Al determinar las energías y constantes de red para el metal Li a granel y los óxidos de Li, la fase posterior implica la construcción de la superficie bidimensional, que servirá como catalizadores catódicos para baterías de Li-O_2.

3.3 Elaboración de γ-Grafino

En la presente investigación, se utilizó γ-Grafino como superficie para catalítica específicamente diseñada para su uso en baterías de litio-oxígeno (Li-O_2), las cuales son de gran interés debido a su alta densidad energética y aplicaciones potenciales en sistemas de almacenamiento de energía sustentable. El proceso de construcción de γ-Grafino se ejecuta meticulosamente a través de la superposición de células individuales, dando como resultado una configuración estructural única que comprende un total de 48 átomos de carbono, proporcionando así una base sustancial para sus propiedades catalíticas. Con el propósito de realizar una comparación integral, tanto la forma prístina de γ-Grafino como la variante de γ-Grafino que ha sido dopada con heteroátomos, específicamente átomos de nitrógeno se utilizan como catalizadores superficiales en nuestro análisis. El prístino γ-Grafino exhibe principalmente dos tipos distintos de huecos, que son parte integral de sus características estructurales y eficacia catalítica. La primera categoría de espacios huecos se genera a partir de una estructura anular hexagonal regular, la cual está compuesta por seis átomos de carbono (denotados como R1), mientras que la segunda categoría emerge de una configuración anular hexagonal irregular, que consta de doce átomos de carbono (denotados como R2), y esta diferenciación estructural se representa visualmente en la Figura 3.3.1. Las longitudes promedio de enlace asociadas con los átomos de carbono en las estructuras R1 y R2 se miden en 1.418 Å y 1.370 Å, respectivamente, lo que indica una variación matizada en el entorno de unión dentro de estos distintos tipos huecos. Las notables discrepancias observadas en las distancias de enlace de carbono son consistentes con las distancias documentadas en la investigación realizada por Peng *et al.,* [62], quienes encontraron la presencia de tres tipos específicos de enlaces de carbono dentro del marco Grafino: el enlace C(sp^2) - C(sp^2) asociado al anillo aromático central, que mide aproximadamente 1,43 Å; el enlace C(sp^2) - C(sp) que une átomos de carbono adyacentes, caracterizada por una longitud aproximada de 1.41 Å y finalmente, el enlace C (sp) - C(sp) que corresponde a los triples enlaces interconectados, que es notablemente más corto a 1.22 Å [56]. La selección de γ-Grafino como catalizador preferido para baterías Li-O_2 se atribuye a su excepcional estabilidad y estructura porosa óptima, que son factores

cruciales para mejorar la eficiencia y el rendimiento del sistema de baterías. Dentro del alcance de este estudio, a γ-Grafino se le asignan tres responsabilidades primarias que son esenciales para su funcionalidad y efectividad como catalizador. El γ-Grafino, como catalizador para baterías de Li-O_2, fue seleccionado entre otros tipos de grafino debido a su alta estabilidad y tamaño de poro. La energía de formación calculada para el γ-Grafino es de 8.074 eV.

a) b)

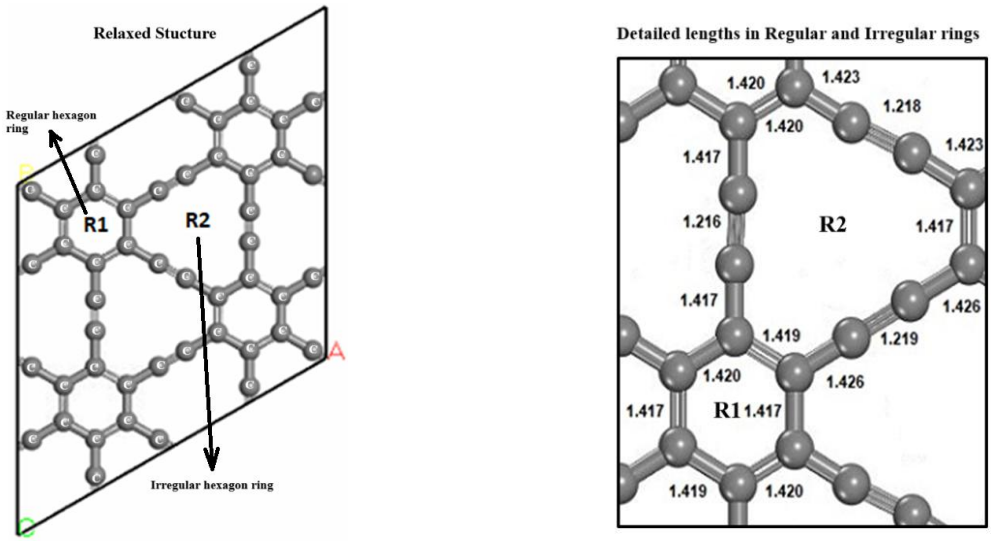

Fig. 3.3.1 a) 2x2 g-Graphyne prístino, b) Detalle de las instancias de enlace en g-Graphyne. Las esferas grises representan átomos de Carbono

3.4 Elaboración de N-γ-Grafino

Para mejorar la eficiencia operativa de la superficie de los catalizadores específicamente utilizada en baterías de litio-oxígeno (Li-O_2), emprendimos el esfuerzo estratégico de introducir heteroátomos en el sistema, con un enfoque particular en la incorporación de átomos de nitrógeno como nuestro dopante de elección. Con el fin de facilitar la generación de un sitio activo dentro del marco estructural de γ-Grafino, ejecutamos un proceso deliberado de sustitución de nitrógeno. Esta sustitución particular fue motivada por hallazgos de investigaciones previas que sugieren que la barrera de energía de activación asociada a la disociación del O_2 molecular es suficientemente baja cuando ocurre en sitios defectuosos dopados con nitrógeno dentro de arquitecturas basadas en grafeno. Las sustituciones de nitrógeno se realizaron específicamente en el sitio S1, el cual fue elegido juiciosamente en base al tipo distintivo de hibridación exhibido por los átomos de carbono ubicados en ese sitio, a saber, hibridación sp. El proceso específico de sustitución de nitrógeno se representa en detalle en la Figura 3.4.1, donde la Figura 3.4.1a ilustra la estructura prístina de γ-Grafino junto a los sitios designados, incluyendo el sitio S1. En contraste, la Figura 3.4.1b proporciona una representación visual de la configuración estructural optimizada después de la sustitución de nitrógeno, dando como resultado lo que se conoce como N-γ-Grafino. Hasta este punto, tanto la γ-Grafino no modificada como su contraparte dopada con nitrógeno, N-γ-Grafino, han sufrido extensas simulaciones teóricas para evaluar su viabilidad como materiales catódicos en aplicaciones de baterías de litio. Además, la energía de formación calculada asociada a γ-Grafino se alinea armoniosamente con resultados previamente documentados, reforzando así la credibilidad y confiabilidad de nuestras metodologías computacionales y hallazgos. La fase posterior de nuestra investigación implicará avanzar en nuestro análisis computacional para proporcionar conocimientos más profundos sobre las propiedades catalíticas bifuncionales tanto de γ-Grafino como de N-γ-Grafino, contribuyendo así a una comprensión más completa de su desempeño en aplicaciones prácticas.

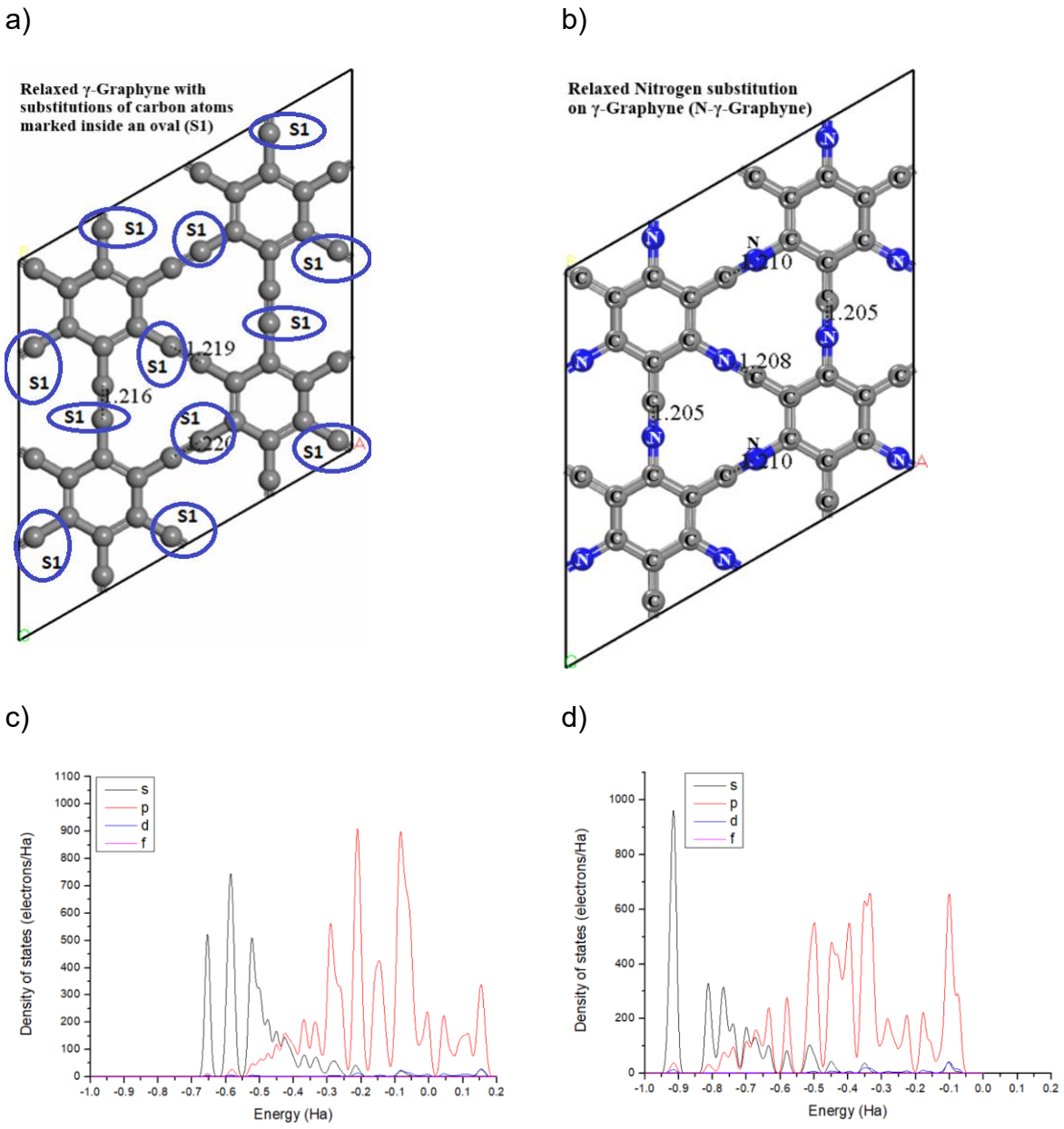

Fig. 3.4.1. a) 2x2 γ-Graphyne prístino, Los sitios S1 indican que un átomo de nitrógeno reemplazo a un átomo de carbono. b) Estructura relajada de N-dopado en γ-Graphyne (N-γ-Graphyne). Las esferas grises son átomos de carbono, y las azules representan átomos de nitrógeno. c) PDO para γ-Graphyne prístino d) PDOS para N-γ-Graphyne.

La Figura 3.4.1 sirve para ilustrar las configuraciones estructurales tanto de γ-Grafino como de N-γ-Grafino, las cuales se clasifican como marcos bidimensionales (2D); el enfoque primario de este análisis es el enlace B-C, un componente crítico de estas estructuras. En el contexto de γ-Grafino $C \equiv C$, la longitud promedio de enlace se mide cuantitativamente en 1.218 Å, mientras que para N-γ-Grafino $C - N$ esta longitud

promedio de enlace es ligeramente más corta, registrada en 1.207 Å, lo que indica que, si bien estas dos estructuras son de hecho muy similares en términos de sus dimensiones, exhiben características geométricas distintas que las diferencian entre sí.

Para proporcionar un análisis más detallado de los cambios de la estructura electrónica en la estructura dopada con N, se calculó la densidad parcial de estados (PDOS), que se grafican en las Figuras 3.4.1c y 3.4.1d para la γ-Grafino prístino y la N-γ-Grafino respectivamente. En la γ-Grafino prístino de la Figura 3.4.1c, el nivel de Fermi (E = 0) se alinea con una cierta densidad de estados. Por el contrario, en la N-γ-Grafino de la Figura 3.4.1d, la PDOS se desplaza notablemente en la región ocupada (HOMO). El desplazamiento descendente del nivel de Fermi sugiere un aumento de la densidad electrónica en los estados ocupados, lo cual es característico del dopaje con nitrógeno en materiales a base de carbono [63]. La PDOS para la N-γ-Graphyne muestra estados adicionales en el rango de energía de -0,9 Ha a -0,5 Ha, que están ausentes en la γ-Graphyne sin dopar. Esto implica que los átomos de nitrógeno introducen estados electrónicos localizados, modificando la estructura de bandas [64]. Dado que el nitrógeno tiene un electrón de valencia adicional al carbono, actúa como donante de electrones. El aumento de la densidad electrónica ocupada sugiere que ciertas regiones del material se vuelven ricas en electrones, lo que aumenta su potencial electrocatalítico.

3.5 Interacción de γ-Grafino prístino y γ-Grafino dopado con nitrógeno (N-γ-Grafino) con O_2

Al considerar la funcionalidad de las baterías de litio-aire, es imperativo reconocer que la interacción entre el oxígeno molecular (O_2) y el material del cátodo debe prevenirse activamente durante los períodos de operación estática; en otros términos, no es necesario que las moléculas de O_2 sufran adsorción sobre las superficies de γ-Grafino / N-γ-Grafino cuando la batería se encuentra en un estado de equilibrio, ni carga ni descarga.

a) b)

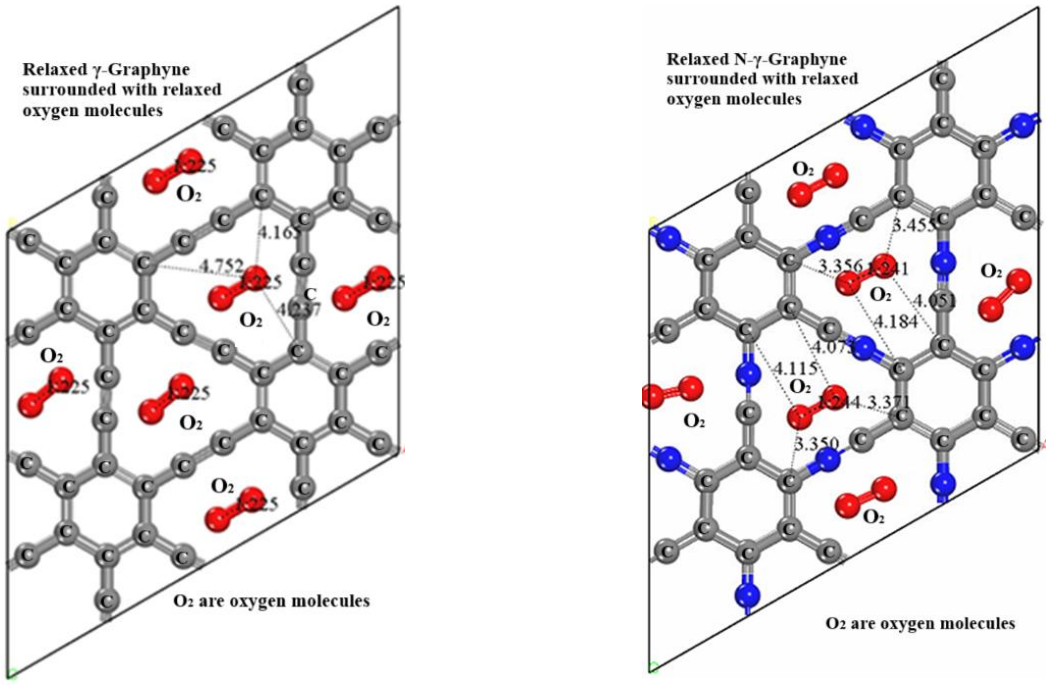

Fig. 3.5.1. a) Estructura relajada de 2x2 γ-Graphyne prístino con 12 moléculas de oxígeno. b) Estructura relajada de N-γ-Graphyne con 12 moléculas de oxigeno

La investigación en curso se centra en el examen y análisis integral de las características y propiedades estructurales de γ-Grafino y N-γ-Grafino cuando estos materiales se sitúan dentro de un ambiente saturado de oxígeno molecular, específicamente O_2, con el fin de recopilar y compilar meticulosamente datos experimentales que expliquen el comportamiento y las interacciones de estas estructuras distintivas en presencia de una atmósfera rica en oxígeno. En la Figura 3.5.1, se pueden observar las geometrías

optimizadas tanto de γ-Grafino como de N-γ-Grafino, cada una de las cuales está envuelta por moléculas de O_2; los resultados indican que la longitud molecular de cada molécula de oxígeno permanece sin cambios en comparación con la de una molécula de oxígeno aislada, que se mide en 1,225 Å, y esta longitud es congruente con las mediciones reportadas por Huber *et al.,* [65] quienes documentaron una longitud de longitud de longitud de 1.205 Å, lo que afirma que, en esta etapa de la investigación, las moléculas de oxígeno no presentan signos de adsorción en las superficies de las capas γ-Grafino y N-γ-Grafino. Para evaluar críticamente y verificar el fenómeno de no adsorción de O_2 molecular en las superficies de las estructuras γ-Grafino y N-γ-Grafino, es necesario proporcionar una evaluación detallada; específicamente para el caso que involucra γ-Grafino, la energía promedio asociada a la enésima molécula de oxígeno molecular (O_2) que se presume adsorbida sobre la estructura γ-Grafino se determina mediante la aplicación de la siguiente ecuación, que servirá de base fundamental para un análisis ulterior.

$$E_{ave} = \frac{[E(\gamma - Graphyne) + n\,E(O_2) - E(\gamma - Graphyne + n\,O_2)]}{n} \qquad \textit{Ecuación 3.5.1}$$

Dónde $E(\gamma - Graphyne)$ es la energía acumulada de γ-Grafino, $E(O_2)$ es la energía de una molécula solitaria de O_2, y finalmente $E(\gamma - Graphyne + n\,O_2)$ es la energía acumulada de n moléculas de O_2 adheridas a γ-Grafino. La energía de adsorción (E_{ad}) de unión de la enésima molécula de O_2 adherida al γ-Grafino se calcula de acuerdo con la ecuación 3.5.2.

$$E_{ad} = E(\gamma - Graphyne + (n-1)O_2) + E(O_2) - E(\gamma - Graphyne + nO_2) \qquad \textit{Ecuación 3.5.2}$$

Donde $E(\gamma - Graphyne + (n-1)O_2)$ es la energía total de $(n-1)$ de la molécula de O_2 adsorbida en γ-Grafino, finalmente n es la cantidad de moléculas de O_2 adsorbidas en γ-Grafino. Los valores y calculados se resumen en la Tabla 3.5.1.

Tabla 3.5.1. E_{ave} y E_{ad} valores de g-Graphyne-nO2 estructura. Los valores de n están entre 1 y 8.

Sistema	Energía de adsorción promedio (Å)	Energía de adsorción de enlace (Å)
γ-Grafino -O_2	0.0819	0.0820
γ-Grafino -2O_2	0.0763	0.0706
γ-Grafino -3O_2	0.0757	0.0768
γ-Grafino -4O_2	0.0761	0.0773
γ-Grafino -5O_2	0.0755	0.0732
γ-Grafino -6O_2	0.0755	0.0750
γ-Grafino -7O_2	0.0754	0.0749
γ-Grafino -8O_2	0.0750	0.0749

Para N-γ-Grafino, la energía promedio de la adsorción (E_{ave}) de la enésima molécula de O_2 se determina usando la ecuación posterior.

$$E_{ad} = E(\gamma - Graphyne + (n-1)O_2) + E(O_2) - E(\gamma - Graphyne + nO_2) \qquad \textit{Ecuación 3.5.3}$$

Donde $E(N-\gamma-Graphyne)$ se define la energía total de N-γ-Grafino, $E(O_2)$ especifica la energía de una molécula de O_2 aislada, y $E(N-\gamma-Graphyne+n\,O_2)$ representa la energía total de n moléculas de O_2 adsorbidas sobre N-γ-Grafino. La energía de adsorción (E_{ad}) de unión de la enésima molécula de O_2 sobre N-γ-Grafino se deriva de la ecuación posterior.

$$E_{ad} = E(N-\gamma-Graphyne + (n-1)O_2) + E(O_2) - E(N-\gamma-Graphyne + nO_2) \qquad \textit{Ecuación 3.5.4}$$

Donde $E(N-\gamma-Graphyne+(n-1)O_2)$ presenta la energía total de la molécula de $(n-1)\,O_2$ sobre N-γ-Grafino. Finalmente n indica la cantidad de moléculas de O_2 adsorbidas en γ-Grafino. Los valores calculados se compilan en la Tabla 3.5.2.

Tabla 3.5.2. E_{ave} y E_{ad} valores de N-γ-Graphyne-nO_2 estructura. Los valores de n están entre 1 y 8.

Sistema	Energía de adsorción promedio (Å)	Energía de adsorción de enlace (Å)
N-γ-Grafino -O_2	0.1190	0.1182
N-γ-Grafino -2O_2	0.1187	0.1170
N-γ-Grafino -3O_2	0.1187	0.1176
N-γ-Grafino -4O_2	0.1185	0.1173
N-γ-Grafino -5O_2	0.1189	0.1172
N-γ-Grafino -6O_2	0.1185	0.1173
N-γ-Grafino -7O_2	0.1190	0.1182
N-γ-Grafino -8O_2	0.1187	0.1170

Las tablas 3.5.1 y 3.5.2 demuestran que las moléculas de oxígeno no se adsorben sobre las superficies γ-Grafino y N-γ-Grafino. En las baterías de Li-aire, el material catalizador del cátodo encapsula moléculas de oxígeno, lo que requiere la ausencia de interacción entre el material del cátodo y el oxígeno cuando se descarga la batería.

3.6 Evaluación de la actividad catalítica

En la superficie catódica de las baterías de litio-oxígeno, los intrincados procesos de la reacción de reducción de oxígeno (ORR) y la reacción de evolución de oxígeno (OER) cambian secuencialmente durante las respectivas fases de descarga y carga, subrayando con ello las transformaciones electroquímicas dinámicas que se producen en estos sistemas de almacenamiento de energía. Para simular meticulosamente la evolución estructural que acompaña a estas reacciones, se deliberaron y formularon tres pasos distintos de reacción superficial a partir de una síntesis integral tanto de observaciones experimentales como de análisis teóricos, tal como se articula en las ecuaciones uno y dos. Durante el proceso de descarga, el oxígeno molecular (O_2) que interactúa con la superficie catódica de X-γ-Grafino sufre una reacción con iones de litio (Li+) y electrones (e^-) para producir óxido de litio adsorbido (LiO_2), en donde el paso posterior implica la interacción de esta especie adsorbida con iones y electrones de litio adicionales, lo que culmina en la formación de peróxido de litio (Li_2O_2), especie que además se compromete con el litio iones y electrones para producir el producto de descarga final, específicamente denotado como $(Li_2O_2)_2$. Por el contrario, la reacción de evolución de oxígeno (OER) representa el proceso termodinámicamente inverso relativo a la ORR, por lo que, durante la fase de carga, el dióxido de litio adsorbido $(Li_2O_2)_2$ se somete progresivamente a des-litiación, resultando en la liberación de oxígeno molecular (O_2). En última instancia, este oxígeno molecular se libera de la superficie de X-γ-Grafino, lo que significa la finalización del proceso de carga y la restauración del potencial electroquímico de la batería. Los pasos elementales que caracterizan tanto a la ORR como a la OER implican fundamentalmente la participación de pares ion-electrón representados como ($Li^+ + e^-$), lo que inherentemente plantea retos para la computación directa mediante métodos de teoría funcional de densidad (DFT), debido a las complejidades asociadas a diversos factores como entornos de solución y efectos de solvatación que influyen significativamente en la dinámica de reacción. El potencial químico asociado a la especie μ ($Li^+ + e^-$) se articula en función de μ (Li) y el potencial U, donde μ(Li) denota el potencial químico del litio y U representa el potencial electroquímico. En este contexto, se postula que las barreras energéticas que separan

los pasos individuales en el mecanismo de reacción son lo suficientemente mínimas como para que no impongan limitaciones cinéticas adicionales al inicio de niveles de corriente medibles durante los procesos electroquímicos. En la Sección 3.1 se realiza un análisis detallado de la formación de energía para el óxido de litio (Li_2O) y el peróxido de litio (Li_2O_2), mientras que en este apartado se evalúa específicamente la formación de energía correspondiente a Li_2O, Li_2O_2, $(Li_2O)_2$, y $(Li_2O_2)_2$, específicamente en las superficies γ-Grafino y γ-Grafino dopadas con N.

$$\Delta G_f^0 = G^0_{(Li_xO_y)_z-X-\gamma-Graphyne} - G^0_{(Li_xO_y)_z} - G^0_{X-\gamma-Graphyne} \qquad \textit{Ecuación 3.6.1}$$

Donde $G^0_{(Li_xO_y)_z X-\gamma-Graphyne}$ es la energía de formación del cátodo (X-γ-Grafino, en esta instancia X representa el heteroátomo para el caso del cátodo con sustitución) y los productos de reacción (Óxidos de litio), $G^0_{(Li_xO_y)_z}$ es la energía de formación de productos de reacción en baterías de Li-aire $G^0_{(Li_xO_y)_z X-\gamma-Graphyne}$ es la energía de formación de una γ-Grafino de 2x2 celdas aisladas. En la tabla 3.5.1 se sintetizan las energías de formación. La Figura 3.6.1 ilustra la estructura relajada para la formación de productos de reacción en una batería de Li-aire; en este escenario, el material del cátodo es γ-Grafino. Las figuras 11a), 11b), 11c), 11d) representan la formación de Li_2O, Li_2O_2, $(Li_2O)_2$, $(Li_2O_2)_2$ respectivamente en γ-Grafino prístino. Es pertinente señalar que los productos de óxido situados en γ-Grafino se predican sobre la estructura a granel (Figura 1). Los productos generados en las baterías de Li-aire están situados teóricamente en los nano poros más grandes de γ-Grafino.

Para el caso del catalizador de cátodo no prístino (N-γ-Grafino), también se ejecuta la investigación teórica para baterías de Li-aire; de manera similar se realizan estructuras relajadas para el catalizador cátodo formado para N-γ-Grafino, y este proceso se delinea en la Figura 6. Los óxidos de litio en ambos escenarios se posicionan en nano poros más grandes; adicionalmente, se calculan las energías de formación para el cátodo predicadas en N-γ-Grafino. Si se evalúan las energías de formación para un cátodo basado en γ-Grafino y N-γ-Grafino, podemos comparar esas energías para escudriñar el

rendimiento de un cátodo. Todos los procesos o reacciones que sucedieron en una batería de Li-aire ya han sido examinados en referencia [18], para esta razón este trabajo sobre γ-Grafino también se calcula utilizando la ecuación 3.6.1.

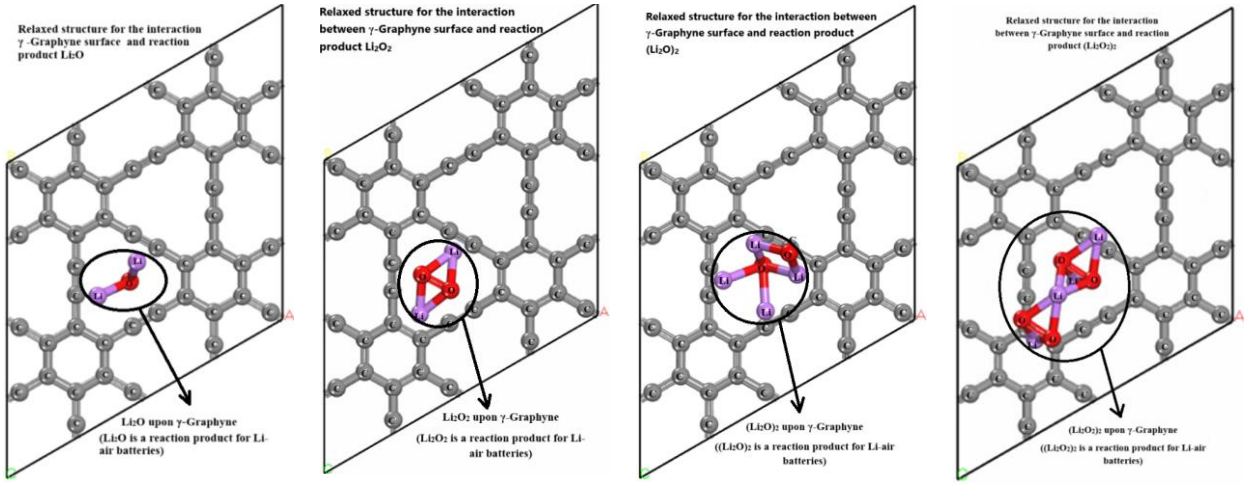

a) b) c) d)

Fig. 3.6.1. Estructura relajada con la formación de productos de baterías Li-air para γ -Graphyne. 11a), 11b), 11c),11d) Muestran la formación para Li_2O, Li_2O_2, $(Li_2O)_2$, $(Li_2O_2)_2$ respectivamente en γ -Graphyne prístino.

Todas las energías de formación computadas están encapsuladas en la Tabla 3.6.1; los hallazgos indican que las energías son elevadas cuando se evalúan en una configuración a granel aislada. Además, cuando se emplea γ-Grafino como catalizador en baterías de Li-O_2, las energías de formación para los productos de reacción disminuyen, lo que sugiere que la superficie de γ-Grafino mejora la actividad catalítica para las baterías de Li-aire. Además, cuando se utiliza un cátodo conectado a tierra en N-γ-Grafino como componente catódico en baterías de Li-O_2, se alcanzan las energías mínimas de formación para los productos de reacción, lo que indica que el cátodo basado en N-γ-Grafino sirve como el catalizador más eficaz para las baterías de Li-aire en esta investigación. Este resultado se anticipa a la luz de estudios anteriores.

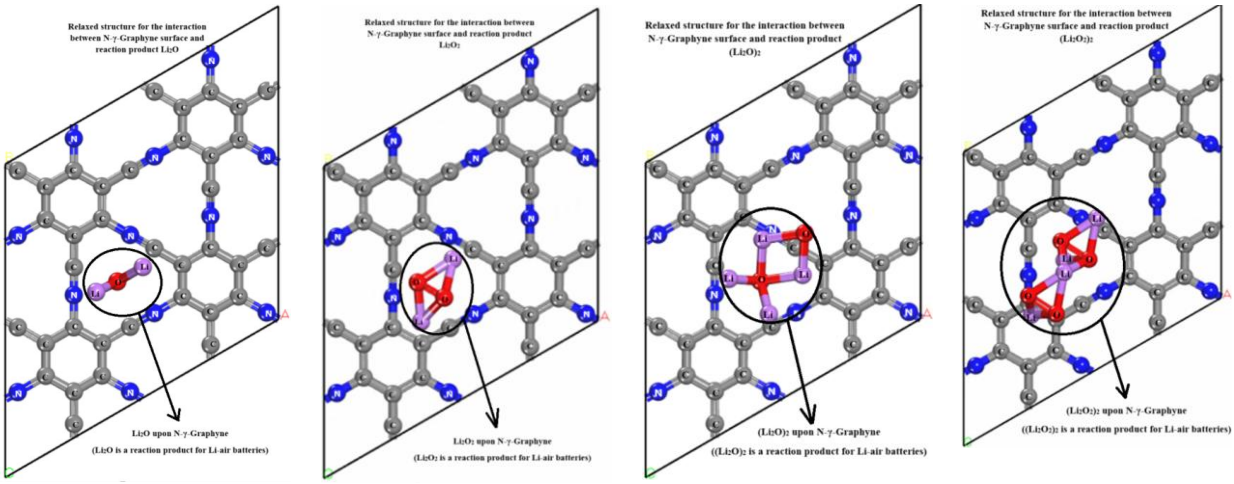

a) b) c) d)

Fig. 3.6.2. Estructuras optimizadas con la formación de productos en baterías Li-air para N-γ-Grafino. 12a), 12b), 12c), 12d) Muestran la formación para Li_2O, Li_2O_2, $(Li_2O)_2$, $(Li_2O_2)_2$ respectivamente en N-γ-Grafino.

En otros términos, es factible construir un catalizador de cátodo para baterías de Li-aire a base de material carbonáceo; los cálculos teóricos indican que la configuración γ-Grafino como catalizador en baterías de Li-aire potencia la síntesis de óxidos de litio sobre la estructura γ-Grafino. De acuerdo con estudios previos, el dopaje o la sustitución dentro de un material carbonáceo disminuye las energías de formación. En esta investigación, la configuración N-γ-Grafino exhibe la eficacia más favorable para el catalizador catódicos de las baterías Li-O_2, proporcionando así una base teórica sustancial para el avance de un cátodo práctico utilizado en baterías de Li-aire. En la tabla 3.6.1, las energías de formación experimental derivadas de las referencias [58] y [59] se comparan contra de energías computadas.

Tabla 3.6.1. ΔG_f^0 Valores calculados para N-g-Graphyne-nO_2 estructura. Los valores de n están entre 1 y 8.

		Energías de formación calculadas ΔG_f^0 (eV)		
Producto de reacción	Experimental Bulk (eV)	Bulk aislado	En γ -Grafino	En N-γ -Grafino
Li_2O	5.826	5.406	5.293	5.019
$(Li_2O)_2$	N/D	N/D	10.863	9.542
Li_2O_2	5.918	5.586	5.475	5.138
$(Li_2O_2)_2$	N/D	N/D	11.041	10.947

3.7 Dopado con boro

Para el caso del catalizador de cátodo no prístino (B-γ-Grafino), también se ejecuta la investigación teórica para baterías de Li-aire; de manera similar se realizan estructuras relajadas para el catalizador formado para B-γ-Grafino, y este proceso se delinea en la Figura 3.7.1. Los óxidos de litio en ambos escenarios se posicionan en nano poros más grandes; adicionalmente, se calculan las energías de formación para el cátodo predicadas en B-γ-Grafino . Se evalúan las energías de formación para un cátodo basado en γ-Grafino y B-γ-Grafino, podemos comparar esas energías para escudriñar el rendimiento de un cátodo. Todos los procesos o reacciones que sucedieron en una batería de Li-aire ya han sido examinados en referencia [18], para esta razón, este trabajo sobre γ-Grafino también se calcula utilizando la ecuación 3.6.1.

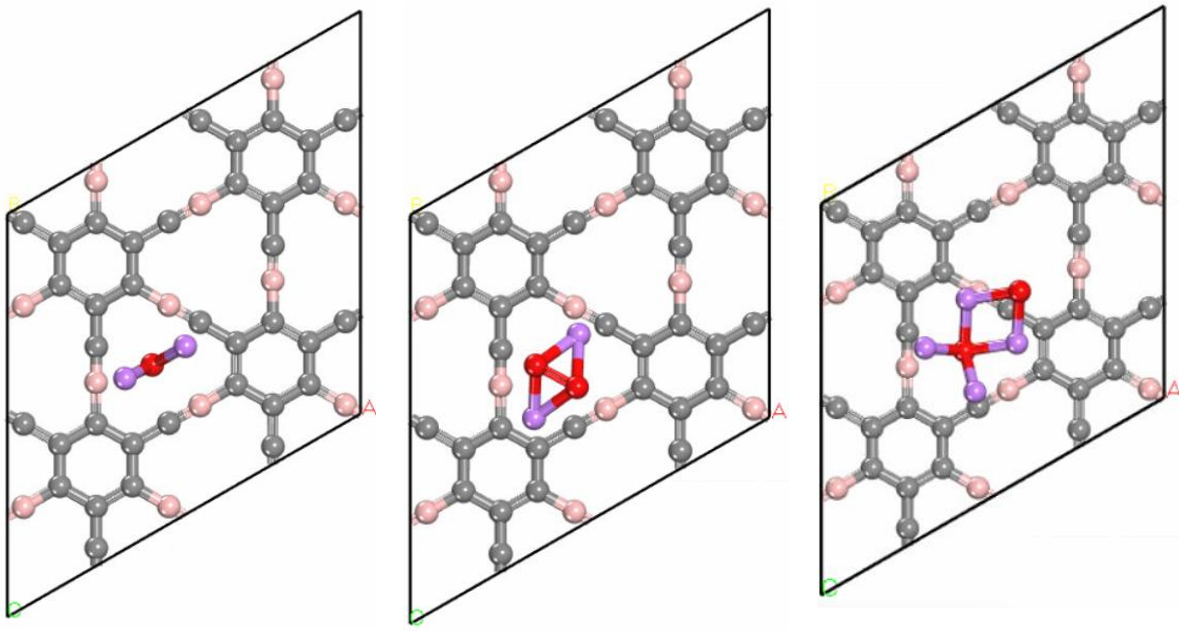

a) b) c)

Fig. 3.7.1. Estructura relajada con la formación de productos en baterías Li-air para B-γ -Graphyne. 13a), 13b), 13c) Muestran la formación para Li_2O, Li_2O_2, $(Li_2O)_2$, $(Li_2O_2)_2$ respectivamente en B-γ -Graphyne.

Tabla 3.7.1. ΔG_f^0 Valores calculados para B-g-Graphyne-nO2 structura. Los valores de n estan entre 1 y 8.

	Energías formación		
	Experimental Bulk (eV)	Calculado Bulk (eV)	Calculado (eV) Sobre grafino dopado
Li_2O	5.826	5.406	5.2178
$(Li_2O)_2$	N/D	N/D	10.5907
Li_2O_2	5.918	5.586	5.3358

Todas las energías de formación computadas están encapsuladas en la Tabla 3.7.1, los hallazgos indican que las energías son elevadas cuando se evalúan en una configuración de grafino prístino. Además, cuando se emplea γ-Grafino como catalizador en baterías de Li-O_2, las energías de formación para los productos de reacción disminuyen, lo que sugiere que la superficie de γ-Grafino mejora la actividad catalítica para las baterías de Li-aire. Además, cuando se utiliza un cátodo dopado B-γ-Grafino como componente catódico en baterías de Li-O_2, se alcanzan las energías mínimas de formación para los productos de reacción, lo que indica que el cátodo basado en B-γ-Grafino sirve como el catalizador más eficaz para las baterías de Li-aire en esta investigación. Este resultado se anticipa a la luz de estudios anteriores.

Tabla 3.7.2 comparación de las energías de formación calculadas sobre gama grafino prístino, dopado con Nitrógeno y dopado con Boro

	Energías formación				
	Experimental Bulk (eV)	Calculado Bulk (eV)	Calculado (eV) Sobre grafino Pristino	Calculado (eV) Sobre B-y-grafino Boro	Calculado (eV) Sobre N-y-grafino
Li_2O	5.826	5.406	5.293	5.2178	5.019
$(Li_2O)_2$	N/D	N/D	10.863	10.5907	9.542
Li_2O_2	5.918	5.586	5.475	5.3358	5.138
$(Li_2O_2)_2$	N/D	N/D	11.041	TBD	10.947

En otros términos, es factible construir un catalizador de cátodo para baterías de Li-aire a base de material carbonáceo; los cálculos teóricos indican que la configuración γ-Grafino como catalizador en baterías de Li-aire potencia la síntesis de óxidos de litio sobre la estructura γ-Grafino. De acuerdo con estudios previos, el dopaje o la sustitución dentro de un material carbonáceo disminuye las energías de formación. En esta investigación, la configuración N-γ-Grafino exhibe la eficacia más favorable para el catalizador catódicos de las baterías Li-O_2, proporcionando así una base teórica sustancial para el avance de un cátodo práctico utilizado en baterías de Li-aire. En la tabla 3.7.2, las energías de formación experimental derivadas de las referencias [58] y [59] se comparan contra de energías computadas.

4. Conclusiones

Esta investigación se dirigió a mejorar el rendimiento general del catalizador utilizado en las baterías de litio-aire (Li-aire), que han recibido una atención significativa en el ámbito de las tecnologías de almacenamiento de energía. Para fundamentar nuestros cálculos, calculamos las energías de formación empleando DFT a través del software Biovia Material Studio Dmol^3, y para asegurar la precisión de nuestro enfoque computacional, se utilizó una base compuesta por una celda unitaria 2x2 de γ-Grafino así como una celda unitaria 2x2 de N-γ-Grafino; además, estas investigaciones se complementaron aún más mediante la realización de cálculos de optimización, en los que determinamos el energías de adsorción pertenecientes a moléculas de oxígeno en los materiales catódicos antes mencionados a través de ecuaciones de energía de adsorción establecidas. Derivados de esta investigación las moléculas de oxígeno no presentan reacción con el cátodo, un resultado que se alinea con nuestras expectativas iniciales, ya que sería bastante ineficiente que el cátodo se involucre en reacciones con moléculas de oxígeno aisladas de una manera propicia para el funcionamiento de la batería. En última instancia, los productos de reacción generados dentro de las baterías de litio-aire, específicamente cuando se sitúan sobre un sustrato γ-Grafino y N-γ-Grafino, están bien documentados en la literatura existente, lo que indica que el cátodo debe funcionar eficazmente como catalizador para facilitar el proceso de litiación, que ocurre cuando un ion de litio (Li^+) interactúa con moléculas de oxígeno, desempeñando el cátodo un papel fundamental en el soporte y catalización de esta reacción esencial. En consecuencia, se procedió a calcular las energías de formación para productos de reacción específicos como óxido de litio (Li_2O), peróxido de litio (Li_2O_2), así como sus respectivos dímeros, a saber $(Li_2O)_2$y $(Li_2O_2)_2$, para obtener conocimientos más profundos sobre sus perfiles energéticos. Los resultados de nuestra investigación revelan que el material del cátodo basado en γ-Grafino potencia significativamente las energías de formación; sin embargo, es el material del cátodo derivado del N-γ-Grafino el que emerge como el candidato superior para su aplicación en baterías de litio-aire, demostrando una reducción aproximada del 15% en las energías de formación para los productos de reacción Li_2O, Li_2O_2, $(Li_2O)_2$, $(Li_2O_2)_2$. Este hallazgo sugiere fuertemente que el desarrollo de cátodos

construidos a partir de materiales basados en carbono para aplicaciones de baterías de litio-aire no solo es factible, sino que también tiene el potencial de contribuir a una reducción en los costos de fabricación asociados con la producción en masa de tales sistemas avanzados de almacenamiento de energía. Por todo el preámbulo y los datos obtenidos en el presente trabajo se puede afirmar teóricamente un incremento de la actividad electrocatalítica al desarrollar un cátodo de grafino dopado con heteroátomos para reacciones de reducción de oxígeno en electrolitos no acuosos, para su uso en baterías de Litio-aire, dando como resultado la completa afirmación de la hipótesis del presente trabajo.

Referencias

[1] B. Richter *et al.*, “HOW AMERICA CANLOOK WITHIN TO ACHIEVE ENERGY SECURITY ANDREDUCE GLOBAL WARMING,” vol. 80, no. 4, pp. S1–S109, Dec. 2008, doi: 10.1103/RevModPhys.80.S1.

[2] C. McGlade and P. Ekins, “The geographical distribution of fossil fuels unused when limiting global warming to 2°C,” *Nature*, vol. 517, no. 7533, pp. 187–190, Jan. 2015, doi: 10.1038/nature14016.

[3] D. Welsby, J. Price, S. Pye, and P. Ekins, “Unextractable fossil fuels in a 1.5 °C world,” *Nature*, vol. 597, no. 7875, pp. 230–234, Sep. 2021, doi: 10.1038/s41586-021-03821-8.

[4] H. Kumar, S. Rajan, and A. K. Shukla, “Development of lithium-ion batteries from micro-structured to nanostructured materials: Its issues and challenges,” *Sci Prog*, vol. 95, no. 3, pp. 283–314, 2012, doi: 10.3184/003685012X13421145651372.

[5] B. Zhu *et al.*, “Semiconductor Electrochemistry for Clean Energy Conversion and Storage,” Dec. 01, 2021, *Springer*. doi: 10.1007/s41918-021-00112-8.

[6] B. Dunn, H. Kamath, and J.-M. Tarascon, “Electrical Energy Storage for the Grid: A Battery of Choices System power ratings, module size.” [Online]. Available: http://science.sciencemag.org/

[7] J.-M. Tarascon and M. Armand, “Issues and challenges facing rechargeable lithium batteries,” 2001. [Online]. Available: www.nature.com

[8] V. Ramadesigan, P. W. C. Northrop, S. De, S. Santhanagopalan, R. D. Braatz, and V. R. Subramanian, “Modeling and Simulation of Lithium-Ion Batteries from a Systems Engineering Perspective,” *J Electrochem Soc*, vol. 159, no. 3, pp. R31–R45, 2012, doi: 10.1149/2.018203jes.

[9] K. Lingyu *et al.*, “Sustainable regeneration of high-performance LiCoO2 from completely failed lithium-ion batteries,” *J Colloid Interface Sci*, vol. 640, Jun. 2023, doi: https://doi.org/10.1016/j.jcis.2023.03.021.

[10] W. Zhi-Hai and Y. Yang-Xin, “Theoretical study on catalytic performance of Ti2B monolayer as cathodes of Li-O2 and Na-O2 batteries promoted by surface functionalization,” *Appl Surf Sci*, vol. 666, no. 160380, Sep. 2024, Accessed: Oct. 05, 2024. [Online].

[11] K. M. Abraham and Z. Jiang, “A Polymer Electrolyte-Based Rechargeable lithium/Oxygen Battery,” 1996.

[12] D. Wang, X. Mu, P. He, and H. Zhou, “Materials for advanced Li-O2 batteries: Explorations, challenges and prospects,” Jun. 01, 2019, *Elsevier B.V.* doi: 10.1016/j.mattod.2019.01.016.

[13] J. L. Shi *et al.*, “Improving the structural stability of Li-rich cathode materials via reservation of cations in the Li-slab for Li-ion batteries,” *Nano Res*, vol. 10, no. 12, pp. 4201–4209, 2017, doi: 10.1007/s12274-017-1489-3.

[14] D. Wu *et al.*, “Metal-organic frameworks as cathode materials for Li-O2 batteries,” *Advanced Materials*, vol. 26, no. 20, pp. 3258–3262, 2014, doi: 10.1002/adma.201305492.

[15] J. Ren, N. Zhang, and P. Liu, "Li adsorption on nitrogen-substituted graphyne for hydrogen storage," *Fullerenes, Nanotubes and Carbon Nanostructures*, vol. 29, no. 3, pp. 212–217, 2020, doi: 10.1080/1536383X.2020.1830066.

[16] D. Zhai *et al.*, "Disproportionation in Li-O2 batteries based on a large surface area carbon cathode," *J Am Chem Soc*, vol. 135, no. 41, pp. 15364–15372, Oct. 2013, doi: 10.1021/ja403199d.

[17] I. C. Jang, Y. Hidaka, and T. Ishihara, "Li metal utilization in lithium air rechargeable batteries," *J Power Sources*, vol. 244, pp. 606–609, 2013, doi: 10.1016/j.jpowsour.2013.01.049.

[18] K. Yoo, S. Banerjee, and P. Dutta, "Modeling of volume change phenomena in a Li-air battery," *J Power Sources*, vol. 258, pp. 340–350, 2014, doi: 10.1016/j.jpowsour.2014.02.044.

[19] W. Liang, L. Zhenjie, G. Limin, and P. Zhangquan, "Understanding oxygen electrochemistry in aprotic LiO2 batteries," *Green Energy & Environment*, vol. 2, no. 3, pp. 186–203, 2017.

[20] H. Cheng and K. Scott, "Improving performance of rechargeable Li-air batteries from using Li-Nafion® binder," *Electrochim Acta*, vol. 116, pp. 51–58, Jan. 2014, doi: 10.1016/j.electacta.2013.11.018.

[21] E. Nasybulin, W. Xu, M. H. Engelhard, Z. Nie, X. S. Li, and J. G. Zhang, "Stability of polymer binders in Li-O2 batteries," *J Power Sources*, vol. 243, pp. 899–907, 2013, doi: 10.1016/j.jpowsour.2013.06.097.

[22] D. Sharon, V. Etacheri, A. Garsuch, M. Afri, A. A. Frimer, and D. Aurbach, "On the challenge of electrolyte solutions for Li-air batteries: Monitoring oxygen reduction and related reactions in polyether solutions by spectroscopy and EQCM," *Journal of Physical Chemistry Letters*, vol. 4, no. 1, pp. 127–131, Jan. 2013, doi: 10.1021/jz3017842.

[23] Y. Wang, D. Zheng, X. Q. Yang, and D. Qu, "High rate oxygen reduction in non-aqueous electrolytes with the addition of perfluorinated additives," *Energy Environ Sci*, vol. 4, no. 9, pp. 3697–3702, Sep. 2011, doi: 10.1039/c1ee01556g.

[24] F. Li, T. Zhang, Y. Yamada, A. Yamada, and H. Zhou, "Enhanced cycling performance of LI-O2batteries by the optimized electrolyte concentration of litfsa in glymes," *Adv Energy Mater*, vol. 3, no. 4, pp. 532–538, Apr. 2013, doi: 10.1002/aenm.201200776.

[25] X. Liu, B. Cui, S. Liu, and Y. Chen, "Progress of Non-Aqueous Electrolyte for Li-Air Batteries," *Journal of Materials Science and Chemical Engineering*, vol. 03, no. 05, pp. 1–8, 2015, doi: 10.4236/msce.2015.35001.

[26] J. L. Shui, H. H. Wang, and D. J. Liu, "Degradation and revival of Li-O2 battery cathode," *Electrochem commun*, vol. 34, pp. 45–47, 2013, doi: 10.1016/j.elecom.2013.05.020.

[27] Q. Qiu *et al.*, "Cathode electrocatalyst in aprotic lithium oxygen (Li-O2) battery: A literature survey," *Catal Today*, vol. 420, Aug. 2023, doi: 10.1016/j.cattod.2023.114138.

[28] C. Ruiqi *et al.*, "Rational design of boron-nitrogen coordinated active sites towards oxygen reduction reaction in aluminum-air batteries with robust integrated air cathode," *J Power*

Sources, vol. 556, Feb. 2023, Accessed: Oct. 05, 2024. [Online]. Available: https://www.sciencedirect.com/science/article/abs/pii/S0378775322014537

[29] Y. Gu *et al.*, "MnIII-enriched α-MnO2 nanowires as efficient bifunctional oxygen catalysts for rechargeable Zn-air batteries," *Energy Storage Mater*, vol. 23, pp. 252–260, Dec. 2019, doi: 10.1016/j.ensm.2019.05.006.

[30] J. Mao, P. Guo, T. Zhang, S. Zhang, and C. Liu, "A first-principle study on hydrogen storage of metal atoms (M = Li , Ca , Sc , and Ti) coated B 40 fullerene composites," *Comput Theor Chem*, vol. 1181, p. 112823, 2020, doi: 10.1016/j.comptc.2020.112823.

[31] Sahar Ziraki, Mansour Kanani, Babak Hashemi, and Mohammad Mohsen Loghavi, "Effect of sodium and yttrium co-doping on electrochemical performance of LiNi0.8Co0.15Al0.05O2 cathode material for Li-ion batteries: Computational and experimental investigation," *J Energy Storage*, vol. 70, Oct. 2023, doi: https://doi.org/10.1016/j.est.2023.107983.

[32] X. Peng *et al.*, "Hierarchically Porous Carbon Plates Derived from Wood as Bifunctional ORR/OER Electrodes," *Advanced Materials*, vol. 31, no. 16, Apr. 2019, doi: 10.1002/adma.201900341.

[33] B. Wang *et al.*, "Simple-Cubic Carbon Frameworks with Atomically Dispersed Iron Dopants toward High-Efficiency Oxygen Reduction," *Nano Lett*, vol. 17, no. 3, pp. 2003–2009, Mar. 2017, doi: 10.1021/acs.nanolett.7b00004.

[34] J. Chen, C. Li, and Y. Chen, "Understanding the effect of functional groups on carbon nanotube towards oxygen reduction reaction," *Mater Today Energy*, vol. 16, Jun. 2020, doi: 10.1016/j.mtener.2020.100400.

[35] Y. Wenyu *et al.*, "P2-type layered oxide cathode with honeycomb-ordered superstructure for sodium-ion batteries," *Energy Storage Mater*, vol. 69, May 2024, Accessed: Oct. 05, 2024. [Online]. Available: https://www.sciencedirect.com/science/article/abs/pii/S2405829724002514

[36] W. Jiajun *et al.*, "Theoretical study of catalytic performance of WN MXenes as cathodes for Li-O2 batteries Effects of surface functionalization and atomic layers," *Appl Surf Sci*, vol. 638, Nov. 2023, doi: https://doi.org/10.1016/j.apsusc.2023.158027.

[37] Z. Peng, S. A. Freunberger, Y. Chen, and P. G. Bruce, "A Reversible and Higher-Rate Li-O 2 Battery." [Online]. Available: https://www.science.org

[38] M. Kim, E. Yoo, W. S. Ahn, and S. E. Shim, "Controlling porosity of porous carbon cathode for lithium oxygen batteries: Influence of micro and meso porosity," *J Power Sources*, vol. 389, pp. 20–27, Jun. 2018, doi: 10.1016/j.jpowsour.2018.03.080.

[39] R. G. Parr, "Density Functional Theory of Atoms and Molecules," in *Horizons of Quantum Chemistry*, K. Fukui and B. Pullman, Eds., Dordrecht: Springer Netherlands, 1980, pp. 5–15.

[40] Dassault Systèmes, "BIOVIA, Dassault Systèmes, Materials Studio," 2025, *San Diego*: 8.0.

[41] L. C, Y. W, and P. RG., "Development of the Colle-Salvetti correlation-energy formula into a functional of the electron density," *Phys Rev B Condens Matter*, vol. 37, no. 2, pp. 785–789, 1988, doi: doi: 10.1103/physrevb.37.785. PMID: 9944570.

[42] I.-O. Frank J, A. J.S., T.-G. Nayely, G.-R. Abraham, and V.-G. Armando, "DFT study for hydrogen storage on γ-Boron-Graphyne decorated with Li atoms," *Comput Theor Chem*, vol. 1214, p. 113764, Aug. 2022, doi: https://doi.org/10.1016/j.comptc.2022.113764.

[43] P. Robert G. and W. Yang, *Density Functional Theory of Atoms and Molecules*. Oxford University Press - Clarendon Press , 1994.

[44] B. Delley, "From molecules to solids with the DMol3 approach," *J Chem Phys*, vol. 113, no. 18, pp. 7756–7764, 2000, doi: 10.1063/1.1316015.

[45] W. Kohn, "Nobel Lecture: Electronic structure of matter—wave functions and density functionals," *Rev. Mod. Phys*, vol. 71, no. 5, pp. 1253--1266, 1999, doi: 10.1103/RevModPhys.71.1253.

[46] W. Kohn and L. J. Sham, "PHYSICAL REVIEW Self-Consistent Equations Including Exchange and Correlation Effects*."

[47] D. P. J. Atkins Peter, *Physical Chemistry for the Life Sciences*. United States and Canada: Oxford University, 2006.

[48] B. Delley, "An all-electron numerical method for solving the local density functional for polyatomic molecules," *J Chem Phys*, vol. 92, no. 1, pp. 508–517, 1990, doi: 10.1063/1.458452.

[49] Z. Ma *et al.*, "A review of cathode materials and structures for rechargeable lithium-air batteries," *Energy Environ Sci*, vol. 8, no. 8, pp. 2144–2198, 2015, doi: 10.1039/c5ee00838g.

[50] A. Ruiz-Puigdollers and P. Gamallo, "DFT study of the role of N- and B-doping on structural, elastic and electronic properties of α-, β- and γ-graphyne," *Carbon N Y*, vol. 114, pp. 301–310, Apr. 2017, doi: 10.1016/j.carbon.2016.12.026.

[51] B. deB. Darwent, *Bond Dissociation Energies In Simple Molecules*, vol. 1. 1970.

[52] N. Narita, S. Nagai, S. Suzuki, and K. Nakao, "Electronic structure of three-dimensional graphyne."

[53] J. H. P. Sánchez, A. V. García, L. A. D. Guzmán, and I. P. Zaragoza, "Calibrating density functionals with DMol3 applied on lithium oxide battery," *Revista Mexicana de Fisica*, vol. 71, no. 1, pp. 1–11, 2025, doi: 10.31349/RevMexFis.71.010402.

[54] F. Faglioni, B. V. Merinov, and W. A. Goddard, "Room-Temperature Lithium Phases from Density Functional Theory," *Journal of Physical Chemistry C*, vol. 120, no. 48, pp. 27104–27108, Dec. 2016, doi: 10.1021/acs.jpcc.6b08168.

[55] H. Föppl, "Die Kristallstrukturen der Alkaliperoxyde," *ZAAC - Journal of Inorganic and General Chemistry*, vol. 291, no. 1–4, pp. 12–50, 1957, doi: 10.1002/zaac.19572910104.

[56] R. W. G. Wyckoff, *Crystal structures*, vol. 1. 1963. doi: 10.1107/s0365110x65000361.

[57] Y. Xu and W. A. Shelton, "O2 reduction by lithium on Au(111) and Pt(111)," *Journal of Chemical Physics*, vol. 133, no. 2, Jul. 2010, doi: 10.1063/1.3447381.

[58] C. Kittel, *Solid State Physics*, 8th ed. 2005.

[59] M. W. Chase, “NIST-JANAF Thermochemical Tables,” 1998.

[60] J. Zemann, “ Crystal structures, 2 nd edition. Vol. 1 by R. W. G. Wyckoff ,” *Acta Crystallogr*, vol. 18, no. 1, pp. 139–139, 1965, doi: 10.1107/s0365110x65000361.

[61] K. H. Yun, Y. Hwang, and Y. C. Chung, “Effective catalytic media using graphitic nitrogen-doped site in graphene for a non-aqueous Li-O2 battery: A density functional theory study,” *J Power Sources*, vol. 277, pp. 222–227, 2015, doi: 10.1016/j.jpowsour.2014.12.021.

[62] Q. Peng *et al.*, “New materials graphyne, graphdiyne, graphone, and graphane: review of properties, synthesis, and application in nanotechnology,” *Nanotechnol Sci Appl*, vol. 10, no. 7, pp. 1–29, 2014.

[63] D. Deng, K. S. Novoselov, Q. Fu, N. Zheng, Z. Tian, and X. Bao, “Catalysis with two-dimensional materials and their heterostructures,” *Nat Nanotechnol*, vol. 11, no. 3, pp. 218–230, Mar. 2016, doi: 10.1038/nnano.2015.340.

[64] H. R. Jiang, T. S. Zhao, L. Shi, P. Tan, and L. An, “First-Principles Study of Nitrogen-, Boron-Doped Graphene and Co-Doped Graphene as the Potential Catalysts in Nonaqueous Li-O2 Batteries,” *Journal of Physical Chemistry C*, vol. 120, no. 12, pp. 6612–6618, 2016, doi: 10.1021/acs.jpcc.6b00136.

[65] K. P. Huber and G. Herzberg, *MOLECULAR SPECTRA and MOLECULAR -STRUCTURE IV. CONSTANTS OF DIATOMIC MOLECULES*, 1st ed. 1978.

Anexos

Listado de producción científica:

1. Armando Vera-Garcia a, J.H. Pacheco-Sanchez a, Frank J. Isidro-Ortega, Abraham Gonzalez-Ruíz c, J.S. Arellano (2025). Theoretical study of catalytic performance of X-γ-Graphyne as cathodes for lithium-air batteries. https://doi.org/10.1016/j.comptc.2025.115197.

2. J. H. Pacheco Sanchez, A. Vera Garcia, and L. A. Desales Guzman (2025). Calibrating density functionals with DMol^3 applied on lithium oxide battery. https://doi.org/10.31349/RevMexFis.71.010402

3. J. H. Pacheco Sanchez, A. Vera Garcia and Frank J. Isidro-Ortega Opinion About Increasing use of Li-Air Batteries https://biomedgrid.com/fulltext/volume15/opinion-about-increasing-use-of-li-air-batteries.002110.php

4. Frank J. Isidro-Ortega, J.S. Arellano, Nayely Torres-Gómez, Abraham González-Ruíz, Armando Vera-Garcia. DFT study for hydrogen storage on γ-Boron-Graphyne decorated with Li atoms. https://doi.org/10.1016/j.comptc.2022.113764

Computational and Theoretical Chemistry 1248 (2025) 115197

Contents lists available at ScienceDirect

Computational and Theoretical Chemistry

journal homepage: www.elsevier.com/locate/comptc

Theoretical study of catalytic performance of X-γ-Graphyne as cathodes for lithium-air batteries

Armando Vera-Garcia[a], J.H. Pacheco-Sanchez[a], Frank J. Isidro-Ortega[b,*], Abraham González-Ruíz[c], J.S. Arellano[b]

[a] División de Estudios de Posgrado e Investigación, Instituto Tecnológico de Toluca, Metepec C.P. 52149, Estado de México, Mexico
[b] Área de Física Atómica Molecular Aplicada, Universidad Autónoma Metropolitana Azcapotzalco, C.P. 02200 Azcapotzalco, Ciudad de México, Mexico
[c] Instituto Nacional de Investigaciones Nucleares, Carretera México - Toluca, S/N, Ocoyoacac, C.P. 52750, Estado de México, Mexico

ARTICLE INFO

Keywords:
Li-air batteries
Cathode catalyst for Li air batteries
Energy formation
N-doped
γ-Graphyne

ABSTRACT

Lithium-air batteries (Li—O_2) are considered one of the most promising energy storage and conversion device candidates for future mobility applications, such as electric vehicles, due to their ultrahigh theoretical energy density (up to ~3600 Wh kg^{-1}). The main goal in this work is to study an electrochemical catalytic model for a cathode in Li—O_2 batteries to simulate the OER during the discharging process. Density Functional Theory (DFT) calculations were performed to investigate γ-Graphyne and N-γ-Graphyne (N-Doped γ-Graphyne) as the potential cathode catalyst for Li—O_2 batteries. γ-Graphyne and N-γ-Graphyne surfaces exhibit high stability according to calculations, the pristine surface exhibits a slight improvement in the formation energy of Li_xO_2, moreover, the N-Doped surface can reduce the significant formation energy of Li_xO_2 in the OER. Calculations explain the catalytic mechanism and identify the active sites to perform N-doping on pristine γ-Graphyne. This study demonstrates a feasible approach to achieve designed γ-Graphyne and N-γ-Graphyne as cathode catalysts for Li air batteries, which is promising for cost reduction in mass production of Li-air batteries.

1. Introduction

It is estimated that world power consumption stands at 19 TW and is expected to triple in 2050 [1]. Currently, most of this demand is covered by the utilization of fuels. In other words, fossil fuels have been a traditional energy source over the last century. It is well known that fossil fuels like coal, petroleum, gas, etc. have caused severe forest degradation, atmospheric pollution, and global warming [2], adding fossil fuels is non-renewable, and these disadvantages for fossil fuels make many efforts in investigations to find eco-friendly energy sources. Consequently, there is an urgent call for scientific and technological advancements to develop advanced energy storage systems with high efficiencies and minimal or zero carbon emissions [1,3]. In this regard over the last few decades, electrochemical energy storage devices have been put forward to fulfill the burgeoning energy demand for several applications such as renewable energy storage, portable devices, and electric vehicles [4,5]. Electrochemical devices, including fuel cells, batteries, and electrolyzers, have great potential for large-scale clean energy conversion and storage applications. In clean energy conversion, fuel cells directly convert the chemical energy from fuels into electricity with high efficiency and low emissions. In contrast, in clean energy storage, a battery is a typical storage device with high energy density, good reversibility and durability [6]. Batteries represent an excellent energy storage technology for the integration of renewable resources. Compact size makes batteries well suited for use at distributed locations, and they can provide frequency control to reduce variations in local solar output and to mitigate output fluctuations, i.e., wind and solar farms [7]. For this reason, there has been a push towards developing more sustainable and environmentally friendly batteries [7]. Lithium- ion (Li-ion) batteries are becoming the most popular device for energy storage in portable electronic devices, Li-ion batteries provide one of the best energy-to-weight ratios, and low self-discharge when not in use [8,9]. Li-ion batteries are currently achieving the ambitious goal of electrifying transportation, this entails replacing gasoline engines in automobiles with packs of secondary batteries. But its limited gravi- metric energy density in commercial Li-ion batteries (~200 Wh kg^{-1}) hinders their effective use for long-range drives in medium to heavy vehicles [10]. However, Li—O_2 batteries have a high theoretical

* Corresponding author.
E-mail address: fisidroo@toluca.tecnm.mx (F.J. Isidro-Ortega).

https://doi.org/10.1016/j.comptc.2025.115197
Received 23 November 2024; Received in revised form 13 March 2025; Accepted 20 March 2025
Available online 22 March 2025

capacity density (up to ~3600 Wh kg^{-1}) due to the low mass of oxygen and lithium making them a potential next-generation rechargeable batteries [11,12]. Li—O_2 batteries are composed of lithium metal anode, electrolyte and oxygen cathode, and realize the reversible charge and discharge process through the oxygen reduction reaction (ORR) between lithium and oxygen and oxygen and the evolution reaction (OER) of lithium peroxide decomposition [11]. However, extensive exploration is still required due to the significant disparity between the theoretical and practical capacities of Li—O_2 batteries. It is well known that Li—O_2 batteries are divided according to the type of electrolyte: 1. water sys- tem, 2. aprotic, 3. solid state, and 4. mixed aqueous/aprotic, these types of Li—O_2 have distinct electrochemical reactions and varying open- circuit voltages for each kind of Li—O_2 battery. However, most of the research is focused on aprotic Li—O_2 batteries [13–16]. A major advantage of aprotic electrolytes is the spontaneous formation of a barrier between the anode and electrolyte that protects the lithium metal from further reaction with the electrolyte. In aprotic electrolyte, the discharge product of lithium oxide or peroxide forms at the cathode following the next electrochemical reaction of $2Li + O_2 \rightarrow Li_2O_2$ (lithium peroxide) or $4Li + O_2 \rightarrow 2Li_2O$ (lithium oxide) [17]. In this work, the electrochemical reaction is based on an aprotic electrolyte. Industrial production for Li—O_2 batteries can occur after solving many problems and challenges before commercial adoption. It is well known that various issues affect Li—O_2 battery performance, such as Li anode im- provements, which are reviewed in [18,19]. Operating atmosphere [20], binder [21,22], solvents [23,24], and lithium salts [25,26] would also make meaningful contributions to enhanced overall battery per- formance, such as poor cyclability and low energy efficiency. However, the dominating factor identified is the low level of performance for the air cathode [27]. Many efforts have been made to improve the efficiency of Li—O_2 batteries. The research on the cathode side mainly focuses on the performance of catalysts towards ORR and OER, the ideal cathode for Li—O_2 batteries should possess the following characteristics: highly efficient catalytic active sites, plentiful and interconnected pores favorable electron/mass/O-containing species transfer, as well as strong stability and durability [28]. Platinum-based materials are currently the most efficient ORR electrocatalysts. However, the scarcity and high cost of Pt significantly restrain their large-scale commercial applications [29]. For this reason, it is urgent to develop low-cost ORR electro- catalysts. Nowadays, various materials such as non-noble metal and carbon-based materials have been investigated [30–32]. Carbon-based materials receive great interest due to low cost, environmental friend- liness, and large-scale availability. However, the ORR catalytic activity of carbon-based materials is still unsatisfactory, strategies including doping metallic or non-metallic heteroatoms and introducing intrinsic vacancies in carbon-based materials have been reported for creating efficient active sites and lowering reaction barriers for ORR [33–35]. Some studies to improve the catalyst in cathodes for metal-air batteries are enlisted: Ziraki et al. [32], studied the effect of Na and Y dopants and the simultaneous addition of Na and Y on the electrochemical perfor- mance of a cathode material, which was investigated computationally using DFT. They report that the major factor affecting the structural stability of cathode material during the de-lithiation process is con- firming the significant impact of doping on reducing the oxygen release rate [32]. Wu et al. [11], develop two-dimensional Ti_2B 2D material monolayers as cathode catalyst of Li—O_2 and Na—O_2 batteries by den- sity functional theory (DFT) calculations. Their results demonstrate new options from 2D materials for cathode catalysts of Li—O_2 / Na—O_2 batteries and provide a new insight into the catalyst design by surface modification [11]. Cheng et al. [29] proposed a pre-self-assembled strategy to prepare controllable B—N coordinated active sites anchored on carbon supports as an efficient electrocatalyst for ORR using DFT calculations, their superior ORR performance is attributed to the intrinsically high activity of the B—N coordinated active sites, which is confirmed through the analysis of ECSA [29]. Yin et al. [36] develop a Li-Ni-Cu co-substituted $Na_{0.67}Li_{0.1}(Mn_{0.7}Ni_{0.2}Cu_{0.1})_{0.9}O_2$ (NLMNC) sample. They carried out DFT calculations to reveal the reaction mechanism of NLMNC. Besides, the DFT results showed that the anionic redox reaction occurs near the Mn ions. In contrast, the Ni ions are stable, and their results lead the way for practical applications of layered oxides in sodium-ion batteries (SIBs) [36]. Wang et al. [31] carried out the first-principles calculations to investigate WN MXenes including the pristine $W_{n+1}N_n$ and oxygen–functionalized $W_{n+1}N_nO_2$ (n = 1,2, and 3), as the potential cathode catalyst for Li-air batteries, their calculations suggest that $W_{n+1}N_n$ and $W_{n+1}N_nO_2$ exhibit good electrical conductiv- ities. The O-terminated W_2NO_2 MXene not only has high electrical conductivity but also exhibits ultra-low ORR, OER and total over- potentials (0.12, 0.17 and 0.29 V) indicating its great potential as cathode catalyst in Li—O_2 batteries [31]. Peng et al. [37] prepared a reversible and high-rate Li-air battery using nanoporous gold electrode (NPG) as the cathode and dimethyl sulfoxide (DMSO) as the electrolyte, which were able to achieve a capacity retention of 95 % after 100 cycles. Chen et al. [35] developed a two-step oxidation method by a weak oxidation treatment using H_2O_2 firstly and selectively adjusting the ratio of phenol and carbonyl/quinone. Their results suggested that the topo- logical defects from removing phenol, carbonyl/quinone is the key to enhancing the ORR activity of MWCNTs [35]. Kim et al. [38] disclosed that the discharge capacity was boosted with the increase of porosity and improving the texture of the carbon cathode [38]. In this work, an electrochemical catalytic model for a cathode for Li—O_2 batteries to simulate the ORR/OER during discharging/charging process is devel- oped. We provide theoretical guidance for the design of 2D layer cath- ode catalyst for Li—O_2 batteries, studying the electrocatalytic process of single layer of γ-Graphyne and its functionalized structures, only considering the intrinsic properties of the electrocatalyst. It is well known that Graphyne is an excellent carbon allotrope of recent decades with *sp* and sp^2 hybridized carbon atoms [39]. In this work γ-Graphyne is selected due to its versatile properties, for example: structural, elec- tronic, mechanical, electronic, pore size, surface area (surface area for γ-Graphyne ~3440 m^2/g against surface area for Graphene ~2630 m^2/g), and thermal transport [40–42]. Besides, Graphyne is studied due to its catalyst behavior in carbon materials and is used for many novel applications, for example: Pristine Graphyne and Cu-doped Graphyne have been theoretically proposed as potential nanocarriers for cisplatin anticancer drug [43]. Pristine γ-Graphyne and B-doped γ-Graphyne have been theoretically proposed as potential material for hydrogen storage [44]. Graphyne is also used to design a highly sensitive gas sensor by studying the interaction of boron-halogenated systems on pristine Graphyne [45].

2. Methodology

γ-Graphyne is used as the main surface for a cathode in a Li—O_2 battery. The building process of γ-Graphyne is carried out using super- position of cells (supercell is built by the superposition of 2 × 2 unit cells), this structure contains 48 carbon atoms, the N-doped is developed on γ-Graphyne. All the calculations in this work are performed using Biovia Material Studio Dmol³ [46,47]. Spin-polarized DFT calculations are carried out using the exchange–correlation interaction between electrons described by the generalized gradient approximation (GGA) with the Perdew-Burke-Ernzerhof (PBE) [46,47]. The effect of weak Van der Waals (vdW) interactions was calculated using the empirical correction scheme of the Grimme DFT-D correction method for periodic systems. Besides, the valence electrons are 2s for Li and 2s2p for C and N. A double numerical basis was chosen paired with polarization functions (DNP) in all calculations to get high accuracy calculations. The threshold value of convergence tolerance for energy, maximum force and maximum displacement was set to 1.0×10^{-5} Ha, 0.002 Ha/Å, and 0.002 Å, respectively. Finally, for the Partial Density of states (PDOS) the Monkhorst-Pack grid is set as follows: a = 2: b = 2; c = 1. The Li_2O_2

(F

oppl structure) and Li_2O (antifluorite structure) structures used in this work are the typical structures reported in Li-air batteries studies, to

have standard frames. Free energy for all the structures is calculated including phonon contributions to entropy and vibrational frequencies. The formation energies of each functional group are calculated to evaluate the feasibility of surface functionalization.

The elementary step of the ORR and OER involves ion-electron pairs of ($Li^+ + e^-$). Unfortunately, it is difficult to calculate directly using DFT methods because it involves complex situations such as solution envi- ronments, solvation ions, etc. The chemical potential of $\mu(Li^+ + e^-)$ is determined by $\mu(Li) + eU$ where $\mu(Li)$ is the chemical potential of Li and eU is the potential of an electron. Here, it is assumed that the barriers between the steps are sufficiently small, so there is no additional kinetic limitation on current onsets at a measurable level.

To perform the theoretical study on cathode catalysts for Li—O_2 batteries, it is necessary to know that the performance of a Li-air battery is affected by the products generated at the cathode during charge-discharge processes. The primary discharge product at the cathode is lithium peroxide (Li_2O_2) with a small portion of lithium oxide (Li_2O). The discharge reactions of Li-air batteries with Li_2O_2 as the product can be described by the following equations.

$$Li \leftrightarrow Li^+ + e^- \quad \text{(Anode oxidation)}$$
$$O_2 + 2Li^+ + 2e^- \leftrightarrow Li_2O_2 \quad \text{(Cathode oxygen reduction)}$$
$$2Li + O_2 \leftrightarrow Li_2O_2 \quad \text{(Overall battery reaction)} \qquad (1)$$

The discharge reactions for Li_2O and the overall reaction can be expressed as follows:

$$4Li + O_2 \leftrightarrow 2Li_2O \qquad (2)$$

If Li_2O is the product, reaction (2) is not desirable because it is not very reversible, being not fully rechargeable back to Li and O_2 [48]. The performance of a Li-air battery is affected by the actual products generated at the cathode during charge-discharge processes.

3. Results and discussion

In the present study, we explored two electrochemical catalytic models (γ-Graphyne and N-γ-Graphyne) for a cathode for Li—O_2 batte- ries, the influence of the dopant atom and the doping site. Compare formation energies for reaction products ($Li_2O_{2(s)}$, and $Li_2O_{(s)}$) to eval- uate the cathode performance for Li—O_2 batteries.

3.1. Bulk Li metal and Li oxides

First, the geometry and energies for bulk reaction products are calculated. The lattice parameter for the bulk Li metal, Li_2O_2 F^{oppl} structure (space group P6) [49], and Li_2O antifluorite structure (Fm3m). [50] Are displayed in Table 1. Lattice constants for bulk Li_2O_2 and Li_2O are calculated, and their values are a = b = 3.180, c = 7.703 Å, and 4.658 Å, respectively. Calculated values are in good agreement with the experimental values reported in Ref. [49], (a = b = 3.142, c = 7.65 Å and 4.619 Å) respectively. Fig. 1 shows relaxed structures for bulk $Li_{(s)}$, $Li_2O_{2(s)}$, and $Li_2O_{(s)}$.

The standard free formation energies ΔG_f° (G_f° values include phonon contributions to entropy: $G = E + E^{ZPE} + \Delta U(T) - TS(T)$) for bulk lithium oxides are calculated with the following Eq. [51]:

$$\Delta G_f^\circ = G^\circ_{Li_xO_y(s)} - xG^\circ_{Li_x} - \frac{y}{2}G^\circ_{O_2(g)} \qquad (3)$$

where E is the DFT total energy, and ΔU is the change in internal energy from 0 K to T. E^{ZPE}, ΔU *and* S are calculated from the vibrational fre- quencies associated with the normal modes of the adsorbed species calculated in the harmonic approximation. Calculated values for: Lattice constants, formation energies and vibrational frequencies are summa- rized in Table 1.

Many studies report that GGA functionals overestimate the O—O bond energy in O_2 [51,54]. For this reason, is combined the total en- ergies of H_2O ($\Delta H^\circ_{f,H_2O} = -241.83$ *kJ/mol*), reported in Ref [55]. The H_2 was calculated using the DFT calculation, as follows:

$$G_{O_2} = 2E_{H_2O} - 2E_{H_2} - 2\Delta H^\circ_{f,H_2O} \qquad (4)$$

Calculated values of the formation energies obtained in this work are 1.537, −5.586 and − 5.406 eV for the Li bulk, Li_2O_2 bulk and Li_2O bulk, respectively. These values are in good agreement with the results re- ported in Ref. [52] and Ref. [53]. Once the energies and lattice constant for bulk Li metal and Li oxides (reaction products) are calculated, the next step is to build the 2D surface, which will be used as cathode cat- alysts for Li—O_2 batteries.

3.2. Cathode catalysts surfaces: γ-Graphyne and N-γ-Graphyne

This study uses pristine γ-Graphyne and N-doped γ-Graphyne as cathode catalyst surfaces for Li—O_2 batteries. The functionalized structure is an N-doped γ-Graphyne, due to many studies indicate that N-doped carbon-based materials exhibit superior electrocatalytic activity (presence of a dopant atom in the unit cell induced energy levels at or close to the Fermi level and converted the semiconductor Graphyne into metallic in nature) [56]. The γ-Graphyne has two kinds of hollows. One type of hollow is formed for a regular hexagon ring (R1) and the second is formed for an irregular hexagon ring (R2). R1 and R2 are shown in Fig. 2. The average bond lengths in R1 and R2 are 1.418 Å and 1.370 Å respectively. The unexpected variations in carbon bond lengths are ac- cording to the lengths reported by Peng et al. [57]. Peng et al. reported the existence of three distinct categories of carbon bonds within

Table 1
Symmetry, lattice constants and energetics for bulk Li $_{(s)}$ metal and $Li_2O_{2\,(s)}$ and Li_2O $_{(s)}$ oxides.

	Symmetry	Lattice constants (Å)		Formation energies (eV)		Vibrational frequencies	
		Experimental	Calculated	Experimental	Calculated	Experimental	Calculated
Li $_{(s)}$	Bcc (IM-3 M)	3.49 [49]	3.509 Å	1.63 [52]	−1.537	–	–
$Li_2O_{2\,(s)}$	Foppl (P63)	a = b = 3.142, c = 7.65 [49]	a = b = 3.180, c = 7.703	−5.918 [53]	−5.586	795 [51]	767.17
$(Li_2O_2)_{2\,(s)}$	Foppl (P63)	a = b = 3.142, c = 7.65 [49]	a = b = 3.180, c = 7.703	–	−11.159	–	767.17
$Li_2O_{(s)}$	Antifluorite (FM-3 M)	4.619 [50]	4.658	−5.826 [53]	−5.406	523 [51]	547.05
$(Li_2O)_{2\,(s)}$	Antifluorite (FM-3 M)	4.619 [50]	4.658	–	−11.045	–	547.05

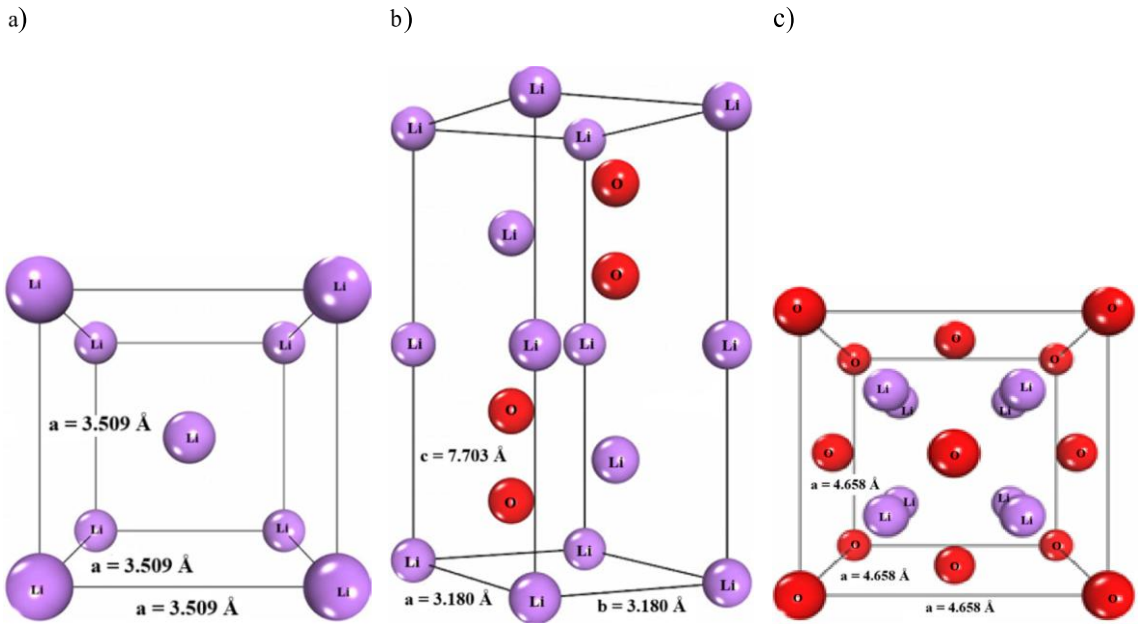

Fig. 1. Relaxed structures for: a) bulk Li $_{(s)}$ bcc; b) $Li_2O_{2\,(s)}$; c) $Li_2O_{(s)}$. blue and red spheres represent Li and O atoms respectively. (For interpretation of the references to colour in this figure legend, the reader is referred to the web version of this article.)

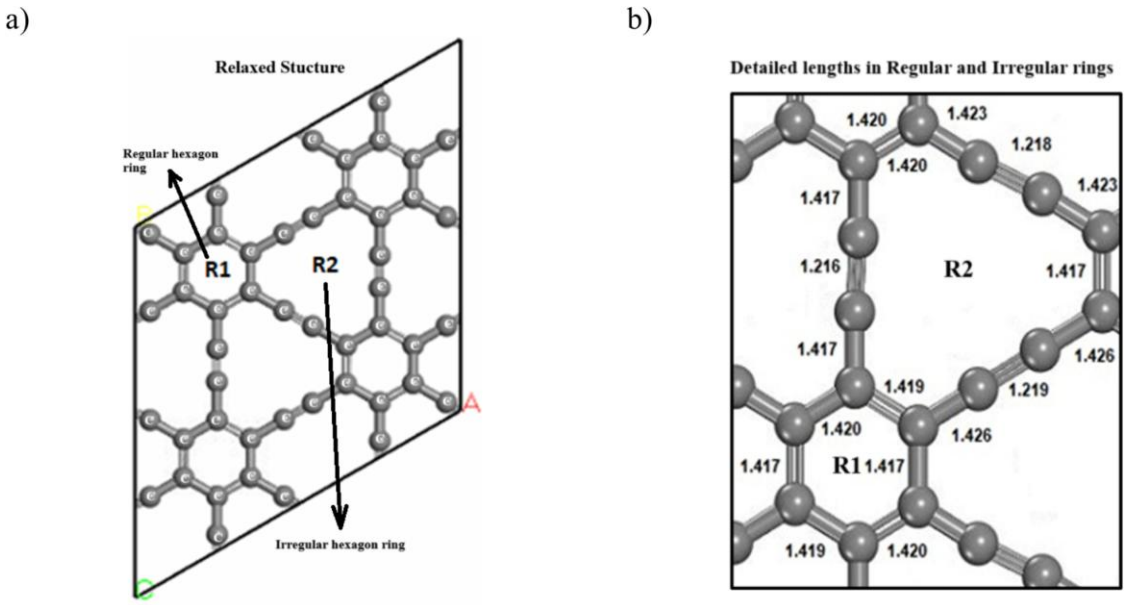

Fig. 2. a) Pristine 2 × 2 γ-Graphyne, b) detailed lengths bonds in γ-Graphyne. The Gray spheres represent carbon atoms.

Graphyne: C(sp^2) — C(sp^2) for the central aromatic ring (1.43 Å), C(sp^2) — C(sp) connecting the adjacent *C* = *C*, and *C* ≡ *C* bonds (1.41 Å). Finally, C (sp) — C(sp) for the linked triple bonds (1.22 Å) [57]. γ-Graphyne, as a cathode catalyst for Li—O_2 batteries, was selected among other kinds of Graphyne due to its high stability and porous size. The calculated formation energy for γ-Graphyne is 8.074 eV.

N-doped enhances the electrocatalytic activity for Graphyne [56]. Furthermore, the activation energy barrier for O_2 dissociation is suffi- ciently low at the N-doped defective site in graphene structures [58,59]. Calculations are performed to select the most effective site for the Mulliken charge and geometry optimization. The calculations reveal that the N-doped at sites S1 is thermodynamically the most stable. The N-doped γ-Graphyne is illustrated in Fig. 3. Fig. 3a shows the pristine γ-Graphyne and sites S1 (N-doped sites). Fig. 3b shows the relaxed

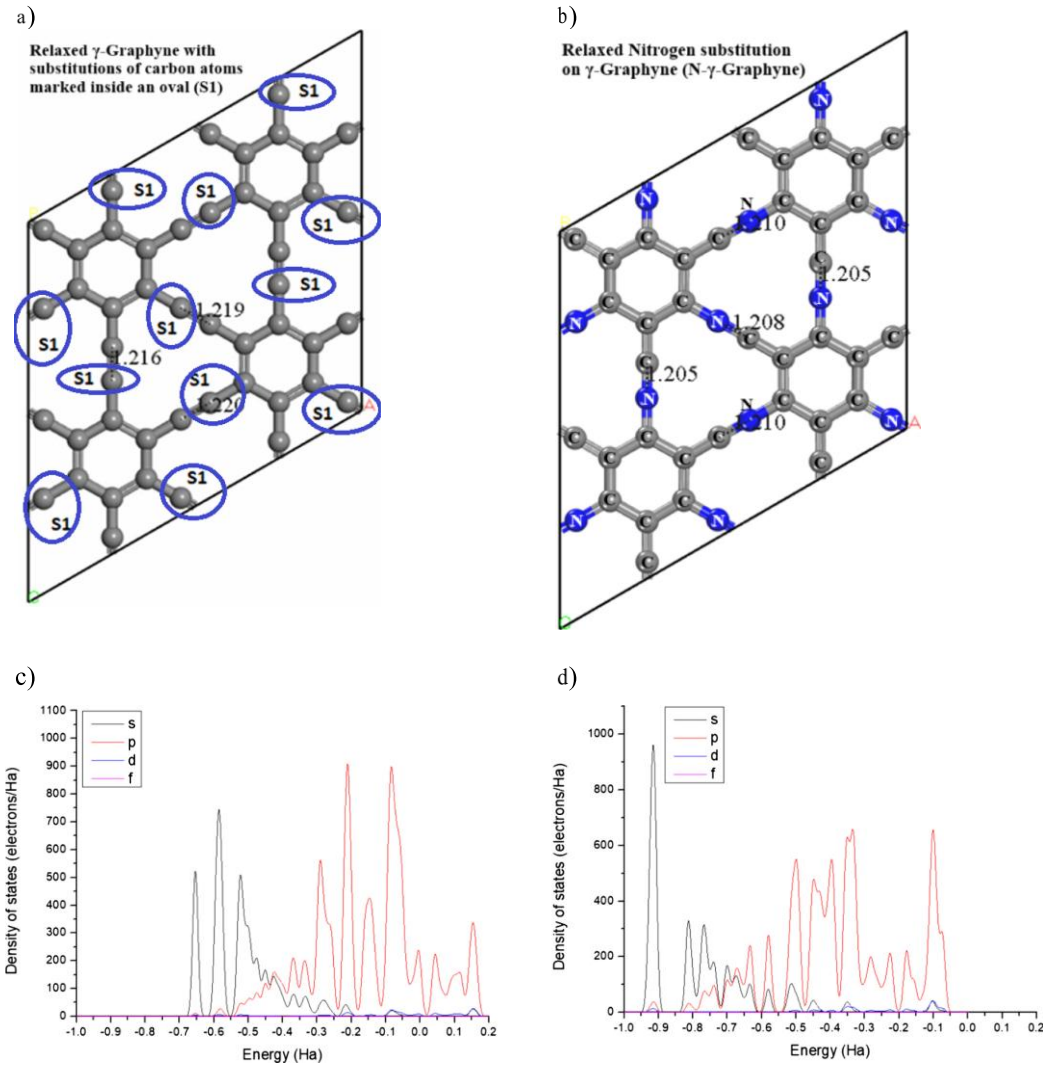

Fig. 3. a) Pristine 2 × 2 γ-Graphyne, sites S1 indicate that a nitrogen atom will replace carbon atoms. b) relaxed structure of N-doped on γ-Graphyne (N-γ-Graphyne). The gray spheres represent carbon atoms, and blue spheres represent nitrogen atoms. c) PDOS for pristine γ-Graphyne d) PDOS for pristine N-γ-Graphyne. (For interpretation of the references to colour in this figure legend, the reader is referred to the web version of this article.)

structure of N-doped γ-Graphyne (N-γ-Graphyne), with a calculated formation energy of 7.259 eV. γ-Graphyne, and N-γ-Graphyne configurations of cathode catalyst surfaces in a lithium battery have been theoretically simulated. Moreover, the calculated formation energy for γ-Graphyne (8.074 eV) aligns with the results reported by Kim et al. (7.95 eV/atom) [42]. These results indicate the reliability of our computational calculations.

Fig. 3 shows the structural configurations of γ-Graphyne and N- γ-Graphyne, which are two-dimensional structures. In γ-Graphyne $C \equiv C$ the average bond length is 1.218 Å, and in N-γ-Graphyne $C - N$ the average bond length is 1.207 Å, this indicates that while γ-Graphyne and N-γ-Graphyne exhibit close proximity in terms of bond lengths, the geometric configuration of each structure is distinct.

To provide a more detailed analysis of the electronic structure changes in N-doped structure, the partial density of states (PDOS) was calculated, which are plotted in Figure 3c and 3d for pristine γ-Graphyne and N- γ-Graphyne respectively. In pristine γ-Graphyne Figure 3c, the Fermi level (E = 0) aligns with a certain density of states. In contrast, in N-γ-Graphyne Figure 3d, the PDOS shifts notably in the occupied region (HOMO). The downward shift of the Fermi level suggests an increase in electron density in occupied states, which is characteristic of nitrogen doping in carbon-based materials [60]. The PDOS for N-γ-Graphyne shows additional states in the energy range of -0.9 Ha to -0.5 Ha, which are absent in the undoped γ-Graphyne. This implies that nitrogen atoms introduce localized electronic states, modifying the band structure [61]. Since nitrogen has one extra valence electron compared to carbon, it acts as an electron donor. The increase in occupied electron density suggests that certain material regions become electron-rich, enhancing their electrocatalytic potential. Use charge density maps or density of states (DOS) plots to explain how active sites are formed and how they contribute to reduced formation energy.

The next step is developing the calculation to give information about

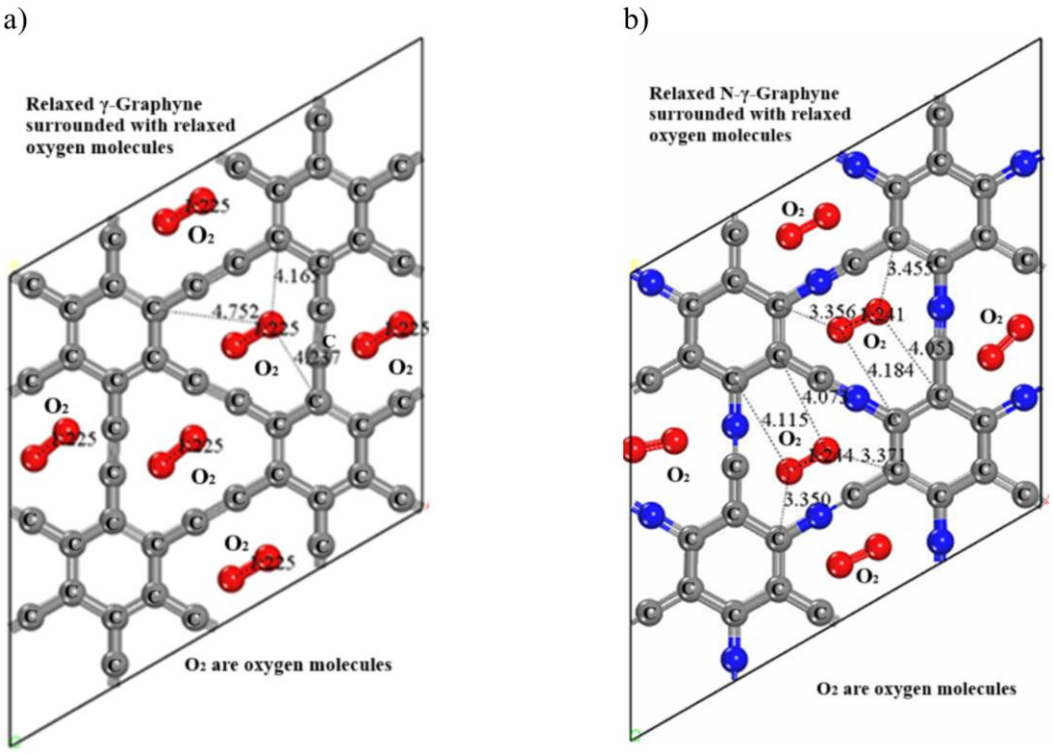

Fig. 4. a) Relaxed structure for pristine 2 × 2 γ-Graphyne rounded by 12 oxygen molecules. b) Relaxed structure for N-γ-Graphyne rounded by 12 oxygen molecules. The gray spheres represent carbon atoms, blue spheres represent nitrogen atoms, red spheres represent oxygen atoms.

the bi-functional catalyst of γ-Graphyne & N-γ-Graphyne.

3.3. γ-Graphyne and N-γ-Graphyne within an oxygen environment

In the practical context of Li-air batteries, avoiding the reaction between O_2 molecules and the cathode component during periods of static operation (when the battery is not in the charging or discharging pro- cesses) is essential. In other words, it is necessary to ensure that the adsorption phenomenon, whereby O_2 molecules attach themselves to the surface of γ-Graphyne or N-γ-Graphyne, does not occur when the battery remains in a state of inactivity.

To evaluate the performance of γ-Graphyne or N-γ-Graphyne in an oxygen-rich environment. The study of γ-Graphyne and N-γ-Graphyne in the presence of O_2 is conducted Fig. 4 shows relaxed structures for γ-Graphyne and N-γ-Graphyne, with O_2 molecules surrounding each cathode structure surface. The result indicates that the bond length of oxygen molecules interacting with cathode surfaces remains unaltered compared to that of an isolated oxygen molecule (1.225 Å). The bond length for isolated oxygen molecules aligns with the values reported by Huber et al. [62] (1.205 Å), serving as the initial validation that the oxygen molecules are weakly adsorbed on γ-Graphyne and N-γ-Graph- yne surfaces. The average binding energy and binding adsorption energy are calculated to get a comprehensive validation of the adsorption process of the O_2 molecules on γ-Graphyne and N-γ-Graphyne struc- tures. For the case of γ-Graphyne the average binding energy (E_{ave}) of the nth O_2 molecule adsorbed on γ-Graphyne is calculated following next equation.

$$E_{ave} = \frac{[E(\gamma - Graphyne) + n\,E(O_2) - E(\gamma - Graphyne + n\,O_2)]}{n} \quad (5)$$

where $E(\gamma - Graphyne)$ is the total energy of γ-Graphyne, $E(O_2)$ is the energy of an isolated O_2 molecule, and finally $E(\gamma - Graphyne + n\ O_2)$ is the total energy of n O_2 molecules adsorbed on γ-Graphyne. Binding adsorption energy (E_{ad}) of the nth O_2 molecule adsorbed on γ -Graphyne is calculated following the next equation.

$$E_{ad} = E(\gamma - Graphyne + (n-1)O_2) + E(O_2) - E(\gamma - Graphyne + nO_2) \quad (6)$$

where $E(\gamma - Graphyne + (n-1)O_2)$ is the total energy of the $(n-1)$ O_2 molecules adsorbed on γ -Graphyne, finally n is the quantity of O_2 molecules adsorbed on γ -Graphyne. The E_{ave} and E_{ad} calculated values are summarized in Table 2.

For the case of N-γ-Graphyne the average binding energy (E_{ave}) of nth O_2 molecule adsorbed on N-γ-Graphyne is calculated following the next equation.

Table 2

E_{ave} and E_{ad} values for γ-Graphyne-nO_2 structure. n values are between 1 and 8.

System	Average binding energy (eV)	Binding adsorption energy (eV)
γ-Graphyne-O_2	0.0819	0.0820
γ-Graphyne-2O_2	0.0763	0.0706
γ-Graphyne-3O_2	0.0757	0.0768
γ-Graphyne-4O_2	0.0761	0.0773
γ-Graphyne-5O_2	0.0755	0.0732
γ-Graphyne-6O_2	0.0755	0.0750
γ-Graphyne-7O_2	0.0754	0.0749
γ-Graphyne-8O_2	0.0750	0.0749

Table 3

E_{ave} and E_{ad} values for N-γ-Graphyne-nO_2 structure. n values are between 1 and 8.

System	Average binding energy (eV)	Binding adsorption energy (eV)
N-γ-Graphyne-O_2	0.0790	0.1182
N-γ-Graphyne-$2O_2$	0.1187	0.1170
N-γ-Graphyne-$3O_2$	0.1187	0.1176
N-γ-Graphyne-$4O_2$	0.1185	0.1173
N-γ-Graphyne-$5O_2$	0.1189	0.1172
N-γ-Graphyne-$6O_2$	0.1185	0.1173
N-γ-Graphyne-$7O_2$	0.1190	0.1182
N-γ-Graphyne-$8O_2$	0.1187	0.1170

$$E_{ave} = \frac{[E(N-\gamma-Graphyne) + n\,E(O_2) - E(N-\gamma-Graphyne + n\,O_2)]}{n} \quad (7)$$

where $E(N-\gamma-Graphyne)$ is the total energy of N-γ-Graphyne, $E(O_2)$ is the energy of an isolated O_2 molecule, and finally $E(N-\gamma-Graphyne+n\,O_2)$ is the total energy of n O_2 molecules adsorbed on N-γ-Graphyne. Binding adsorption energy (E_{ad}) of the nth O_2 molecule adsorbed on N-γ -Graphyne is calculated following the next equation.

$$E_{ad} = E(N-\gamma-Graphyne+(n-1)O_2) + E(O_2) - E(N-\gamma-Graphyne+nO_2) \quad (8)$$

where $E(N-\gamma-Graphyne+(n-1)O_2)$ is the total energy of the $(n-1)$ O_2 molecule adsorbed on N-γ-Graphyne, finally n is the quantity of O_2 molecules adsorbed on γ-Graphyne. The E_{ave} and E_{ad} calculated values are summarized in Table 3.

Tables 2 and 3 corroborate the initial validation (oxygen molecules are weakly adsorbed on γ-Graphyne and N-γ-Graphyne surfaces). Oxy- gen molecules do not exhibit reaction behavior on the surfaces of γ-Graphyne and N-γ-Graphyne. The E_{ave} values for γ-Graphyne and N- γ-Graphyne structures are observed to be within the range of 0.0750–0.0819 eV and 0.1185–0.1190 eV respectively. The E_{ad} vales for γ-Graphyne and N-γ-Graphyne structures are further noted to be within the range of 0.0732–0.0820 eV and 0.1170–0.1182 eV respectively. The calculated E_{ave} and E_{ad} values for γ-Graphyne and N-γ-Graphyne surfaces are indicative of physisorption. Typical physisorption values range from 15 kJ/mol to 50 kJ/mol (0.155 to 0.518 eV). The conventional values associated with physisorption are within 15 kJ/mol to 50 kJ/mol (0.155 to 0.518 eV). Oxygen molecules are binding to the surfaces of γ-Graphyne and N-γ-Graphyne through relatively weak interactions, specifically van der Waals forces.

4. Evaluation of cathode catalysts surfaces activity

On the cathodic surface of Li—O_2 batteries, the ORR and OER occur during the discharging and charging process. This study considered three surface reaction steps grounded in experimental and theoretical findings (eqs. 1 and 2) to model the structural evolution. Initially, during the discharge process O_2 on cathodic surfaces (γ-Graphyne and N- γ-Graphyne) reacts with ($Li^+ + e^-$) to yield an adsorbed LiO_2. The subsequent phase involves the reaction of the adsorbed LiO_2 with ($Li^+ + e^-$) to produce Li_2O_2, which further reacts with ($Li^+ + e^-$) to generate the final discharge product $(Li_2O_2)_2$. The OER represents the inverse mechanism of the ORR. During the charging phase, the adsorbed species $(Li_2O_2)_2$ undergoes a gradual delithiation process resulting in the for- mation of O_2. Finally, O_2 is liberated from cathodic surfaces (γ-Graphyne and N-γ-Graphyne), concluding the charging process.

Table 4

ΔG_f^0 Calculated formation energies associated with the formation of Li_2O, Li_2O_2, $(Li_2O)_2$, and $(Li_2O_2)_2$ structures adsorbed on γ-Graphyne and N-γ- Graphyne surfaces.

	Calculated formation energies ΔG_f^0 (eV)	
Reaction product	On γ -Graphyne	On N-γ -Graphyne
Li_2O	5.293	5.019
$(Li_2O)_2$	10.863	9.542
Li_2O_2	5.475	5.138
$(Li_2O_2)_2$	11.041	10.947

To assess the relative ease or difficulty associated with the formation of Li_2O, Li_2O_2, $(Li_2O)_2$, and $(Li_2O_2)_2$ structures adsorbed on γ-Graphyne and *N*-γ- Graphyne surfaces, calculation of formation energies of reac- tion products upon cathode surfaces (on γ-Graphyne and *N*-γ- Graphyne) is conducted using the following equation:

$$\Delta G_f^0 = G^0_{(Li_xO_y)_z-X-\gamma-Graphyne} - G^0_{(Li_xO_y)_z} - G^0_{X-\gamma-Graphyne} \quad (9)$$

where $G^0_{(Li_xO_y)_zX-\gamma-Graphyne}$ denotes the formation energy associated with the cathode surfaces (for the expression X-γ-Graphyne it is to be noted that X does not possess a value for the γ-Graphyne surface, whereas X is denoted as N for N-γ- Graphyne surface) and the reactions products (Lithium oxides), $G^0_{(Li_xO_y)_z}$ is the formation energy of isolated reactions products (Li_2O, Li_2O_2, $(Li_2O)_2$, or $(Li_2O_2)_2$). $G^0_{(Li_xO_y)_zX-\gamma-Graphyne}$ is the formation energy of isolated cathodic surfaces (γ-Graphyne or N- γ-Graphyne). All calculated formation energies are summarized in Table 4.

4.1. Reaction products formation process upon the cathode catalysts surfaces

Fig. 5 shows the relaxed configuration regarding the formation of reaction products upon cathode surfaces in a Li-air battery, where the cathode is γ-Graphyne. Figs. 5a), 5b), 5c), 5d) delineate the formation of Li_2O, Li_2O_2, $(Li_2O)_2$, and $(Li_2O_2)_2$ respectively upon γ-Graphyne surface. Notably, the reaction product (Lithium oxides) positioned on γ-Graph- yne are derived from the bulk structure depicted in Fig. 1. The reaction products formed within Li-air batteries are theoretically situated on the bigger pores of γ-Graphyne surface.

A theoretical study of the N-doped cathode catalyst surface (*N*-γ-the Graphyne) was conducted on Li-air batteries. Relaxed configuration about the cathode catalyst formed for *N*-γ-the Graphyne surface was performed. Relaxed configuration regarding the formation of reaction products upon cathode surfaces in a Li-air battery, where the cathode is N-γ-Graphyne. Figs. 6a), 6b), 6c), 6d) delineate the formation of Li_2O, Li_2O_2, $(Li_2O)_2$, and $(Li_2O_2)_2$ respectively upon N-γ-Graphyne surface. Also, it is essential to note that the reaction products (Lithium oxides) positioned on N-γ-Graphyne are derived from the bulk structure depic- ted in Fig. 1. The reaction products formed within Li-air batteries are theoretically situated on the bigger pores of N-γ-Graphyne surface.

4.2. Performance cathode catalysts surfaces

In this last section, a comprehensive analysis of the performance of cathode catalyst surfaces is developed. In section 3.1 (Bulk Li metal and Li oxides), the calculated values of the formation energies for the Li bulk, Li_2O bulk, $(Li_2O)_2$ bulk, Li_2O_2 bulk, $(Li_2O_2)_2$ bulk, are presented 5.406, 11.045, 5.586, and 11.159 eV respectively. These values demonstrate commendable concordance with the results reported in Ref. [52] and Ref. [53] (see Table 1). While in section 4 (Evaluation of Cathode cat- alysts surfaces activity) the formation energies of reaction products upon

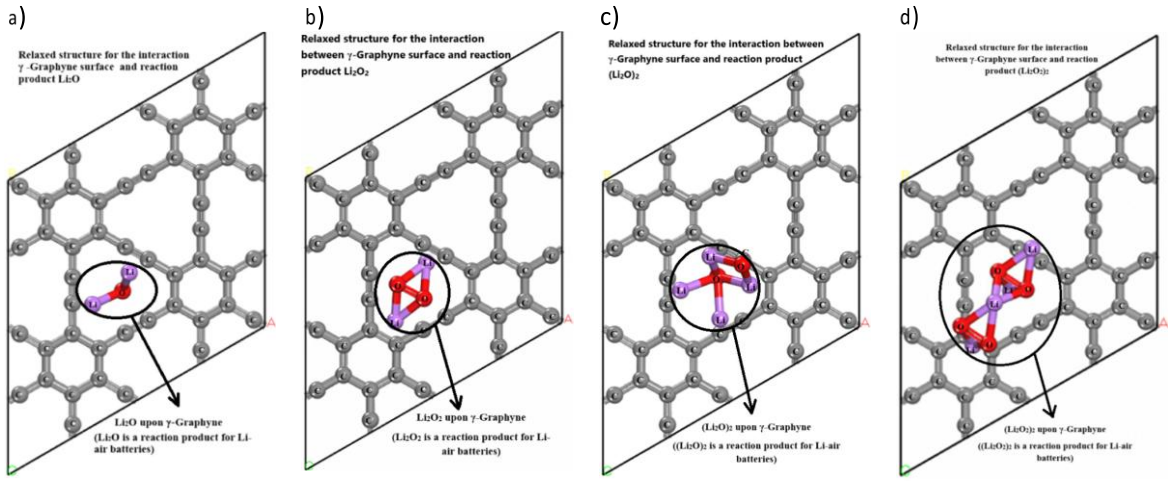

Fig. 5. Relaxed structure for the formation of reaction products on γ-Graphyne surface. 5a), 5b), 5c), 5d) show the formation for Li_2O, Li_2O_2, $(Li_2O)_2$, $(Li_2O_2)_2$ respectively on γ -Graphyne. The gray spheres represent carbon atoms, red spheres represent oxygen atoms, and purple spheres represent lithium atoms. (For interpretation of the references to colour in this figure legend, the reader is referred to the web version of this article.)

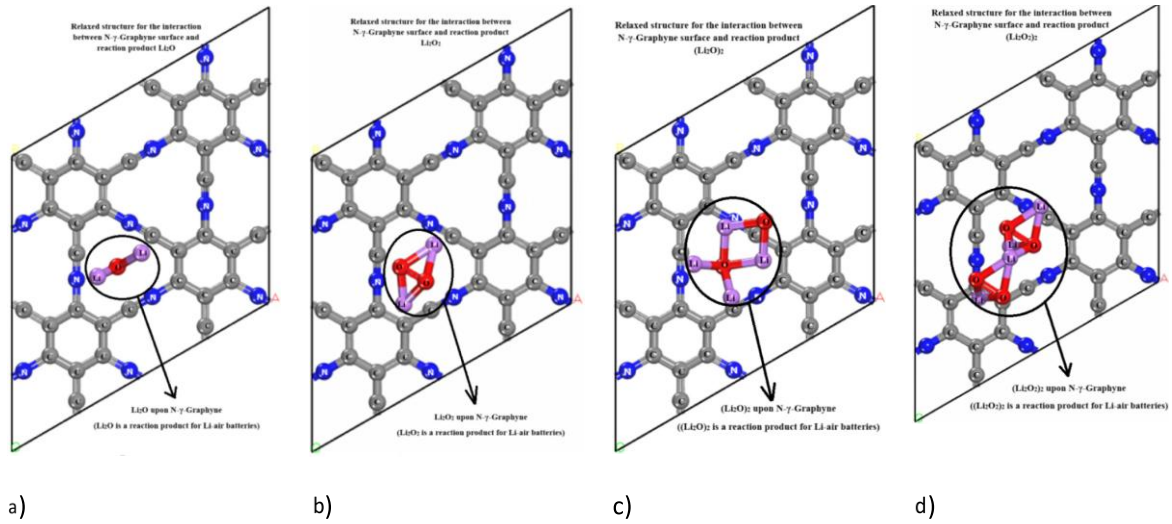

Fig. 6. Relaxed structure for the formation of reaction products on N-γ-Graphyne. 5a), 5b), 5c), 5d) show the formation for Li_2O, Li_2O_2, $(Li_2O)_2$, $(Li_2O_2)_2$ respectively on N-γ-Graphyne. The gray spheres represent Carbon atoms, red spheres represent Oxygen atoms, the blue spheres represent nitrogen atoms, and purple spheres represent lithium atoms. (For interpretation of the references to colour in this figure legend, the reader is referred to the web version of this article.)

Table 5
ΔG_f Reported formation energies associated with the formation of Li_2O, Li_2O_2. structures adsorbed on γ-Graphyne and N-γ- Graphyne surfaces.

	Formation energies (eV)		Calculated formation energies ΔG_f (eV)		
Column A	Column B	Column C	Column D	Column E	Column F
Reaction product	Exp. bulk	Ref. [63]	Isolated bulk	On γ -Graphyne	On N-γ - Graphyne
Li_2O	5.826	5.51	5.406	5.293	5.019
$(Li_2O)_2$	–	–	11.045	10.863	9.542
Li_2O_2	5.918	5.63	5.586	5.475	5.138
$(Li_2O_2)_2$	–	–	11.159	11.041	10.947

ref. [53]

cathode surfaces (on γ-Graphyne and *N*-γ-Graphyne) are presented as 5.293, 10.863, 5.475, 11.041 eV for Li_2O, $(Li_2O)_2$, Li_2O_2, $(Li_2O_2)_2$ respectively for γ-Graphyne surface. And take values as 5.019, 9.542, 5.138, 10.947 eV for Li_2O, $(Li_2O)_2$, Li_2O_2, and $(Li_2O_2)_2$ respectively for N-γ-Graphyne surface. Finally, Yun et al. [63] report the formation en- ergies of reaction products on graphitic N doping surface as 5.51 and 5.63 eV for Li_2O, Li_2O_2, respectively. All these results are summarized in Table 5.

With the data presented in Table 5, a comprehensive analysis of the performance of cathode catalyst surfaces can be conducted. Column B exhibits the highest values for the formation energy for Li_2O, and Li_2O_2 (5.51, and 5.63 eV respectively). Yun et al. [63] (Column C) reports a reduction in formation energies for the reaction products Li_2O, and Li_2O_2 with their respective values being 5.51 and 5.63 eV, the cathode

studied by Yun et al.is a Graphitic N-doped surface. The diminution of formation energies signifies a convenience related to the formation of Li_2O and Li_2O_2. Consequently, the generation of reaction products Li_2O and Li_2O_2 on the Graphitic N-doped surface examined by Yun et al. [63] is more favorable than the formation of these identical products in bulk isolated. In alignment with the preceding concept, column D delineates the formation energies about bulk configurations of the reaction prod- ucts (Li_2O, $(Li_2O)_2$, Li_2O_2, $(Li_2O_2)_2$). Columns E and F elucidate the re- action energies associated with the identical reaction products while varying the cathode catalytic material. In column E, the reaction prod- ucts are formed on γ-Graphyne, whereas in column F, the reaction products are formed on N-γ-Graphyne. Based on the preceding analysis, it may be inferred that the catalytic cathodic surface N-γ-Graphyne significantly facilitates the formation of reaction products, thereby endowing N-γ-Graphyne with a pronounced catalytic efficacy regarding the reaction products. Furthermore, the γ-Graphyne surface contributes to the formation of reaction products compared to the energy associated with bulk products. Consequently, it can be inferred that, within the scope of this investigation, N-γ-Graphyne emerges as the most effective catalyst for synthesizing the reaction products, yielding enhancements on formation energies compared to γ-Graphyne.

In other words, this research provides insights into the feasibility of developing a cathode catalyst for lithium-air batteries utilizing Graph- yne. This provides a significant theoretical foundation for advancing a practical cathode catalyst in lithium-air batteries.

5. Conclusions

In this manuscript, we conduct an extensive investigation focused on evaluating the improvement in the performance of cathode catalysts employed in Li-air batteries. We employed Density Functional Theory (DFT) using Biovia Material Studio Dmol³ to calculate the formation energies. To validate the calculation, the calculated formation energy for γ-Graphyne and N-γ-Graphyne are 8.074 eV and 7.259 eV, respec- tively. Those results indicate the reliability of our computational cal- culations. The performance of catalyst cathode materials is evaluated using a base consisting of 2 × 2 cell γ-Graphyne, the 2 × 2 cell N- γ-Graphyne, additionally employing optimization calculations and for- mation energy assessment. The adsorption energies for oxygen mole- cules on the cathode materials are computed utilizing adsorption energy equations. The findings illustrate that oxygen molecules exhibit considerable inertness, rendering them unlikely to react with a catalyst cathode medium; this outcome is anticipated, as it would be inefficient for the cathode to engage with isolated oxygen molecules. Ultimately, the reaction products generated within Li-air batteries are examined on γ-Graphyne and N-γ-Graphyne; it is well established that the catalyst cathode must function as a catalyst to facilitate the lithiation process, which occurs when a Li^+ ion interacts with oxygen molecules, with the cathode supporting and catalyzing this reaction. The results demon- strate that the cathode based on γ-Graphyne enhances the formation energies; however, the cathode based on N-γ-Graphyne emerges as the superior alternative for application in Li-air batteries, resulting in an approximate reduction of 15 % in formation energies for the reaction products Li_2O, Li_2O_2, $(Li_2O)_2$, $(Li_2O_2)_2$ This theoretically suggests the feasibility of developing a cathode catalyst for Li-air batteries utilizing Graphyne, which may reduce costs associated with the mass production of Li-air batteries.

CRediT authorship contribution statement

Armando Vera-Garcia: Writing – review & editing, Writing – orig- inal draft, Methodology, Investigation, Formal analysis, Data curation, Conceptualization. **J.H. Pacheco-Sanchez:** Validation, Supervision, Resources, Project administration, Investigation, Funding acquisition, Formal analysis, Conceptualization. **Frank J. Isidro-Ortega:** Validation, Supervision, Methodology, Formal analysis. **Abraham Gonz**

ález-Ruíz: Writing – review & editing, Visualization, Validation, Methodology, Investigation. **J.S. Arellano:** Writing – review & editing, Visualization, Validation, Supervision.

Declaration of competing interest

The authors declare the following financial interests/personal re- lationships which may be considered as potential competing interests: Armando Vera reports financial support, administrative support, and equipment, drugs, or supplies were provided by National Technology of Mexico. If there are other authors, they declare that they have no known competing financial interests or personal relationships that could have appeared to influence the work reported in this paper.

Acknowledgements

We thank Instituto Tecnologico de Toluca (ITTOL) for allowing us the facilities to develop the project. In addition, and finally, we thank the Consejo Nacional de Humanidades, Ciencias y Tecnologías (Conahcyt) for a grant awarded with number CVU 635564, thanks to all those mentioned, because without them.

Data availability

The authors do not have permission to share data.

References

[1] B. Richter, et al., How America Canlook Within to Achieve Energy Security Andreduce Global Warming vol. 80, 4, Dec. 2008, pp. S1–S109, https://doi.org/10.1103/RevModPhys.80.S1.

[2] C. McGlade, P. Ekins, The geographical distribution of fossil fuels unused when limiting global warming to 2 C, Nature vol. 517 (7533) (Jan. 2015) 187–190, https://doi.org/10.1038/nature14016.

[3] D. Welsby, J. Price, S. Pye, P. Ekins, Unextractable fossil fuels in a 1.5 C world, Nature vol. 597 (7875) (Sep. 2021) 230–234, https://doi.org/10.1038/s41586- 021-03821-8.

[4] H. Kumar, S. Rajan, A.K. Shukla, Development of lithium-ion batteries from micro-structured to nanostructured materials: its issues and challenges, Sci. Prog. vol. 95 (3) (2012) 283–314, https://doi.org/10.3184/003685012X13421145651372.

[5] H, K, V, L, F, A, A, What have we learned by multiscale models on improving the cathode storage capacity of Li-air batteries recent advances and remaining challenges, Renew. Sust. Energ. Rev. vol. 154 (Oct. 2022), https://doi.org/10.1016/j.rser.2021.111849.

[6] B. Zhu, et al., Semiconductor Electrochemistry for Clean Energy Conversion and Storage, Dec. 01, Springer, 2021, https://doi.org/10.1007/s41918-021-00112-8.

[7] B. Dunn, H. Kamath, J.-M. Tarascon, Electrical Energy Storage for the Grid: A Battery of Choices, Science (2011), https://doi.org/10.1126/science.1212741.

[8] J.-M. Tarascon, M. Armand, Issues and Challenges Facing Rechargeable Lithium Batteries [Online]. Available: www.nature.com, 2001.

[9] V. Ramadesigan, P.W.C. Northrop, S. De, S. Santhanagopalan, R.D. Braatz, V. R. Subramanian, Modeling and simulation of Lithium-ion batteries from a systems engineering perspective, J. Electrochem. Soc. vol. 159 (3) (2012) R31–R45, https://doi.org/10.1149/2.018203jes.

[10] K. Lingyu, et al., Sustainable regeneration of high-performance LiCoO2 from completely failed lithium-ion batteries, J. Colloid Interface Sci. vol. 640 (Jun. 2023), https://doi.org/10.1016/j.jcis.2023.03.021.

[11] W. Zhi-Hai and Y. Yang-Xin, "Theoretical study on catalytic performance of Ti2B monolayer as cathodes of Li-O2 and Na-O2 batteries promoted by surface functionalization," Appl. Surf. Sci., vol. 666, 160380.

[12] K.M. Abraham, Z. Jiang, A Polymer Electrolyte-Based Rechargeable lithium/Oxygen Battery, 1996.

[13] D. Wang, X. Mu, P. He, H. Zhou, Materials for Advanced Li-O2 Batteries: Explorations, Challenges and Prospects, Jun. 01, Elsevier B.V, 2019, https://doi.org/10.1016/j.mattod.2019.01.016.

[14] J.L. Shi, et al., Improving the structural stability of Li-rich cathode materials via reservation of cations in the Li-slab for Li-ion batteries, Nano Res. vol. 10 (12) (2017) 4201–4209, https://doi.org/10.1007/s12274-017-1489-3.

[15] D. Wu, et al., Metal-organic frameworks as cathode materials for Li-O2 batteries, Adv. Mater. vol. 26 (20) (2014) 3258–3262, https://doi.org/10.1002/ adma.201305492.

[16] J. Ren, N. Zhang, P. Liu, Li adsorption on nitrogen-substituted graphyne for hydrogen storage, Fuller. Nano. Carbon Nanostruct. vol. 29 (3) (2020) 212–217, https://doi.org/10.1080/1536383X.2020.1830066.

[17] D. Zhai, et al., Disproportionation in Li-O2 batteries based on a large surface area carbon cathode, J. Am. Chem. Soc. vol. 135 (41) (Oct. 2013) 15364–15372, https://doi.org/10.1021/ja403199d.

oppl, Die Kristallstrukturen der Alkaliperoxyde, ZAAC - J. Inorg. Gen. Chem. vol. 291 (1–4) (1957) 12–50, https://doi.org/10.1002/zaac.19572910104.

[50] J. Zemann, Crystal structures, 2 nd edition. Vol. 1 by R. W. G. Wyckoff, Acta Crystallogr. vol. 18 (1) (1965) 139, https://doi.org/10.1107/ s0365110x65000361.

[51] Y. Xu, W.A. Shelton, O2 reduction by lithium on au(111) and Pt(111), J. Chem. Phys. vol. 133 (2) (2010), https://doi.org/10.1063/1.3447381.

[52] C. Kittel, Solid State Physics, 8th ed., 2005.

[53] M.W. Chase, NIST-JANAF Thermochemical Tables, 1998.

[54] K.H. Yun, Y. Hwang, Y.C. Chung, Effective catalytic media using graphitic nitrogen-doped site in graphene for a non-aqueous Li-O2 battery: a density functional theory study, J. Power Sources vol. 277 (2015) 222–227, https://doi.org/10.1016/j.jpowsour.2014.12.021.

[55] N. I. of S. and T. (U.S.), NIST Chemistry Webbook: NIST, NIST, 2000.

[56] B. Bhattacharya, U. Sarkar, The effect of boron and nitrogen doping in electronic, magnetic, and optical properties of graphyne, J. Phys. Chem. C vol. 120 (47) (Dec. 2016) 26793–26806, https://doi.org/10.1021/acs.jpcc.6b07478.

[57] Q. Peng, et al., New materials graphyne, graphdiyne, graphone, and graphane: review of properties, synthesis, and application in nanotechnology, Nanotechnol. Sci. Appl. vol. 10 (7) (2014) 1–29.

[58] H.R. Jiang, T.S. Zhao, L. Shi, P. Tan, L. An, First-principles study of nitrogen-, boron-doped graphene and co-doped graphene as the potential catalysts in nonaqueous Li-O2 batteries, J. Phys. Chem. C vol. 120 (12) (2016) 6612–6618, https://doi.org/10.1021/acs.jpcc.6b00136.

[59] J. Kang, J.S. Yu, B. Han, First-principles design of graphene-based active catalysts for oxygen reduction and evolution reactions in the aprotic Li-O2 Battery, J. Phys. Chem. Lett. vol. 7 (14) (2016) 2803–2808, https://doi.org/10.1021/acs.jpclett.6b01071.

[60] D. Deng, K.S. Novoselov, Q. Fu, N. Zheng, Z. Tian, X. Bao, Catalysis with two-dimensional materials and their heterostructures, Nat. Nanotechnol. vol. 11 (3) (Mar. 2016) 218–230, https://doi.org/10.1038/nnano.2015.340.

[61] H.R. Jiang, T.S. Zhao, L. Shi, P. Tan, L. An, First-principles study of nitrogen-, boron-doped graphene and co-doped graphene as the potential catalysts in nonaqueous Li-O2 batteries, J. Phys. Chem. C vol. 120 (12) (2016) 6612–6618, https://doi.org/10.1021/acs.jpcc.6b00136.

[62] K.P. Huber, G. Herzberg, Molecular Spectra and Molecular -Structure iv. Constants of Diatomic Molecules, 1st ed, 1978.

[63] K.H. Yun, Y. Hwang, Y.C. Chung, Effective catalytic media using graphitic nitrogen-doped site in graphene for a non-aqueous Li-O2 battery: a density functional theory study, J. Power Sources vol. 277 (Mar. 2015) 222–227, https://doi.org/10.1016/j.jpowsour.2014.12.021.

[18] I.C. Jang, Y. Hidaka, T. Ishihara, Li metal utilization in lithium air rechargeable batteries, J. Power Sources vol. 244 (2013) 606–609, https://doi.org/10.1016/j.jpowsour.2013.01.049.

[19] K. Yoo, S. Banerjee, P. Dutta, Modeling of volume change phenomena in a Li-air battery, J. Power Sources vol. 258 (Jul. 2014) 340–350, https://doi.org/10.1016/j.jpowsour.2014.02.044.

[20] "Understanding oxygen electrochemistry in aprotic LiO2 batteries _ Elsevier Enhanced Reader".

[21] H. Cheng, K. Scott, Improving performance of rechargeable Li-air batteries from using Li-Nafion® binder, Electrochim. Acta vol. 116 (Jan. 2014) 51–58, https://doi.org/10.1016/j.electacta.2013.11.018.

[22] E. Nasybulin, W. Xu, M.H. Engelhard, Z. Nie, X.S. Li, J.G. Zhang, Stability of polymer binders in Li-O2 batteries, J. Power Sources vol. 243 (2013) 899–907, https://doi.org/10.1016/j.jpowsour.2013.06.097.

[23] D. Sharon, V. Etacheri, A. Garsuch, M. Afri, A.A. Frimer, D. Aurbach, On the challenge of electrolyte solutions for Li-air batteries: monitoring oxygen reduction and related reactions in polyether solutions by spectroscopy and EQCM, J. Phys. Chem. Lett. vol. 4 (1) (2013) 127–131, https://doi.org/10.1021/jz3017842.

[24] Y. Wang, D. Zheng, X.Q. Yang, D. Qu, High rate oxygen reduction in non-aqueous electrolytes with the addition of perfluorinated additives, Energy Environ. Sci. vol. 4 (9) (Sep. 2011) 3697–3702, https://doi.org/10.1039/c1ee01556g.

[25] F. Li, T. Zhang, Y. Yamada, A. Yamada, H. Zhou, Enhanced cycling performance of LI-O2batteries by the optimized electrolyte concentration of litfsa in glymes, Adv. Energy Mater. vol. 3 (4) (Apr. 2013) 532–538, https://doi.org/10.1002/aenm.201200776.

[26] X. Liu, B. Cui, S. Liu, Y. Chen, Progress of non-aqueous electrolyte for Li-air batteries, J. Mater. Sci. Chem. Eng. vol. 03 (05) (2015) 1–8, https://doi.org/10.4236/msce.2015.35001.

[27] J.L. Shui, H.H. Wang, D.J. Liu, Degradation and revival of Li-O2 battery cathode, Electrochem. Commun. vol. 34 (2013) 45–47, https://doi.org/10.1016/j.elecom.2013.05.020.

[28] Q. Qiu, et al., Cathode electrocatalyst in aprotic lithium oxygen (Li-O2) battery: a literature survey, Catal. Today vol. 420 (Aug. 2023), https://doi.org/10.1016/j. cattod.2023.114138.

[29] C. Ruiqi, et al., Rational design of boron-nitrogen coordinated active sites towards oxygen reduction reaction in aluminum-air batteries with robust integrated air cathode, J. Power Sources vol. 556 (Feb. 2023). Accessed: Oct. 05, 2024. [Online]. Available: https://www.sciencedirect.com/science/article/abs/pii/S0378775 322014537.

[30] Y. Gu, et al., MnIII-enriched α-MnO2 nanowires as efficient bifunctional oxygen catalysts for rechargeable Zn-air batteries, Energy Storage Mater. vol. 23 (Dec. 2019) 252–260, https://doi.org/10.1016/j.ensm.2019.05.006.

[31] W. Jiajun, et al., Theoretical study of catalytic performance of WN MXenes as cathodes for Li-O2 batteries effects of surface functionalization and atomic layers, Appl. Surf. Sci. vol. 638 (Nov. 2023), https://doi.org/10.1016/j. apsusc.2023.158027.

[32] Sahar Ziraki, Mansour Kanani, Babak Hashemi, Mohammad Mohsen Loghavi, Effect of sodium and yttrium co-doping on electrochemical performance of LiNi0.8Co0.15Al0.05O2 cathode material for Li-ion batteries: computational and experimental investigation, J. Energy Storage vol. 70 (Oct. 2023), https://doi.org/ 10.1016/j.est.2023.107983.

[33] X. Peng, et al., Hierarchically porous carbon plates derived from wood as bifunctional ORR/OER electrodes, Adv. Mater. vol. 31 (16) (Apr. 2019), https://doi.org/10.1002/adma.201900341.

[34] B. Wang, et al., Simple-cubic carbon frameworks with atomically dispersed Iron dopants toward high-efficiency oxygen reduction, Nano Lett. vol. 17 (3) (Mar. 2017) 2003–2009, https://doi.org/10.1021/acs.nanolett.7b00004.

[35] J. Chen, C. Li, Y. Chen, Understanding the effect of functional groups on carbon nanotube towards oxygen reduction reaction, Mater. Today Energy vol. 16 (Jun. 2020) https://doi.org/10.1016/j.mtener.2020.100400.

[36] Y. Wenyu, P2-type layered oxide cathode with honeycomb-ordered superstructure for sodium-ion batteries, Energy Storage Mater 69 (2024) 103424, https://doi.org/ 10.1016/j.ensm.2024.103424.

[37] L. Battery, Z. Peng, S.A. Freunberger, Y. Chen, P.G. Bruce, A reversible and higher-rate Li-O 2 battery, Science vol. 337 (6094) (1979) 563–566, 2012.

[38] M. Kim, E. Yoo, W.S. Ahn, S.E. Shim, Controlling porosity of porous carbon cathode for lithium oxygen batteries: influence of micro and meso porosity, J. Power Sources vol. 389 (Jun. 2018) 20–27, https://doi.org/10.1016/j. jpowsour.2018.03.080.

[39] Q. Peng, et al., New materials graphyne, graphdiyne, graphone, and graphane: review of properties, synthesis, and application in nanotechnology, Nanotechnol. Sci. Appl. vol. 10 (7) (2014) 1–29.

[40] Q. Peng, W. Jib, S. De, Mechanical properties of graphyne monolayers : a first-principles study, Phys. Chem. Chem. Phys. vol. 14 (2012) 13385–13391, https://doi.org/10.1039/c2cp42387a.

[41] J. Deb, R. Mondal, U. Sarkar, H. Sadeghi, Thermoelectric properties of pristine graphyne and the bn-doped graphyne family, ACS Omega vol. 6 (31) (Aug. 2021) 20149–20157, https://doi.org/10.1021/acsomega.1c01538.

[42] B.G. Kim, H.J. Choi, Graphyne: hexagonal network of carbon with versatile Dirac cones, Phy. Rev. B Condens. Matter. Mater. Phy. vol. 86 (11) (Sep. 2012), https://doi.org/10.1103/PhysRevB.86.115435.

[43] D. Jyotirmoy, K. Ajit, G. Nandini, S. Utpal, C. Brahmananda, Copper decorated graphyne as a promising nanocarrier for cisplatin anti-cancer drug a DFT study, Appl. Surf. Sci. vol. 622 (Jun. 2023) 156885, https://doi.org/10.1016/j.apsusc.2023.156885.

[44] I.-O. Frank, T.-G. Nayely, G.-R. Abraham, V.-G. Armando, DFT study for hydrogen storage on γ-boron-Graphyne decorated with Li atoms, Comput. Theor. Chem. vol. 1214 (Aug. 2022) 113764, https://doi.org/10.1016/j.comptc.2022.113764.

[45] J. Deb, B. Bhattacharya, N.B. Singh, U. Sarkar, First principle study of adsorption of boron-halogenated system on pristine graphyne, Struct. Chem. vol. 27 (4) (Aug. 2016) 1221–1227, https://doi.org/10.1007/s11224-016-0747-4.

[46] B. Delley, From molecules to solids with the DMol3 approach, J. Chem. Phys. vol. 113 (18) (2000) 7756–7764, https://doi.org/10.1063/1.1316015.

[47] B. Delley, An all-electron numerical method for solving the local density functional for polyatomic molecules, J. Chem. Phys. vol. 92 (1) (1990) 508–517, https://doi.org/10.1063/1.458452.

[48] Z. Ma, et al., A review of cathode materials and structures for rechargeable lithium-air batteries, Energy Environ. Sci. vol. 8 (8) (2015) 2144–2198, https://doi.org/10.1039/c5ee00838g

Atomic and Molecular Physics Revista Mexicana de Física **71** 010402 1–11 JANUARY-FEBRUARY 2025

Calibrating density functionals with $DMol^3$ applied on lithium oxide battery

J. H. Pacheco Sánchez, A. Vera García, and L. A. Desales Guzmán

TecNM / Instituto Tecnológico de Toluca,
Av. Tecnológico s/n. Col. Agrícola Bellavista, Metepec 52149, Edo. Mex., México.

I.-P. Zaragoza

TecNM / Instituto Tecnológico de Tlalnepantla,
Av. Mario Colín s/n. Col. La Comunidad, Tlalnepantla de Baz 54070, Edo. Mex., México.

Received 6 February 2023; accepted 23 August 2024

Density functional theory - based methods constitute part of the computational techniques considered for finding energy, temperature, pressure, density, electronic structure, and more, of materials and other systems. There is not a general density functional for solving either one or another system, rather there are approximations to the exchange-correlation functional designed to apply this theory, and the density functional for the system in study is usually selected through the Jacob's Ladder. The purpose of this article is to calibrate by means of selecting multiple density functionals, for calculating potential energy curves on a specific system, and comparing these results with literature values to determine the most suitable functional. With this theory, when a calculation becomes cyclical means that it does not converge after thousands of steps or iterations. The use of thermal smearing calculations can achieve the convergence of the molecular systems. The density functional is calibrated at insignificant thermal smearing values (around 0.005 Hartrees), because the calculated minimum energy is still consistent against experimental values. This level of theory allows searching for stable reaction products. Among the interactions developed to find a suitable density functional are Li + O, Li + O_2, Li + CO, $2LiO^-$ + $C_{38}H_8$. We select GGA-PBE-Grimme as the most suitable density functional. The resulting information is for applying it to infer about charge/discharge of a rechargeable battery, according to the porosity of the cathode.

Keywords: DFT functionals; potential energy curves; battery ion lithium-oxigen; beta-carbyne.

DOI: https://doi.org/10.31349/RevMexFis.71.010402

1. Introduction

The aim of this study is to optimize one way to select a more proper density functional for the studied system in DFT (Density Functional Theory) through calculations of potential energy curves. DFT-based methods are to find potential energy curves by calculating single points step by step among other things. It is known that it does not exist a general functional for solving any different problem. Among the models of density functional designed to apply DFT for the material in study, Jacob's Ladder is a tool for selecting one proper. In this case, with a generalized gradient approximation (GGA) we used BP, VWN-BP, PBE, RPBE, PBE-Grimme, and we also used hybrid GGA with B3LYP, and B3LYP-Grimme. Then, constructing potential energy curves by single point calculations on one system by various density functional for choosing one of them after calibrating each one according to the experimental value. The result is to infer charge/discharge of a rechargeable battery, according to the porosity of the cathode. Furthermore, when a DFT calculation becomes cyclical, there is no convergence after thousands of iterations, however using thermal smearing calculations the convergence of the molecular systems is possible. At thermal smearing values around 0.005 Ha the density functional is calibrated. On this level of theory, we can be able to search stable reaction products.

The thermal smearing computation shows a heating or increase in the temperature of the system, which is not significant when the values are around 0.005 Ha [1], depending on the material used. The latter is based on the change of temperature (T [K]) and pressure (P [atm]) due to thermal smearing variation δE [Ha] at a volume of 638 Å^3 as shown in Table I of Ref. [2], and a graph corroborating the variation of the energy as a function of the thermal smearing. However, a widely research on this aspect has been carried out in the reference [3] providing reliable convergent results at 0.0001 Ha (0.00272 eV) in cluster calculations $DMol^3$ according to the La and Lu atoms adsorbed on graphene. In the best case, we can achieve a better approximation towards experimental (or theoretical) values when the density functional is calibrated. In the worst case, we can find a density functional that can achieve calculations for the system in study. Here, DFT theory is to search for a stable molecular intermediate of reactions as: Li + O, Li + O_2, Li + CO, $2LiO^-$ + $C_{38}H_8$, which are among those to be developed to obtain information for choosing a functional to infer about the material used in the cathode of a rechargeable battery, because lithium ion is the material of its anode. A rechargeable battery consists of two electrodes (anode and cathode) separated by a membrane. In this case, we propose β-Graphyne as the main material of the cathode.

β-Graphyne is an allotrope of carbon that has diamond-like properties; that is to say, carbons fully bond with other carbons without bonding with another different atom such as hydrogen. There are three known types of graphyne:$\alpha - \beta - \gamma$-graphyne. Graphyne spreads out like a flat mesh just as graphene does it, but with uniform, non-random porosity. With graphyne, what we intend is to build ordered activated carbon, which has a pore size distribution that can be manipulated, depending on the facilities provided by the graphyne type. It is known that there are batteries or cells with catalytic carbon support, which in the best case is activated carbon with random porosity. Activated carbon has the property of being of high porosity, or a large superficial area, with a dispersion from small to large pores, whereby the pore size distribution is not uniform [4-8].

Research on rechargeable batteries (cells) is still open for industrial applications, such as electric vehicles and electromobile devices (cell phones and laptops). The focus is on rechargeable Li-ion batteries, and on electrical energy storage devices which must have high energy density. For this, $metal$-O_2 batteries (Zn-O_2, Al-O_2, Li-O_2) are attractive. These batteries are characterized by having oxygen among their electroactive materials. This simplifies the design and increases the energy density of a battery. For the anode of $metal$-O_2 battery, the metal used can be for example: Ca, Al, Fe, Cd and Zn [9]. Research on Zn-O_2 and Li-O_2 batteries is of interest, and the former is a mature technology. Major part of it, is contemplated in non-rechargeable batteries [9]. Table II in Ref. [10] gives the most common commercial battery systems.

Zinc-oxide Zn-O_2 batteries have a theoretical energy density of 1 kWh/kg, five times above current lithium batteries [11]. Lithium-oxide Li-O_2 or Li-air batteries are an alternative with high theoretical gravimetric energy density ($11 - 13$ kWh/kg). There are four types of cells with respect to the electrolyte used: aprotic, aqueous, solid and hybrid aqueous/aprotic. The efficiency of Li-air batteries is lower than 70 %, the low charge and discharge speeds or effect of charge/discharge which is its cyclability, are limitations of this type of battery. Therefore, it is sought to develop materials with better stability, and better efficiency in the reaction and transport kinetics [11]. Li-CO_2 rechargeable batteries with graphene support are designed, identifying the discharge product with first principles calculations [12]. It is concluded that its kinetic parameters must be improved to achieve the efficiency of Li-O_2 batteries [12]. To fabricate and characterize long-cycle Li-O_2 rechargeable cells, a lithium metal anode, a membrane laminate made of glass-ceramic and polymer-ceramic materials, and a solid-state cathode made of air and carbon are needed [13].

The cells (or batteries) are thermally stable with a recharge capacity between 30 and 105°C. A cell achieves 40 discharge/charge cycles. The reproducibility of its design allows the manufacture of safe, rechargeable lithium-air batteries with high energy density [13]. In the development [14] of non-aqueous LiO_2 batteries based on LiOH to avoid instability of their typical discharge products: LiO_2 and Li_2O_2. The use of the redox pair I^-/I_3^- is introduced to mediate the oxidation and reduction reactions of LiOH-based, and ionic liquid containing Li and water to demonstrate reversible Li-O_2 battery cycle based on LiOH. The addition of the ionic liquid increases the oxidizing power of I_3, changing the charging mechanism from the formation of IO/IO_3 to the evolution of O_2 [14].

We build here potential energy curves for several different density functionals used in DFT with the generalized gradient approximation for choosing one, which better approximate to experimental values. We also accomplish some calculations for the interaction between Lithium ion and β-graphyne. From this, we obtained two curves in one graph exhibiting activating and dissociation energies. Our final aim is to get a value for the specific surface area, which can be used to get an average porosity of the material used, which we think it is the main reason for a good efficiency of a battery.

2. Methodology

With the use of Density Functional Theory $DMol^3$ [15] from BIOVIA Materials Studio software [16] calculations of minimum energy are carried out. This level of theory is useful to figure out systems properties up to tens of electrons in a spatial dependence of the electron density. $DMol^3$ software allows calculations for energy, geometry optimization, dynamics, transition states, elastic constants, reaction kinetics and electron transport. A molecular simulation is useful given its ability as alternative to experimental synthesis [17]. The facilities provided by DFT allow atom-atom, atom-molecule, molecule-molecule interactions to be calculated, of which simple cases are facing a lithium atom and an oxygen atom, a lithium atom and an oxygen molecule, a lithium atom with a molecule of CO, a molecular unit of β-graphyne with an ion of lithium oxide. For example, lithium dioxide can be obtained at least in two ways. One is with the interaction between a lithium atom and an oxygen molecule, and the other is the interaction of a lithium dimer with a carbon dioxide molecule.

DFT [18-21] is employed to perform energy calculations essential for constructing potential energy surfaces that allow observing the adsorption of the two reactants. At thermal smearing values around 0.005 Ha the system encounters a change in temperature, which is slight and insignificant when the values are around 0.005 Ha. It is at these values that a density functional can be calibrated. In this case, this level of theory makes it possible to search for stable reaction products. Geometry optimization calculations allows equilibrium, and consequently stability of a complex intermediate molecule formed between the reactants; in this case, they conduct to the formation of a lithium oxide molecule. Single point step by step calculations can take us to get the interaction between a lithium atom and an oxygen molecule. This is through the construction of potential energy surfaces (curves

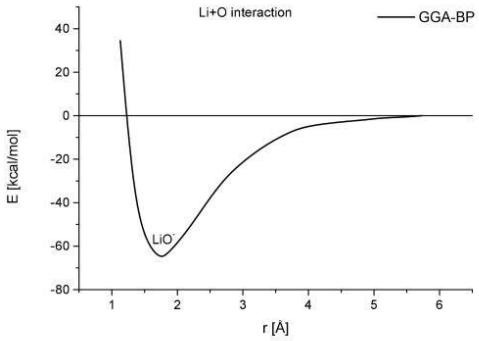

FIGURE 1. Well of potential of $Li+O$ interaction with equilibrium point at (1.76Å, 66.88 kcal/mol) by means of BP functional.

in our cases), which are also all-electron, $DMol^3$ software with DFT-GGA level of theory using a set of DND bases for Hartree-Fock spin unrestricted, and density functional: BP, VWN-BP, PBE, RPBE, PBE-Grimme, B3LYP, and B3LYP Grimme. The same method is used for choosing frequency calculations, which is an additional option for achieving either energy or geometry optimization calculations. When calculations become cyclical without converging, we use thermal smearing to break out the cyclical process, although sometimes a slight bulge appears in the potential wells.

3. Results

First, the interaction between a lithium atom and an oxygen atom is obtained, as it is seen in Fig. 1. Single-point calculations of all-electron interaction between a lithium atom and an oxygen atom are in a level of theory DFT-GGA-BP-UHF carried out with DND 3.5 basis set using 0.003 Ha of thermal smearing, because at 3.73 Å, of separation distance between the two atoms, calculations turn to be cyclical without smearing. This potential energy curve is completed for thermal smearing of 0.003 Ha since 3.7 Å, and shows the formation of a lithium oxide ion LiO^- with a bond that corresponds to chemisorption due to the size of the potential well, which is around 66.88 kcal/mol (see Fig. 1) with length bond of 1.762 Å. The error in the energy calculation is 14.0% with respect to the dissociation energy value of $D_0 = 3.37$ eV (77.8 kcal/mo) for the $X^2\Pi$ state reported by means of $ab\ initio$ CI [22] wave functions calculations, with bond length of 1.695Å, for a reference configuration $1\sigma^2 2\sigma^2 3\sigma^2 4\sigma 5\sigma 1\pi^3$ that properly dissociates Li:^{2}S and O:^{3}P [22]. This theoretical computed $ab\ initio$ CI energy is in complete agreement with the experimental value 3.39 ± 0.26 eV [78.175 ± 5.996 kcal/mol] reported on Ref. [23].

The formation of LiO^- with an overestimation greater than 10% when compared against experimental results does not say that it is an appropriate density functional for the calculations. Figure 2 shows a pertinent analysis that allows us an adequate use of thermal smearing to calibrate the chosen density functional whenever possible. In this case, we see that as larger the thermal smearing, the dissociation energy is closer to the experimental value, but the temperature/pressure inadequately grows. Then, for thermal smearing of 0.01 Ha the equilibrium (1.727Å, -70.818 kcal/mol) point has an energy with 9% error respect to that on Ref. [22]. A bond length with error of 1.89% compared against the $ab\ initio\ CI$ value of Ref. [22] mentioned in the previous paragraph, which is a theoretical result in excellent agreement with the experimental one. It must be noticed that in Fig. 2 normalized means a translational position of the curve in the graph as it is shown in Fig. 2a), which is not applied in Fig. 2b).

However, in all electron calculations using GGA-PBE-GRIMME-UHF with 0.032 Ha of thermal smearing and DND basis set with file 4.4 as seen in Fig. 3, the equilibrium point is obtained at (1.651Å, -73.844 kcal/mol), and has an energy with a 5.32% error.

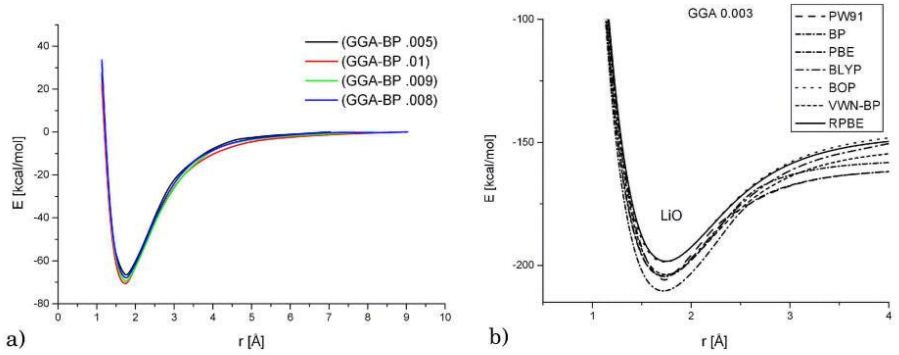

FIGURE 2. Potential energy curves for interaction between lithium and oxygen atoms a) normalized with BP functional at 0.005, 0.01, 0.009, and 0.008 Ha values of thermal smearing, b) without normalizing with PW91, BP, PBE, BLYP, BOP, VWN-BP, RPBE functionals.

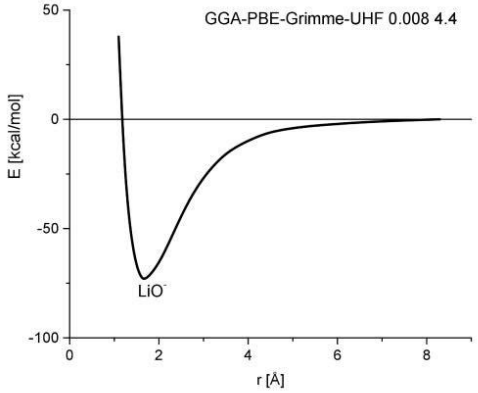

FIGURE 3. Potential energy curve of Li+O interaction using thermal smearing of 0.032 Ha and DND basis set with 4.4 file with PBE-Grimme functional.

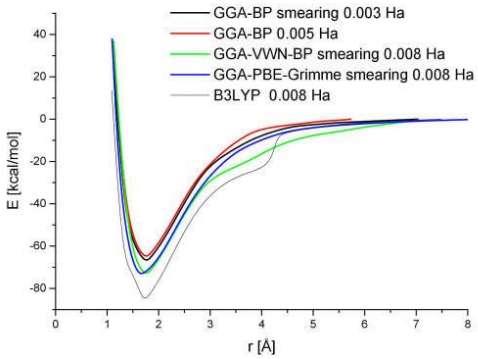

FIGURE 4. Selected functionals BP, VWN-BP and B3LYP to calculate the potential well of the $Li + O$ interaction. The LiO^- formation appears at each different equilibrium points.

The Fig. 4 exhibits a notable enhancement in the approximation to *ab initio* CI results of Ref. [22]. The 5.8% percentage of error in the equilibrium energy point (1.749Å, -73.27 kcal/mol) of GGA-VWN-BP is consequently lower than 10%. In addition, with GGA-PBE-Grimme functional, the calculated energy shows an error of 5.32%, and it is the closest approximation to that one against which we are comparing. Finally, the potential curve of the B3LYP functional exhibits this hybrid functional, with a potential well very irregular, and an equilibrium point (1.722Å, -83.825 kcal/mol) having an error of 7.7% in the energy with respect to the *ab initio* CI value of Ref. [22]. However, since $E_{\text{B3LYP}} > E_{\text{EXP}}$ there is no consistency in having a potential well below the experimental energy, and it only occurs due to the step that shows the potential energy curve built with B3LYP, which risks the credibility of this density functional.

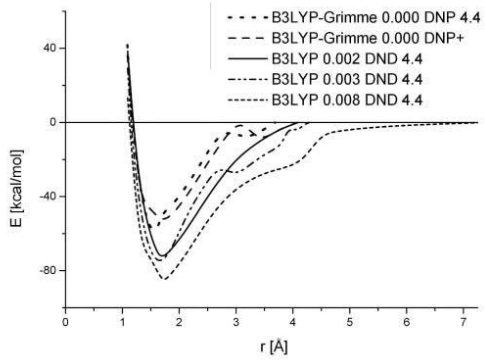

FIGURE 5. Trends of B3LYP functional by using 0.000 Ha, 0.002 Ha, 0.003 Ha, 0.008 Ha values of thermal smearing on Li+O interaction, and DNP, DNP+, DND basis set respectively, the file 4.4.

The case of the B3LYP hybrid functional using DND basis set is explored for the Li+O interaction in Fig. 5. By applying thermal smearing at 0.002 Ha, it is a soft behavior obtained, while it is deforming as its thermal smearing value grows. The curves at 0.002 Ha and 0.003 Ha are similar. About this, at least we must see two things: the first is that as the curve is deforming, the equilibrium point in energy is closer to the experimental value, until it significantly exceeds such value. The second is that the trend to zero is clear when thermal smearing value is 0.032 Ha, while at 0.002 Ha no more points can be by our computational resources obtained. It is inferred that calculating without thermal smearing the minimum of the potential energy curve enhances more, given that the scope in the distance would be lower. These trends show that the use of the B3LYP hybrid functional can be adequate according to the system under study. It is important to mention that each curve has been towards zero normalized by itself that is, using its own value to which the step-by-step procedure in single-point calculations are constant or almost constant according to a tolerance, by taking only one single point taken for all the curves to compare them easily.

From the data for the interactions obtained applying step-by-step single-point calculations, the equilibrium points are in Table I listed.

When directly calculating without thermal smearing in Table I, the results stay far of the experimental values. Sometimes, it is good to calculate thermal smearing at certain value, and then to gradually decrease its value until cero, this gives excellent results; however, in this case we chose to apply calculations directly with the thermal smearing value chosen to see clearly the conduct. Potential energy curves for different density functional at 0.003 Ha of thermal smearing can be observed in Fig. 6a) (notice that once system is stable in the calculations, it is easy to decrease the thermal smearing up to zero with good results), where the minimum energy of GGA-VWN-BP is close to the experimental value 2.55 eV

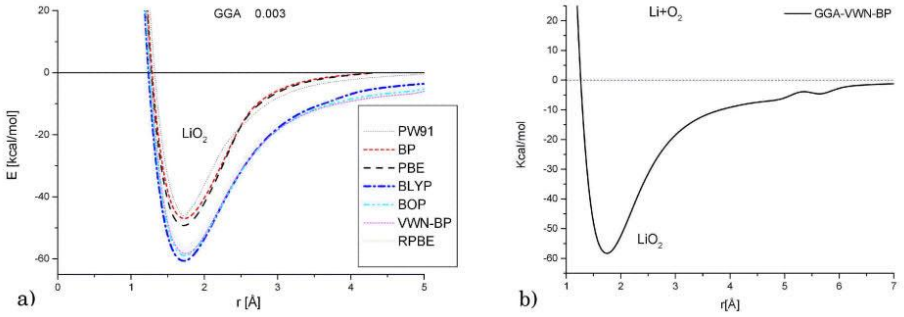

FIGURE 6. Potential energy curves of the interaction between lithium atom and oxygen molecule using the functionals: PW91, BP, PBE, BLYP, BOP, VWN-BP, RPBE. In case of GGA-VWN-BP, the minimum corresponding to the LiO_2 intermediary complex is at the point: a) (1.74Å, −58.32 kcal/mol), b) (1.74Å, −58.53 kcal/mol).

TABLE I. Sensibilizing of equilibrium points [Å, kcal/mol] on Li+O interaction as thermal smearing [Ha] changes for different density functionals.

Functional	Thermal Smearing values [Ha]	Basis set and File	Equilibrium Point [Å, kcal/mol]
UHF GGA-BP	0.000	DND-3.5	(1.730, -65.400)
UHF GGA-BP	0.003	DND-3.5	(1.762, -66.880)
UHF GGA-BP	0.005	DND-3.5	(1.749, -64.810)
UHF GGA-BP	0.032	DND-3.5	(1.709, -70.716)
UHF GGA-BP	0.002	DND-4.4	(1.707, -71.074)
UHF GGA-BP	0.003	DND-4.4	(1.707, -72.325)
UHF GGA-BP	0.005	DND-4.4	(1.705, -71.823)
UHF GGA-BP	0.032	DND-4.4	(1.731, -71.760)
UHF GGA-BP	0.009	DND-4.4	(1.731, -70.282)
UHF GGA-BP	0.010	DND-4.4	(1.695, -68.885)
UHF GGA-VWN-BP	0.003	DND-4.4	(1.706, -72.243)
UHF GGA-VWN-BP	0.005	DND-4.4	(1.731, -69.931)
UHF GGA-VWN-BP	0.032	DND-4.4	(1.699, -73.568)
UHF-GGA-PBE-Grimme	0.032	DND-4.4	(1.697, -73.844)
UHF-GGA-RPBE	0.032	DND	(1.709, -70.716)
B3LYP-Grimme	0.000	DND-4.4	(1.589,-61.696)
B3LYP-Grimme	0.000	DNP+	(1.688,-53.824)
B3LYP	0.002	DND-4.4	(1.693,-72.474)
B3LYP	0.003	DND-4.4	(1.693,-81.764)
B3LYP	0.032	DND-4.4	(1.692,-85.694)

(58.8 kcal/mol) reported on the Ref. [24]; however, GGA-BOP is also very good minimum energy. Here we must comment that in the Ref. [25] the following values were also reported for D_0 dissociation energy Li-O_2 interaction: i) 222 ± 25 kJ/mol (53.06 ± 5.97 kcal/mol) in a flame study measurement by Dougherty *et al.* [26]; ii) 220 kJ/mol (52.58 kcal/mol) semiempirical calculation estimate by Alexander [27]; iii) 302 ± 21 kJ/mol (72.18 ± 5.02 kcal/mol in a flame study measurement by Steinberg and Schofield [28]; iv) ≥ 180 kJ/mol (43.02 kcal/mol) time-resolved kinetics by Plane *et al.* [29]; v) 296 kJ/mol (70.74 kcal/mol) *ab initio* calculation by Plane *et al.*, [29]; vi) 259 kJ/mol (61.9 kcal/mol) *ab initio* calculation by Allen *et al.* [30]. These results indicate a wide diversity in both measurements and theoretical values of D_0 dissociation energy Li-O_2 interaction between lithium (atom) and oxygen

(molecule), then other density functional can approximate another experimental or theoretical value.

In the interaction between a lithium atom and an oxygen molecule Li+O_2, all electron single-point step-by-step calculations at a level of DFT-GGA-BP theory, the potential energy curve show the formation of a LiO_2 lithium oxide molecule with a bond corresponding to chemisorption due to the magnitude of the well of potential, which is 58.53 kcal/mol (see Fig. 6b) in complete agreement with experimental measurements [24]. The measurement of the dissociation energy of the Li-O_2 interaction is: 2.55 eV (58.8 kcal/mol) reported by Nefedov *et al.* [24,31], and 2.3 eV (53.06 kcal/mol) reported by Nefedov *et al.*, [24-26].

Nevertheless, in another case in which all electron single-point calculations of the interaction between a lithium atom and an oxygen molecule now at a level of DFT-GGA-BP theory are carried out with a set of DND-3.5 basis set for Hartree-Fock non-restricted spin. In the potential energy curve, the formation of a LiO_2 lithium oxide molecule is observed with bond corresponding to chemisorption due to the magnitude 47.3 kcal/mol of the well of potential (see Fig. 7).

The difference of 5.32% is good result; however, the need to continue searching is due to the diversity of results in this case, and to the existence of frequency calculations for comparing against experimental results. This is a vibrational methodology to investigate a computational result closest to the experimental value. Experimental values of LiO_2 formation in an argon matrix using infrared spectroscopy that correspond to energy levels are next: 492.4 cm^{-1}, 698.8 cm^{-1}, and 1096.9 cm^{-1} [32]. This last value is equivalent to 3.135 kcal/mol (1 $cm^{-1} = 2,858$ cal/mol); so, it is not possible to compare against our values calculated through potential energy wells since they are more than 10 times larger, and therefore the comparison is not adequate. This leads to the calculation of frequencies with the same DFT-GGA-BP methodology used, which provides the following frequencies (cm^{-1}) for normal modes: i) 7 : 347.8, ii) 8 : 658.3,

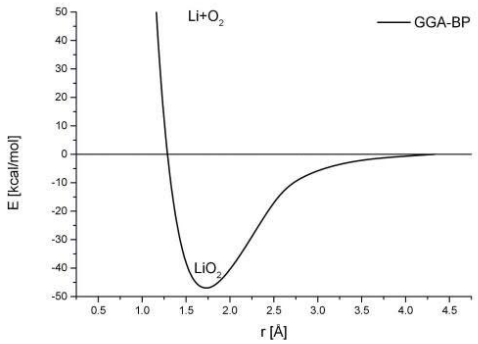

FIGURE 7. Potential energy curve of the interaction between a lithium atom and an oxygen molecule. The minimum at the point (1.7209Å, −47.3265 kcal/mol) corresponds to the LiO_2 intermediary complex by means of BP functional.

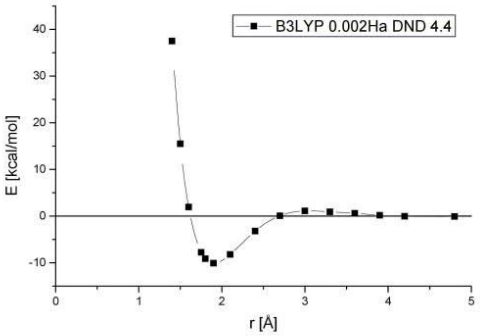

FIGURE 8. Potential energy curve of the Li+CO interaction using B3LYP functional with DND basis set file 4.4, at 0.002 Ha of thermal smearing.

iii) 9 : 1670.8, which are of the same order of magnitude as the experimental values. In addition, the vibrational energy of the zero point is +3.827 kcal/mol that is 18.07% greater than the experimental, and that reveals an adequate comparison.

The B3LYP hybrid functional has been chosen to calculate the Li+CO interaction, and the potential energy curve obtained is in Fig. 8 shown, in which the minimum is located at (1.893 Å, −10.53 kcal/mol), and corresponds to the equilibrium point. The distance at this point is the bond length, and the energy is the dissociation energy value, which in this case is far from the experimental value 1806 cm^{-1} (5.1636 kcal/mol) reported in Ref. [33].

In this case, Fig. 9 shows the application of the density functional ones that behaved best in the interactions Li+O. The eligibility of B3LYP as functional is shown in Fig. 9a), since when comparing it against GGA PBE Grimme, B3LYP gives the best approximation to the experimental value. In Fig. 9b) the calculations are compared without the use of smearing. The minimum of Fig. 9b) when applying the B3LYP hybrid functional is similar to that when thermal smearing 0.002 Ha is used, while by applying GGA-PBE Grimme has the minimum at (2.057Å, −13.423 kcal/mol) with an energy farther to the experimental value than with B3LYP. However, the latter value is in complete agreement with the ab initio result exhibited in reference [34], where the bonding and structure of lithium-ion carbonyl complex Li^+CO was studied at CCSD and MP2 levels of theories, and a global minimum of the Li^+CO complex with bond dissociation energy of 13.7 kcal/mol, and a linear configuration was found.

Finally, the LiO and $C_{38}H_8$ are molecules independently optimized. The optimized lithium oxide molecule turns out to be the LiO^- ion with hydrogen bond type as shown in Fig. 10a) without visible bond. The $C_{38}H_8$ molecular unit of carbons ring type β-graphyne [35] alternates single and triple bonds except at four double bonds observed in Fig. 10a) turns out to be flat after geometry optimization.

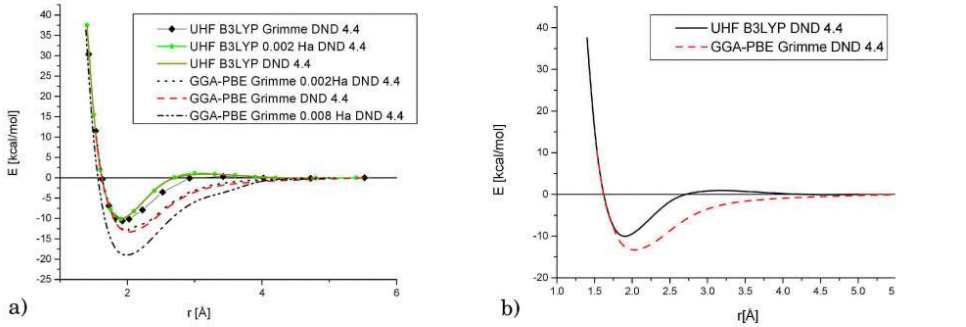

FIGURE 9. a) Comparison among potential energy curves of Li+CO interaction between B3LYP and PBE-Grimme functionals without smearing and at smearing of 0.002 Ha, and 0.008 Ha, b) Specific comparison between B3LYP and PBE-Grimme functionals without smearing.

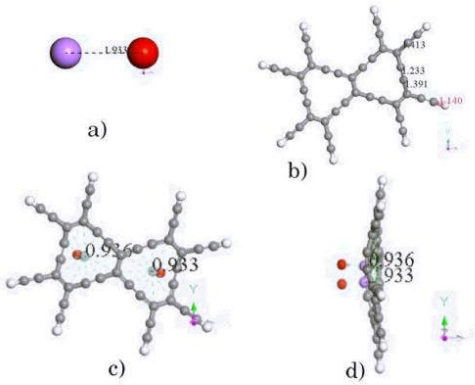

FIGURE 10. Graphyne system with lithium oxide. a) Lithium oxide ion. b) Flat graphyne unit, c) Graphyne unit with two ions of lithium oxide, d) Profile view of the optimized graphyne unit with two lithium oxide ions.

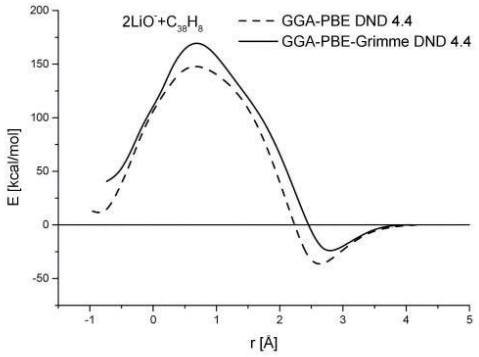

FIGURE 11. Potential energy curves of the 2 LiO^-+$C_{38}H_8$ interaction. Each curve has two critical points, the PBE curve has maximum at the point (0.658Å, 147.59 kcal/mol), and minimum at (2.64 Å, -35.54 kcal/mol); and the PBE-Grimme curve has maximum at (0.658Å, 168.61 kcal/mol), and minimum at (2.78Å, -24.34 kcal/mol).

For which DFT-PBE-Grimme-DND-4.4 is used with thermal smearing of 0.007 Ha, with which the resulting energy is -6588.334 kcal/mol (285.605 eV). Each lithium oxide ion is placed approximately in the center of each carbon ring of Fig. 10b). With this configuration we tried about obtaining the potential energy curve that was not possible to obtain. It was only achieved when the complete system was optimized. In this way, choosing the DFT-GGA-PBE-Grimme density functional in all-electron calculations with not restricted spin of Hartree-Fock, with DND basis set using the 4.4 file, without thermal smearing, 'single point' step by step calculations are made about obtaining potential energy curves $2LiO^-$ vs $C_{38}H_8$, placed as seen in Fig. 10c). Figure 10d) shows that after geometry optimization the molecules of lithium oxide make the graphyne unit no longer flat.

In the Fig. 11, we see the potential energy curves of the $2LiO^-$+$C_{38}H_8$ interaction, where the original energy values were to get energies tending to zero energy translated. Then, maximum and minimum correspond to the energies searched. Each curve has at least two critical points, the PBE curve has a maximum at the point (0.658Å, 147.59 kcal/mol), and a minimum at (2.64Å, -35.54 kcal/mol); and the PBE-Grimme curve has maximum at (0.658Å, 168.61 kcal/mol), and minimum at (2.78Å, -24.34 kcal/mol). The minimums correspond to the formation of an intermediary complex molecule $2LiO^-C_{38}H_8$ for both bond length and dissociation energy.

This lithium oxide ion is a complex case, using another strategy, we were able to get the visible bond between Li and O, and we exhibit in Fig. 12a) such LiO^- ion. Due to the methodology strategy chosen, in this case we proceed to get the adsorption energy using the equation:

$$E_{(\mathrm{ad})} = E_{(\mathrm{LiO^-C38})} - E_{(\mathrm{C38})} - E_{(\mathrm{LiO^-})},$$

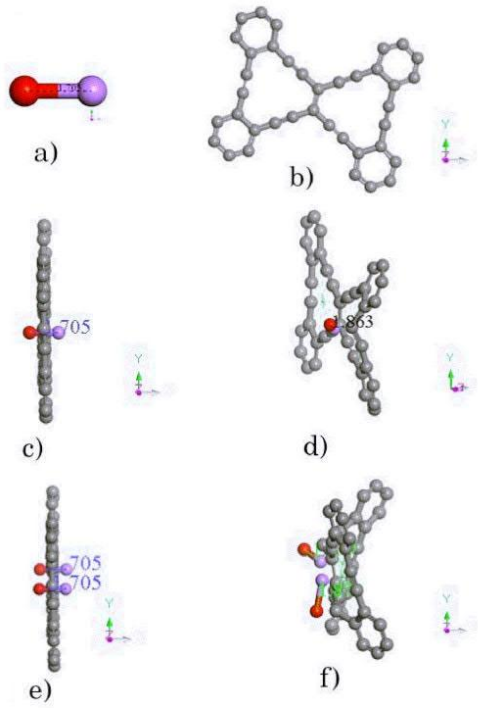

FIGURE 12. β-graphyne system with bonded lithium oxide. a) Lithium oxide ion, b) Flat β-graphyne unit, c) Input for optimization of β-graphyne unit with one ion of lithium oxide, d) Output of the optimized β-graphyne unit with one lithium oxide ion, e) Input for optimization of β-graphyne unit with two ions of lithium oxide, f) Output of the optimized β-graphyne unit with two lithium oxide ions.

where $E_{(\mathrm{LiO^-C38})} = -6001.020$ kcal/mol is the energy of intermediary complex formed with one lithium oxide ion and one unit of β-graphyne, -92.061 kcal/mol is the energy of one lithium oxide ion, and -5852.783 kcal/mol is the energy of one unit of β-graphyne. Then in this case the adsorption energy of one $\mathrm{LiO^-}$ ion and one unit of β-graphyne.

$$E_{(\mathrm{ad})} = -56.354 \text{ kcal/mol}.$$

The adsorption between β-graphyne and lithium-oxide ion is accomplished between one carbon atom attached to β-graphyne and the oxygen atom of Lithium-oxide ion as it is shown in Fig. 12d). Figures 12e) and 12f) exhibit that oxygen is responsible of the planarity deformation of β-graphyne.

Figures 10d), 12d), and 12f) exhibit a charged cathode expecting discharge by the user of the battery.

We achieve one calculation of specific surface area (SSA) [36] on a unit of β-graphyne molecule using the equation

$$A_s = \frac{6}{\rho d},$$

where $\rho = 1.109$ g/cm^3 is the density of the material that was with molecular dynamics calculated using the NPT ensemble at 500 ps; and d is an average diameter of a graphyne unit approximately of 13.2Å. Then the specific surface area in this case is

$$A_s = 4098.5 \frac{\mathrm{m}^2}{\mathrm{g}}.$$

We consider that this is an excellent specific surface area. On the other hand, using SBET measurements of surface area for activated carbon fiber (ACP) the surface area is 1970 m^2/g [37], and our SSA result is 2.32 times greater than this one. We also previously reported activated carbon using burned coconut shells at 900°C a surface area of 452 m^2/g using BET measurements [6,38], which is smaller than our result.

4. Discussion

Calculations on Li+O have been widely analyzed given that calculations are computationally cheaper than those for the other systems, and we compare our results against data information of diatomic molecules on which we found the dissociation energy near to the experimental value. However, our best results appear by comparing against frequency measurements information for Li+O_2 and Li+CO interactions, for which we selected GGA-PBE-Grimme density functional because the results are the most approximated to either experimental or theoretical results. Our analyses have not been exhaustive, because according to our results, and the systems used, we did not consider obtaining more potential energy curves given that van der Waals interactions supported by PBE-Grimme on gas atoms as oxygen is widely recommended in literature, and results of our calculations agree with this fact. On the other hand, when we perform calculations using thermal smearing values lower than 0.002 the number of iterations grows indicating that it is hard to converge.

On the other hand, ab initio calculations for extended ionic models report that LiO bond of 3.774 au (1.997Å) against the experimental value of 3.711 au (1.964Å) in their Table I about M-O bond lengths [39]. Ab initio calculations used to provide bond lengths, harmonic frequencies, and dissociation energies of low-lying electronic states for LiO, $\mathrm{LiO^+}$, $\mathrm{LiO^-}$ allowed the electronic structure [40]. There is a close correspondence in the ground states of molecules in which atoms are replaced by other atoms of the same column from the periodic table. An exception to this occurs with the alkali oxides where LiO has a $^2\Pi$ ground state. Ab initio calculations, Hartree-Fock (HF), generalized valence bond (GVB), and configuration interaction (CI) have allowed to elucidate bonding and to explain its reversal [41]. The ground state geometries of neutral and cationic $\mathrm{Li}_n\mathrm{H}$ ($n = 1-7$) and $\mathrm{Li}_n\mathrm{H}_2$ ($n = 2-6$) clusters are determined in the framework of the SCF and CASSCF procedures. Large-scale CI calculations for valence electrons are to determine stabilities

carried out and ionization potentials (IP) [42]. We are comparing against ab initio CI [22] calculation in agreement with experimental results [23], but another experimental result is $D_0 = 3.49$ eV given at Ref. [43], which is also in agreement with the previous ones.

Using a self-consistent pseudopotential method equilibrium ground-state properties of Mo and Nb transition metals, equilibrium lattice constants, cohesive energies, and bulk moduli, which are in excellent agreement with experiment, have been from calculations obtained [44]. Small nickel clusters were up to the tetramer investigated by the local spin density functional theory. Some competitive states were for the dimer studied. Calculations were by vibrational analysis also followed to discriminate between real minima and saddle points on the potential energy surface. Jahn-Teller deformations played an important role in determining transition-metal cluster geometries. Equilibrium geometries, electronic configurations, binding energies, magnetic moments, and harmonic frequencies were in the work [45] reported. Density-functional theory approach is with fractionally occupied orbitals presented for studying prototypical ferric-ferrous electron-transfer process in liquid water. The use of fractional occupation numbers turned out to be crucial for achieving convergence in most self-consistent calculations because of the open-shell d-multiplet electronic structure of each iron ion and the near degeneracy of the redox groups involved [46].

Density functional theory molecular dynamics (DFT-MD), and classical molecular dynamics using polarizable force fields (PFF-MD) are employed to evaluate the influence of Li^+ on the structure, transport, and electrochemical stability of three potential ionic liquid electrolytes is reported on Ref. [47]. The effect of equilibration methodology and sampling on ab initio molecular dynamics (AIMD) simulations of systems of common solvents and salts found in lithium-oxygen batteries is in Ref. [48] studied.

5. Conclusions

Using Jacob's Ladder, we proposed to work with BP, VWN-BP, PBE, RPBE, PBE-Grimme, B3LYP, and B3LYP Grimme to construct their potential energy curves for comparing between them, and against experimental values. This brief study lead us to the use of one of the functionals (GGA-BP, GGA-PBE-Grimme, or B3LyP) in the systems required to study lithium oxides with carbon LiO^- support for batteries that improve electric charge storage, ready to be used and discharged by the user of the battery. In this case, it is concluded that GGA-PBE-Grimme gives a minimum with lower energy than GGA-PBE. This is more appreciable for charge desorption in this charge storage system.

The reason to consider LiO^- ion is due to its type $X + Y^-$; that is, an oxidation - reduction process in which one atom loses an electron and the other gain it. Electrons lost on lithium ion is a fact when turns on the device with its corresponding battery, and it must be recharged by external charge by plug in the battery, to which lithium ion recovers its original charge again. This is a reversible process.

Then from the three selected, PBE-Grimme is applied to the interaction between two lithium ions and one β-graphyne unit. Their interaction gives a potential energy curve, from which we see one barrier corresponding to the activation energy, and one well of potential corresponding to the dissociation energy.

We observe that any of the two methodologies (potential energy curves or frequencies) used for choosing the better functional is capable for giving suitable selection. In our case, we selected the construction of potential energy curves in this case. However, the last result of adsorption energy has been with a different method calculated. Furthermore, it is observed that oxygen atom in the lithium oxide ion is responsible for deformation of the planarity of β-graphyne since there is a strong interaction between one carbon atom of β-graphyne and the oxygen atom of lithium oxide ion.

The selected β-graphyne unit molecule has an excellent specific surface area. Then, its use as cathode of Li-ion battery might enhance its capability characteristics.

Acknowledgements

We thank to TecNM for supporting this research through the grant 14113.22-P.

1. V.A. Basiuk, Electron smearing in DFT calculations: a case study of doxorubicin interaction with single-walled carbon nanotubes. *Int J Quantum Chem* **111** (2011) 4197-4205.

2. D. Hernández-Benitez, J. H. Pacheco-Sánchez, Optimization of Chitosan+Activated Carbon Nanocomposite. *DFT Study* **3** (2018) 436, https://dx.doi.org/10.32474/AOICS.2018.03.000175.

3. V. A. Basiuk, O. V. Prezhdo, E. V. Basiuk, Thermal smearing in DFT calculations: How small is really small? A case of La and Lu atoms adsorbed on graphene, *Materials Today Communications* **25** (2020) 101595, https://dx.doi.org/10.1016/j.mtcomm.2020.101595.

4. J. Jagiello, A. Ansón, and M.T. Martínez, *J. Phys. Chem. B* **110** (2006) 4531.

5. H. Tanahashi, *J. Appl. Electrochem.* **35** (2005) 1067.

6. L.A. García, I.P. Zaragoza, J.H. Pacheco, A. Bravo, J.L. Contreras, J. Salmones, and G. Arriaga, Study of activated carbons from different source, used to storage hydrogen as energy vector, presented at the 14th International Symposium on Metastable and Nano Materials, Corfu, Greece, 2007.

7. A. Allwar, Bin Md Noor and A. Bin Mohd Nawi, *Journal of Physical Science* **19** (2032) 93.
8. D. Lozano-Castelló, D. Cazorla-Amorós, and A. Linares-Solano, *Energy & Fuels* **16** (2002) 1321.
9. U. Pau. Taylor Peter, Bolton Ronan, Stone Dave, Zhang Xiao-Ping, Martin Chris, Pathways for Energy Storage in the UK Pathways for energy storage in the UK, (2012).
10. M. Winter, R. J. Brodd, What are batteries, fuel cells, and supercapacitors? *Chem. Rev.* **104** (2004) 4245-4269.
11. M. Gil-Austi, L. Zubizarreta-Saenz De Zaitegui, V. Fuster-Roig, and A. Quijano- López, Batteries of the future: challenges and projection, *Dyna*, **92** (2017) 601-605.
12. Z. Zhang *et al.*, The First Introduction of Graphene to Rechargeable Li - CO2 Batteries **, *Angewandte Chemie International Edition*, **127** (2015) 6550, https://dx.doi.org/10.1002/anie.201501214.
13. B. Kumar *et al.*, A Solid-State, Rechargeable, Long Cycle Life Lithium -Air Battery, *Journal of The Electrochemical Society*, **157** (2010) 50, https://dx.doi.org/10.1149/1.3256129.
14. I. Temprano *et al.*, Toward Reversible and Moisture-Tolerant Aprotic Lithium-Air Batteries Toward Reversible and Moisture-Tolerant Aprotic Lithium-Air Batteries, *Joule*, **4** (2020) 2501, https://dx.doi.org/10.1016/j.joule.2020.09.021.
15. B. Delley, An all-electron numerical method for solving the local density functional for polyatomic molecules, *J. Chem. Phys.* **92** (1990) 532, https://dx.doi.org/10.1063/1.458452.
16. BIOVIA Materials Studio (2017) Springer, New York, USA. (DS BIOVIA. Dassault Systèmes BIOVIA. Retrieved 24 January 2017).
17. D. FairÃ©n-JimÃ©nez, Claves de la simulación molecular para el estudio de procesos de adsorción en estructuras metal-orgánicas, *An. Quím.* **106** (2010) 183-190.
18. Kohn, W. v-Representability and density functional theory. *Phys. Rev. Lett.* **51** (1983) 1596-1598.
19. Kohn, W. Density-functional theory for excited states in quasi-local density approximation. *Phys. Rev. A.* **34** (1986) 737-741.
20. Kohn, W., and Sham Self-consistent equations including exchange and correlation effects. *Phys. Rev.* **140** (1965) A1133-A1138.
21. Kohn, W. and Vashishta, P. General density functional theory. In Theory of inhomogeneous Electron Gas. (Lundqvist, S. and March, NH, eds. Plenum, NY, 1983).
22. M. Yoshimine Accurate potential curves and properties for X 2Π and A 2∑+ states of LiO* J. Chem. Phys. **57** (1972) 1132, https://dx.doi.org/10.1063/1.1678366.
23. L. Brewer, G. M. Rosenblatt, *Advan. High Temp. Chem.* **2** (1969) 1.
24. A. P. Nefedov, B. V. Rogov, V. A. Sinel'shchikov, and M. A. Khomkin, Investigation of Distribution of Lithium Atoms in the Boundary Layer of the Flow of Combustion *Products High Temperature,* **38** (2000) 742, https://dx.doi.org/10.1007/BF02755927.
25. J. M. C. Plane, B. Rajasekhar, and L. Bartolotti, Kinetic study of the reaction potassium + oxygen + M (M = nitrogen, helium) from 250 to 1103 K *J. Phys. Chem.,* **94** (1990) 4161,
26. G. J. Dougherty, M. J. McEwan, L. F. Phillips, Some photometric observations of trace additives in dry carbon monoxide flames *Combust. Flame* **21** 1973 253.
27. M. H. Alexander, Semiempirical potential surfaces and dynamical considerations for collisions between alkali metals and molecular oxygen: Li + O2 and Na + O2 a) *J. Chem. Phys.* **69** (1978) 3502, https://dx.doi.org/10.1063/1.437055.
28. M. Steinberg, K. Schofield, The High-Temperature Chemistry and Thermodynamics of Alkali Metals (Lithium, Sodium and Potassium) in Oxygen Rich Flames. Preprint; Western Section, The Combustion Institute, November 1987.
29. J. M. C. Plane, B. Rajasekhar, L. Bartolotti, Theoretical and Experimental Determination of the Lithium and Sodium Superoxide Bond Dissociation Energies, *J. Phys. Chem.* **93** (1989) 3141, https://dx.doi.org/10.1021/j100345a052.
30. W. D. Allen, D. A. Horner, R. DeKock, R. B. Remington, H. F. Schaefer, The Lithium Superoxide Radical: Symmetry Breaking Phenomena and Potential Energy Surfaces. Submitted for publication in Chem. Phys.
31. R.H. Lamoreaux, and D.L. Hildenbrand, High Temperature Vaporization Behavior of Oxides. I. Alkali Metal Binary Oxides. *J. Phys. Chem. Ref Data*, **13** (1984) 151-173.
32. X. Wang, L. Andrews, Infrared spectra, structure and bonding in the LiO2, LiO2Li, and Li2O molecules in solid neon Molecular Physics: *An International Journal at the Interface between Chemistry and Physics*, **107** (2009) 739, https://dx.doi.org/10.1320/00268973202526583.
33. O. Ayed, A. Loutellier, L. Manceron, and J. P. Perchard Interaction between Lithium and Carbon Monoxide. 1. A Matrix Infrared Study. *J. Am. Chem. Soc.* **132** (1986) 8138.
34. J. N. Dawoud, Interaction energies and structures of the Li+(CO)n (n=1-3) complexes. *J. Chem. Sci.* **129** (2017) 543, https://dx.doi.org/10.1007/s12039-017-1275-5.
35. X Kim BG, Choi HJ. Graphyne: Hexagonal network of carbon with versatile Dirac cones. *Phys. Rev. B.* **86** (2012) 115435.
36. D.H. Everett, Basic Principles of Colloid Science. Royal Society of Chemistry, (London 1988).
37. IUPAC commission on Colloid and Surface Chemistry Including Catalysis, *Pure Appl. Chem.* **57** (1985) 603.
38. J.H. Pacheco-Sánchez, IP Zaragoza-Rivera, A Bravo-Ortega, Interaction of small carbon molecules and zinc dichloride: DFT study, *Rev. Mex. Fís.*, **63** (2017) 97-110, https://repositorio.unam.mx/contenidos/4107435.
39. M. Wilson, Extended ionic models from ab initio calculations, *Phil. Trans. R. Soc. London A* **358** (2000) 399-418.
40. A. I. Boldyrev, J. Simons, Paul von FL Schleyer Ab initio study of the electronic structures of lithium containing diatomic molecules and ions. *The Journal of Chemical Physics* **99** (1993) 8793, https://dx.doi.org/10.1063/1.465600.

41. J. N. Allison, R. J. Cave, W. A. Goddard III Alkali Oxides. Analysis of Bonding and Explanation of the Reversal in Ordering of the 2fl and 22+States. *J. Phys. Chem.* **88** (1984) 1262, https://dx.doi.org/10.1021/j150650a049.

42. V. Bonačić Koutecký, J. Gaus, M.F. Guest, L. Češpiva and J. Koutecký, Ab initio CI study of the electronic structure and geometry of neutral and cationic hydrogenated lithium clusters. Predictions and interpretation of measured properties. *Chem. Phys. Lett.* **206** (1993) 528-539

43. K.P. Huber and G. Herzberg, Molecular Spectra and Molecular Structure **Vol. 4** constants of diatomic molecules. Van Nostrand Reinhold C. NY 1979.

44. C.-L. Fu and K.-M. Ho First-principles calculation of the equilibrium ground-state properties of transition metals: Applications to Nb and Mo. *Phys. Rev. B* **28** (1983) 5480-5486.

45. M. C. Michelini, R. Pis Diez, A. H. Jubert A density functional study of small Nickel clusters. *Inter. J. Quant. Chem.*, **70** (1998) 693-701.

46. A. Migliore, P. H.-L. SIt, and M. L. Klein, Evaluation of Electronic Coupling in Transition-Metal Systems Using DFT: Application to the Hexa-Aquo Ferric-Ferrous Redox Couple. *J. Chem. Theory Comput.* **5** (2009) 307, https://dx.doi.org/10.1021/ct800340v.

47. J. B. Haskins, Ch. W. Bauschlicher Jr., and J. W. Lawson, Ab Initio Simulations and Electronic Structure of Lithium-Doped Ionic Liquids: Structure, Transport, and Electrochemical Stability. *J. Phys. Chem. B* **119** (2015) 14705, https://doi.org/10.1021/acs.jpcb.5b06951.

48. E. Crabb, A. France-Lanord, G. Leverick, R. Stephens, Y. Shao-Horn, J.C. Grossman* Importance of Equilibration Method and Sampling for Ab Initio Molecular Dynamics Simulations of Solvent-Lithium-Salt Systems in Lithium-Oxygen Batteries. *J. Chem. Theory Comput.* **5** (2009) 307, https://dx.doi.org/10.1021/acs.jctc.0c03233.

American Journal of Biomedical Science & Research

www.biomedgrid.com

ISSN: 2642-1747

Opinion

Opinion About Increasing use of Li-Air Batteries

Juan Horacio Pacheco Sánchez*, Armando Vera García and Frank Jhonatan Isidro Ortega

Postgraduate Studies and Research Division, Toluca Institute of Technology, Mexico

***Corresponding author:** Juan Horacio Pacheco Sánchez, Postgraduate Studies and Research Division, Toluca Institute of Technology, Mexico.

To Cite This Article: *Juan Horacio Pacheco Sánchez, Armando Vera García, Frank Jhonatan Isidro Ortega. Opinion About Increasing use of Li-Air Batteries. Am J Biomed Sci & Res. 2022 - 15(3). AJBSR.MS.ID.002110.* DOI: 10.34297/AJBSR.2022.15.002110

Received: January 19, 2022; **Published:** January 27, 2022

Opinion

Currently, conventional lead-acid and lithium-ion batteries are inappropriate to withstand conditions and requirements of industrial applications, such as in high-range electric vehicles and electro-mobile devices such as cell phones and laptops. To meet the storage requirements of electrical energy, batteries must develop a higher energy density. The batteries that are currently dominating the field of electromobility are Li-ion batteries. To achieve a requirement of high energy density, metal-O_2 mainly Zn-O_2, Al-O_2, Li-O_2 batteries (O_2 is taken from the air) are attractive as an alternative, to the fact that these have a high theoretical energy density. Metal-O_2 batteries are characterized by oxygen, one of their electroactive materials. Given that oxygen is an electroactive material, in theory this simplifies the design and increases the energy density of a battery cell. For metal-O_2 batteries, there are different technologies based on using different metals as an anode, for example: Ca, Al, Fe, Cd and Zn [1]. Interest has been directed more towards Zn-O_2 and Li-O_2 batteries, of which research into Zn-O_2 batteries is considered to be a sufficiently mature technology, and most of their applications are regarded as stationary or in primary batteries, i.e., non-rechargeable batteries. Currently, there are primary batteries with Zn-O_2 technology. These Zn-O_2 batteries have a theoretical energy density of 1 kWh/kg, which is 5 times higher than the energy density of current Lithium batteries [2]. Li-O_2 or Li-air batteries are considered as an alternative of high theoretical gravimetric energy density (11-13 kWh/kg). For Li-air batteries there are four types of cells according to the type of electrolyte used which are: aprotic, aqueous, solid, and hybrid aqueous/aprotic. The efficiency of Li-air batteries is below 70%, in addition to low charging and discharging speeds and cyclability are the main limitations of this type of battery. Therefore, a series of challenges must be overcome that focus on obtaining materials, with greater stability and greater understanding of the reaction and transport kinetics [2]. On the other hand, Zhang, et al. [3] Introduce graphene to rechargeable Li-CO_2 batteries. To do this, they perform calculations of first principles to identify the discharge product. In addition, they calculate a voltage of 2.66 V for the reaction $4Li+3CO_2=C+2Li_2CO_3$. Their results exhibit good electrochemical activity in Li-CO_2 batteries, including higher capacities, longer cyclabilities, and lower overpotentials. They conclude that their kinetic parameters need to be improved to achieve the efficiency of Li O_2 batteries. They report high discharge capacity (up to 14774 $mAhg^{-1}$) and stable cyclability for 20 cycles at a current density of 50 mAg^{-1} [3,4] perform the manufacture, characterization, and performance of rechargeable and long-cycle Li-O_2 cells. The cells manufactured consist of a lithium metal anode, a membrane laminate made of glass-ceramic materials and polymer-ceramic, plus a solid-state cathode composed of air prepared from coal. The cells showed excellent thermal stability and rechargeability in the temperature range of 30 to 105°C. One cell underwent 40 discharge/charge cycles with excellent reversibility. Its reproducible results are brought to the manufacture of a safe, rechargeable lithium-air battery with high energy density [4]. Although there are a lot of studies that use lithium in batteries in other ways that use oxygen as the main source of electrical energy creation, this and the demonstration of the formation of lithium oxide molecules that will be seen in the following results is enough to infer limitations to the use of lithium and in general of this type of batteries and the use of metal oxides as an energy source.

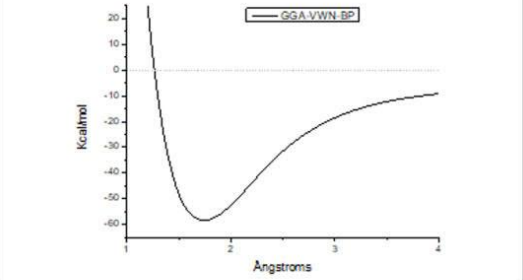

Figure 1: Potential interaction curve of the interaction between one lithium atom and one oxygen molecule.

Single-point all electron calculations of the interaction between one lithium atom and one oxygen molecule using the BIOVIA Materials Studio software with a DFT-GGA theory level by means of VWN-BP functional with a set of DND bases for unrestricted Hartree-Fock space are shown in Figure 1. It is shown that a lithium oxide molecule LiO_2 is indeed formed with very strong bonding corresponding to chemisorption due to the magnitude of the potential well which is around 60Kcal/mol. This means that lithium batteries are effectively powered by molecular oxygen that is in the air. The interesting point is that in near future, the air will be shared among electronic devices and animals. Considering the exponential growth in the use of cell phones, laptops, ipads, etc. the air might be a competition problem mainly among human being and machines. Although the calculations are preliminary, the already well-known facts allow us to express the opinion that the use of metal oxides to generate electric current should be limited to reactions of lithium molecules with CO_2, as an example. Extensive use of reactions among lithium atoms and oxygen molecules for energy storage does not seem pretty good.

References

1. Taylor P, Bolton R, Stone D, Zhang XP, Martin Ch, et al. (2012) Pathways for Energy Storage in the UK. Center for Low Carbon Futures, Uk.
2. MT Gil Austi, L Zubizarreta Saenz De Zaitegui, V Fuster Roig, A Quijano Lopez (2017) Batteries of the future: challenges and projection. Dyna 92(6): 601-605.
3. Zhang Z, Qiang Zhang, Yanan Chen, Jie Bao, Xianlong Zhou, et al. (2015) The First Introduction of Graphene to Rechargeable Li-CO_2. Batteries. Angewandte Chemie International Edition 127(22): 6550-6553.
4. B Kumar (2010) A Solid-State, Rechargeable, Long Cycle Life Lithium-Air Battery. Journal of the Electrochemical Society 157(1): 50-54.

Computational and Theoretical Chemistry xxx (xxxx) 113764

Contents lists available at ScienceDirect

Computational and Theoretical Chemistry

journal homepage: www.elsevier.com/locate/comptc

DFT study for hydrogen storage on γ-Boron-Graphyne decorated with Li atoms

Frank J. Isidro-Ortega [a, *], J.S. Arellano [b], Nayely Torres-Gómez [a], Abraham González-Ruíz [c], Armando Vera-Garcia [a]

[a] División de Estudios de Posgrado e Investigación, Instituto Tecnológico de Toluca, Metepec C.P. 52149, Estado de México, Mexico
[b] Area de Física Atómica Molecular Aplicada, Universidad Autónoma Metropolitana Azcapotzalco, C.P. 02200, Azcapotzalco, Ciudad de México, Mexico
[c] Instituto Nacional de Investigaciones Nucleares, Carretera México-Toluca S/N, Ocoyoacac C.P. 52750, Estado de México, Mexico

ARTICLE INFO

Keywords:
γ-Graphyne
Boron substitution
Lithium decoration
Hydrogen storage
Adsorption isotherm

ABSTRACT

This work reports theoretical calculations for hydrogen storage on γ-B-Graphyne structure using DFT. The pristine γ-Graphyne is a 2D structure, with 2 kinds of hexagonal rings. The boron substitution on a pristine γ-Graphyne is characterized by the formation of a 2D structure, the molecular structure of the boron substitution on a pristine γ-Graphyne is very close to γ-Graphyne structure. Boron substitution on γ-Graphyne is developed to create an active site for metallic decorations. For hydrogen storage, the calculated gravimetric capacity is 6.94 wt%, this result reaches DOE gravimetric targets (6.5 wt%). To measure the hydrogen bonding on the 18Li—γ-B-Graphyne structure, the average binding energies, and adsorption energies for each H_2 molecule are calculated, these values are between 0.321 and 0.353 eV, these values suggest that H_2 adsorption at ambient temperatures is possible. The calculations reveal that Li decoration improves the hydrogen storage conditions. Finally, employing adsorption isotherms calculations, the equilibrium pressure is determined for the 18Li—γ-B-Graphyne.

1. Introduction

According to the Intergovernmental Panel on Climate Change (IPCC), in recent years, the increasing concentrations of carbon dioxide caused by human activities, mainly caused by the usage of fossil fuels is the major reason for global warming. This is associated with problems of sea levels rising and more extreme weather [1]. For those reasons nowadays the development of renewable energy sources such as solar, wind, and tidal are being developed to satisfy energy requirements for today's living. An interesting proposal to replace fossil fuels is hydrogen since there is a great abundance of hydrogen in the earth in form of water. Besides hydrogen is an energy carrier free of carbon pollutants, because its oxidation delivers only water as a by-product. Hydrogen has a high energy content in terms of mass, (143 MJ/kg) which is three times greater than the energy content of gasoline in terms of mass (44.4 MJ/kg). However, in terms of volume, the hydrogen energy content is very low, (0.0108 MJ/L) compared to gasoline (34.8 MJ/L). It is well known that the main challenge to using hydrogen as an alternative fuel is its storage. According to the above background is important to develop a new way to produce and store hydrogen. It is well known that hydrogen storage in physical forms (cryogenic liquid, pressurized gas) is inefficient for this reason, the called "solid-state hydrogen storage" is developing nowadays. Our goal is to study the hydrogen storage in a γ-B-Graphyne supercell, decorated with Li atoms, by DFT calculations. In the last decade, many theoretical studies have been developed about hydrogen storage on host materials, mainly carbon-based materials per its big surface areas, the ideal material for hydrogen storage should be capable of realizing easy adsorption and desorption under ambient conditions [2], also large hydrogen gravimetric densities are required for fuel cell vehicle applications. Currently, the most used standard for hydrogen storage is established by the department of energy of the United States (DOE). According to DOE the gravimetric density target, for hydrogen storage is 6.5 wt% (wt.%) [3]. Many works, techniques, and materials for improving the hydrogen storage conditions have been widely researched to develop the hydrogen economy. Hydrogen storage studies propose many kinds of nanostructures for example metal hydrides [4], zeolites frameworks [5], etc. have been studied. Nevertheless, carbon-based materials such as nanotubes [6–8], graphene [9,10], fullerenes [11,12], ZTC [13,14], and Graphyne [15–18] have been widely investigated as potential hydrogen storage materials due to their low weight, necessary to achieve high gravimetric storage capacity. γ-Graphyne, is of particular interest in this study due to its electronic

Email address: fisidroo@toluca.tecnm.mx

https://doi.org/10.1016/j.comptc.2022.113764
Received 18 January 2022; Received in revised form 21 April 2022; Accepted 25 May 2022
2210-271/© 20XX

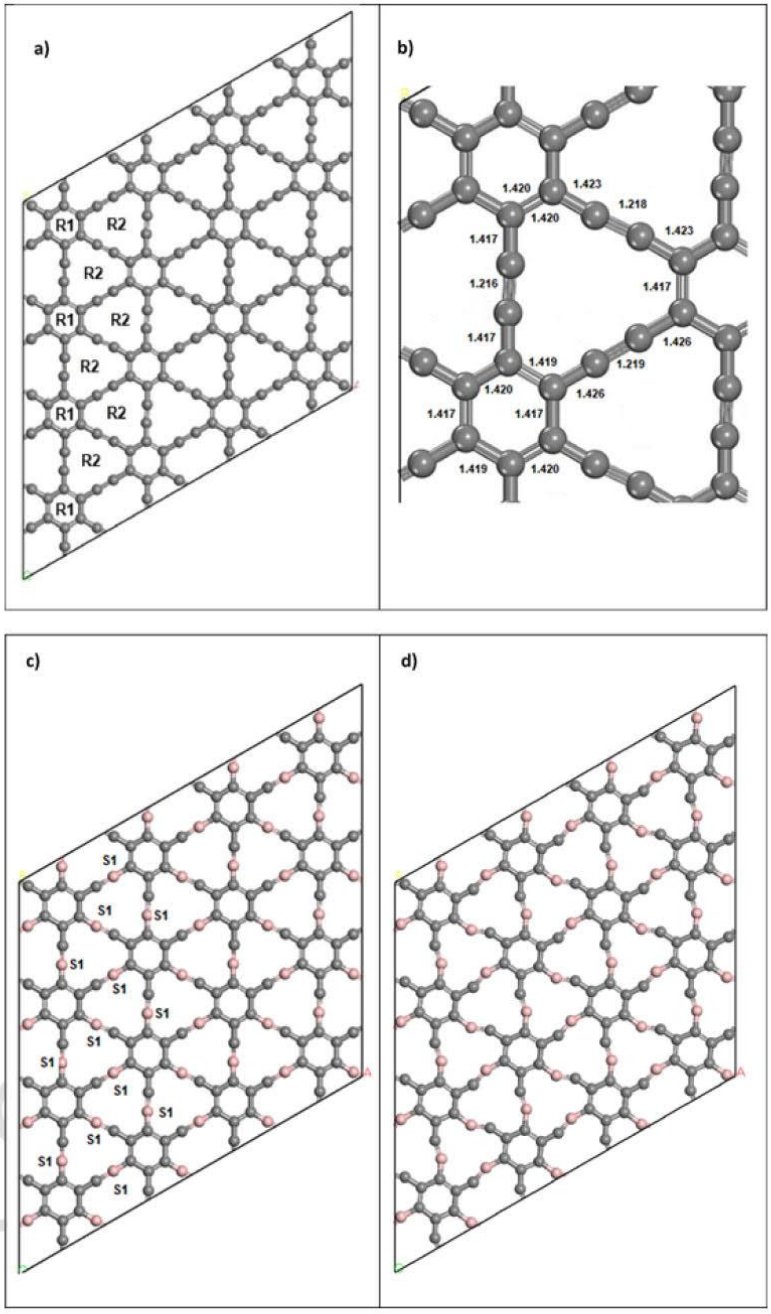

(caption on next page)

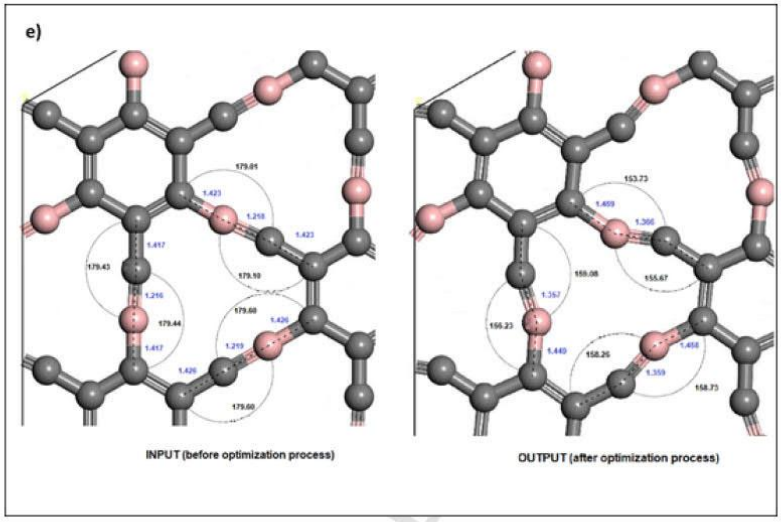

Fig. 1. a) Pristine γ-Graphyne, R1, and R2 represent its two kinds of rings, b) detailed measures in γ-Graphyne structure, c) Input boron substitution on γ-Graphyne, all the substitutions are performed in site S1. b) Output boron substitution on γ-Graphyne. e) Detailed measures in Boron substitution on γ-Graphyne input and output structure, side left and right respectively. Gray spheres represent carbon atoms, pink spheres represent boron atoms. Black numbers are angular measurements. Blue numbers are length measurements.

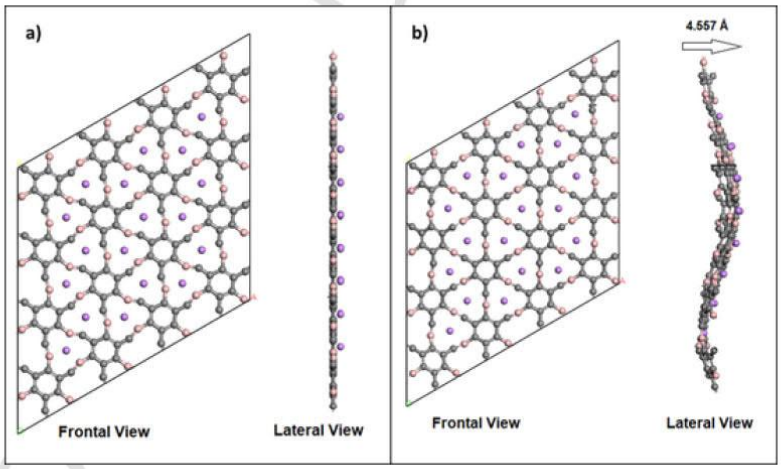

Fig. 2. a) Input of a decoration process on γ-B-Graphyne structure, the input is a 2D structure. b) Output of the decoration process on γ-B-Graphyne structure. The decoration process leads to a unique 3D structure. Gray spheres represent carbon atoms, pink spheres represent boron atoms, and purple spheres represent lithium atoms.

structure, and the size of its pores, which are quite different from other existing materials, including other carbon-based materials such as diamond and graphene [19]. In this study γ-Graphyne is used due to is the most common form of Graphyne [19], besides γ-Graphyne has the advantages of high stability and semiconductor characteristics [20,21]. The novel properties exhibited by γ-Graphyne indicate that γ-Graphyne is a good candidate for hydrogen storage. Besides, works on the experimental synthesis of graphdiyne structures have been reported by Li *et al.* [22], who fabricated large-area ordered graphdiyne films by the Glaser-Hay cross-coupling reaction using hexaethynylbenzene [22], Qiaodan *et al.* [23], have demonstrated a simple and high-yield method to prepare γ-Graphyne. Nowadays the hydrogen storage in carbon-based materials is hampered by some drawbacks, such as their performance at low temperatures, and low adsorption energy. To solve these drawbacks, many techniques to improve the material host are developed, for example, the creation of vacancies [24,25], and the substitution of heteroatoms on carbon materials (for the creation of active sites) [26–28] are developed to increase hydrogen adsorption conditions. Besides decorations of alkaline, alkaline-earth, and transition metals are used to improve adsorption energies per hydrogen molecules [29,30]. In this way the main state of the art about graphyne for hydrogen storage is summarized:

Table 1
Total energies of γ-B-Graphyne structure, γ-B-Graphyne with lithium decoration. Binding energies between the Li atoms and γ-B-Graphyne structure (E_b (Li)), and finally average lengths between the Li atoms and γ-B-Graphyne structure.

System	Total Energy [Ha]	E_b(Li) [eV]	$D_{Li—}$γ-B-Graphyne [Å]
γ-B-Graphyne	−6670.347	–	–
Li	−7.46	–	–
Li—γ-B-Graphyne	−6677.918	3.016	2.562
2Li—γ-B-Graphyne	−6685.489	3.017	2.605
3Li—γ-B-Graphyne	−6693.059	3.001	2.855
4Li—γ-B-Graphyne	−6700.632	3.019	2.624
5Li—γ-B-Graphyne	−6708.2	3.005	2.608
6Li—γ-B-Graphyne	−6715.771	3.003	2.641
7Li—γ-B-Graphyne	−6723.339	2.996	2.619
8Li—γ-B-Graphyne	−6730.909	2.993	2.648
9Li—γ-B-Graphyne	−6738.479	2.994	2.633
10Li—γ-B-Graphyne	−6746.054	3.005	2.631
11Li—γ-B-Graphyne	−6753.624	3.005	2.662
12Li—γ-B-Graphyne	−6761.194	3.003	2.642
13Li—γ-B-Graphyne	−6768.765	3.005	2.652
14Li—γ-B-Graphyne	−6776.331	2.996	2.620
15Li—γ-B-Graphyne	−6783.913	3.016	2.636
16Li—γ-B-Graphyne	−6791.484	3.016	2.626
17Li—γ-B-Graphyne	−6799.053	3.014	2.644
18Li—γ-B-Graphyne	−6806.617	3.002	2.636

First-principles studies of Li-decorated Graphyne for hydrogen storage using density functional have been developed by Guo *et al.* [15], their average adsorption energy of hydrogen is −0.27 eV/H_2. Zhang *et al.* [18], have studied the effect of electric field on Ti-decorated graphyne for hydrogen storage. For the adsorption energy of a single H_2 molecule on the Ti-decorated graphyne, they report 0.41 eV. Each Ti atom can adsorb up to 4 hydrogen molecules and a vertical electric field to the graphyne layer can increase the hydrogen adsorption energy. Yan *et al.* [31], have studied Li decorated oxidized graphyne with DFT. They find that Li atoms can be fixed to oxidized graphyne even more than on pristine graphyne. One Li atom can adsorb 6hydrogen molecules and the hydrogen storage capacity of Li-oxidized-graphyne systems could reach up to 12.03 wt% [31]. On the other hand, Liu *et al.* [32], have reported gravimetric capacities of 5.98 and 5.84 wt% for Na-decorated graphyne and BN-yne (analogous system for graphyne but with alternating B and N atoms). The corresponding adsorption energies are −0.254 and −0.172 eV per hydrogen molecule. Lu *et al.* [33], have developed a comparative study for hydrogen storage in metal decorated graphyne monolayers and graphyne nanotubes. Their results for the hydrogen storage capacity are 4.82, 5.08, 4.88, and 4.76 wt% respectively, for graphyne nanotubes decorated with Li, Ca, Sc, and Ti atoms. The average binding energy of Li atom, for gamma graphyne monolayer and graphyne nanotube, are −0.583 and −0.743 eV/Li atom respectively. Sathe *et al.* [34] have developed a DFT study of dihydrogen adsorption in Li, Mg, Ca and Sc decorated in γ-graphyne (Gγ). The maximum hydrogen weight percentage for those systems are respectively 8.69, 7.73, 8.10, and 6.83 wt%. Ren *et al.* [35], have studied the adsorptions of hydrogen on Li-decorated N-substituted graphyne using DFT calculations, they calculated a higher average binding energy per hydrogen molecule on Li-decorated N-substituted system than on pristine graphyne. The binding energy of Li atom is a little more than 3.10 eV when Li atom is adsorbed on the acetylenic ring, at the hollow site. Their results reveal that up to three hydrogen molecules are binding to one adsorbed Li atom on one side of the system. Zhang *et al.* [17], gave results for Li-decorated porous hydrogen substituted graphyne, denoted as (HsGY). Li atom is adsorbed with a binding energy of −1.91 eV. The gravimetric density is around 11.35 wt% for Li-decorated HsGY on both sides of the system with a value of −0.25 eV for the adsorption energy per hydrogen molecule. The intensive study of graphyne (GY) and graphdiyne (GDY) is because porous hydrogen substituted graphyne (HsGY) nanosheets have been obtained, with good electrochemical properties. The interplanar space in the DFT calculations was fixed as 20 Å with 18C atoms and 6H atoms in the HsGY unit cell, which remains stable at 300 K. Results are given for the systems 4Li-HsGY-nH2, for n = 4, 8,12 and 16. MD (molecular dynamics) for 500 K shows complete desorption of the hydrogen molecules but at 300 K most of the hydrogen molecules begin to be desorbed from the 4Li-HsGY-16H_2 system. These last results give confidence that those systems can be used as good hydrogen storage materials [17]. Gao *et al.* [36], gave results for ab initio molecular dynamics calculations for 300, 350, 400, and 450 K, to predict the hydrogen storage characteristics for one holey graphyne (HGY) sheet modified by the presence of some Li atoms. Up to 4 hydrogen molecules can be attached to one Li atom with −0.22 eV per hydrogen molecule as the average adsorption energy. They give the gravimetric density the high value of 12.8 wt%.

2. Methodology

In this work γ-Graphyne is used as the main structure to adsorb molecular hydrogen. The building of γ-Graphyne is carried out utilizing the superposition of a cell (supercell is built by the superposition of 4x4 unit cells), this structure contains 192 carbon atoms. First a γ-Graphyne structure is optimized. Second, a boron substitution is carried out utilizing geometry optimization calculations. Third, the metallic decoration is performed on functionalized γ-Graphyne. Finally, hydrogen saturation is carried out. The geometry optimizations and energy calculations developed in this work are carried out by numerical calculations using Biovia Materials Studio DFT-DMol^3 software [37,38]. All the geometry optimizations are performed at the level of the generalized gradient approximation (GGA), using the functional Perdew-Burke-Ernzerhof (PBE) [37], for a restricted spin. The double numerical basis sets with polarization functionals (DNP) are used, which has the advantage of being equivalent to the analytical Gaussian 6-31G* basis. All geometry optimizations are obtained until less than 0.001 Ha/Å maximum force values. It is well known that the Grimme method is considered for long-range dispersion correction to generate good adsorption energies. For this reason, it is important for the dispersion correction PBE-Grimme method in developing DFT-based simulations for hydrogen storage systems [39,40]. Therefore, an approximate semi-empirical DFT-D correction scheme proposed by Grimme [41], is considered in the calculations. The dispersion correction parameters for each of the atomic species (C6) are 0.139, 3.114, 1.741, and 1.601 Jnm6/mol, for H, B, C, and Li atoms respectively. Atomic Van der Waals radii are 1.0010, 1.4850, 1.4520, and 0.8250 Å, for H, B, C, and Li atoms respectively. Montecarlo Sorption simulation (Biovia-Materials-Studio using Compass Forcefield and Metropolis method) has been applied on a supercell (triclinic crystal parameters: a = 27.720 Å, b = 27.4729 Å, c = 30 Å, α = 90°, β = 90°, γ = 60°) containing the molecular hydrogen adsorbed on boron substitution γ-Graphyne decorated with Lithium atoms, to build logarithmic adsorption isotherms.

3. Results

The outcome of the computational experiments reported in this work is detailed in three sections. First, the stability for boron substitution on γ-Graphyne is calculated using geometry optimizations besides, the metallic decorations (decoration with Li atoms) on the γ-Graphyne are carried out. Second, the hydrogen adsorption on γ-Graphyne decorated with Li atoms is performed. Finally, the adsorption isotherms are performed.

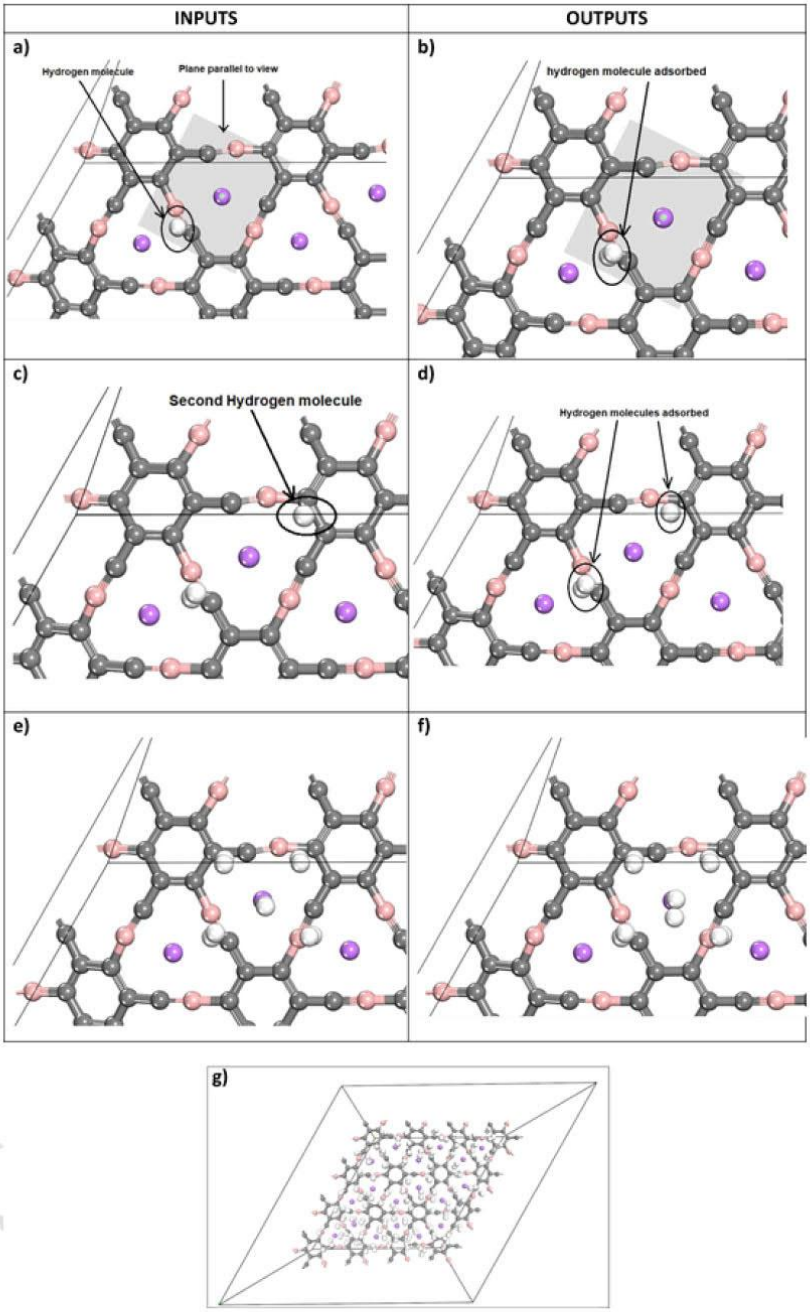

Fig. 3. Hydrogen adsorption process on 18Li—γ-B-Graphyne structure. Inputs show the proposal hypothetical hydrogen adsorption systems, outputs show the geometry optimization process of the hydrogen adsorption hypothetical systems a, b) For the case 18Li—γ-B-Graphyne adsorbing an H_2 molecule. c, d) For the case 18Li—γ-B-Graphyne adsorbing two H_2 molecules. e, f) For the case 18Li—γ-B-Graphyne adsorbing five H_2 molecules. g) For the case 18Li—γ-B-Graphyne adsorbing 90 H_2 molecules.

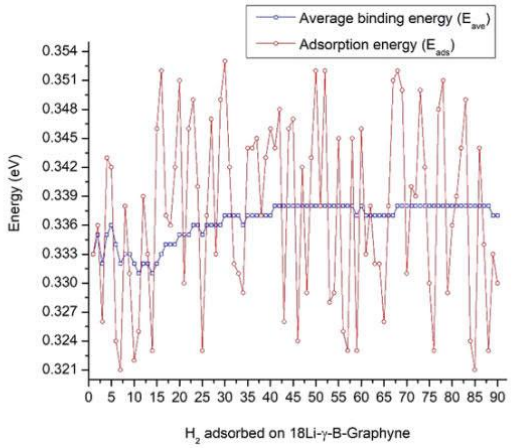

Fig. 4. Curves of average binding energy (E_{ave}), and adsorption energies (E_{ads}) per H_2 molecule.

3.1. Boron substitution on a γ-Graphyne, and decoration with metallic atoms

Is well known that the γ-Graphyne is a 2D stable structure, and the hydrogen storage in pristine carbon material is inefficient due to low binding energies, in other words, pristine carbon nanostructures are chemically too inert to be useful for practical hydrogen storage [42]. γ-Graphyne has mainly 2 kinds of hollows. The first kind of hollow is formed for a regular hexagon ring, built for 6 carbon atoms (R1), and the second kind of hollow is formed for an irregular hexagon ring, built for 12 carbon atoms (R2), this can be seen in Fig. 1a. The average bond lengths in R1 and R2 are 1.418 Å and 1.370 Å respectively; this can be seen in Fig. 1b. The surprising differences in carbon bond distances are according to distances reported by Peng *et al.* [43]. Peng *et al.* reported the existence of three types of carbon bonds in Graphyne: $C(sp^2)$—$C(sp^2)$ for the central aromatic ring (1.43 Å), $C(sp^2)$—C(sp) connecting the adjacent C═C, and C≡C bonds (1.41 Å), Finally, C (sp)–C(sp) for the linked triple bonds (1.22 Å) [43]. The three types of carbon bonds in Graphyne can be seen in Fig. 1b, the average bond length of each type of bond is 1.418 Å, 1.422 Å, and 1.217 Å respectively, these bond lengths can be compared to distances reported by Peng *et al.* [43]. To create an active site in γ-Graphyne a boron substitution is carried out. In other words, the boron substitution is developed to avoid metallic clustering. Atomic substitution on carbon-based materials technique has been reported in the last years [27,44]. The boron substitutions are performed in site S1. The carbon atoms located in site S1 are removed and substituted by boron atoms. Site S1 is selected for the kind of hybridization of carbon atoms (sp hybridization, triple bonds). This is shown in Fig. 1c. The Boron substitution on a γ-Graphyne is performed using geometry optimization calculations. As a result, a stable boron substitution on a γ-Graphyne is obtained, this can be seen in Fig. 1d. The result is a 2D stable structure that contains 48 boron atoms and 144 carbon atoms. The boron-carbon bond is deformed because of the boron substitution process. In pristine γ-Graphyne the average bond length between the carbon atom placed in S1 and its neighbor carbon atoms is 1.319 Å, and the average torsional angle in S1 is 179.36°. In boron substitution γ-Graphyne the average bond length between the boron atom placed in S1 and its neighbor carbon atoms is 1.408 Å and the torsional angle in S1 is 156.95°, this can be seen in Fig. 1e. Hereafter the boron substitution γ-Graphyne will be called γ-B-Graphyne. It is well known that the γ-B-Graphyne, has not been synthesized until now, in order to study the intrinsic stability of γ-B-Graphyne, the cohesive energy (E_{coh}) for γ-Graphyne, and γ-B-Graphyne is calculated following the next equation.

$$E_{coh} = \frac{\left((N_c E_c + N_b E_b) - E_{tot}\right)}{N_c + N_b} \quad (1)$$

Where N_c and E_c are the number of carbon atoms and energy for the carbon atoms respectively. N_b and E_b are the number of boron atoms and energy for the boron atoms respectively ($N_b = 0$ for pristine γ-Graphyne). Finally, E_{tot} is the total energy for γ-Graphyne and γ-B-Graphyne structures. The cohesive energy calculated for pristine γ-Graphyne is 7.171 eV/atom, the cohesive energy value calculated in this work is comparable with DFT calculations of cohesive energies for γ-Graphyne (7.262 eV/atom) reported by Shin *et al.* [45]. The cohesive energy for γ-B-Graphyne is 6.024 eV/atom, this value reveals that the γ-B-Graphyne can be synthesized experimentally. It is important to mention that we assume that the synthesis of boron substitution in γ-Graphyne structure can be carried out due to the following: It is known that discharge plasma milling (P-milling) has been applied to the synthesis of MOF's with added of a carbonaceous matrix [46], and also on Si (or Ge)-based materials [47]. P-milling is a novel and mass production technique to synthesize energy storage materials aiming at overcoming critical issues. This technique could be used to replace a C atom with a B atom in each chain linking carbon.

When a stable γ-B-Graphyne is obtained, the next step is to develop decoration with metallic atoms. In this case, decoration with Li atoms is performed. The decoration with Li atom is performed in R2 site. Decoration in R2 site is due to the porous size. The porous size in R2 is bigger than R1. The Li atom is placed pyramidally on each R2 ring, 18Li atoms are placed in the 4x4 supercell γ-B-Graphyne that is shown in Fig. 2.

Fig. 2a shows the input of a decoration process. The Li atoms are placed pyramidally on R2 of γ-B-Graphyne, which is a 2D structure, the stability is obtained using optimization calculation. Fig. 2b shows the decoration process output. The geometry of the R2 ring returns to the pristine geometry and the electrostatic forces of Li atoms produce a 3D deformation, the maximum amplitude of the 3D deformation is 4.557 Å.

It is well known that metal atoms aggregation or metallic clustering is an important factor for hydrogen storage, this reduces the hydrogen storage capacity, for this reason, is analyzed the binding energy between the γ-B-Graphyne and the Li atoms $E_b(Li)$, which is obtained following the next equation:

$$E_b(Li) = \frac{E(\gamma - B - Graphyne) + xE(Li) - E(Li_x\ \gamma - B - Graphyne)}{x}$$

Where, $E(\gamma\text{-}B\text{-}Graphyne)$ is the total energy of γ-B-Graphyne structure (Fig. 1d). $E(Li)$ is the total energy of an isolated Li atom. $E(Li_x\ \gamma\text{-}B\text{-}Graphyne)$ is the total energy of γ-B-Graphyne structure decorated with Li atoms (Fig. 2b). Finally, x is the number of Li atoms existing in the decorated structure. In this specific case, there are 18Li atoms. $E_b(Li)$ values calculated are summarized in Table 1. According to $E_b(Li)$ values, γ-B-Graphyne structure decorated with Li atoms is a stable structure. The $E_b(Li)$ average value is 3.006 eV. $E_b(Li)$ values indicate that the metallic clustering is avoided due to the large binding energy with the host material (γ-B-Graphyne). The dissociated energy for the Li-Li interaction is 1.088 eV [48]. This energy value is smaller (almost three times smaller) than $E_b(Li)$ value. For this reason, $E_b(Li)$ value ensures that lithium clustering is not possible in this study. The $E_b(Li)$ values corresponding to γ-B-Graphyne are quite large, this is caused by the boron substitution process in γ-Graphyne. The $E_b(Li)$ value corresponding to pristine Graphyne decorated with Li atoms is calculated by Guo *et al.* [15] their $E_b(Li)$ value is −1.35 eV, the negative value of $E_b(Li)$ indicates that the absorption is exothermic. Comparing the value reported by Guo *et al.* [15] against the $E_b(Li)$ values calculated in this work (displayed in Table 1), it is observed that the boron substitution process in

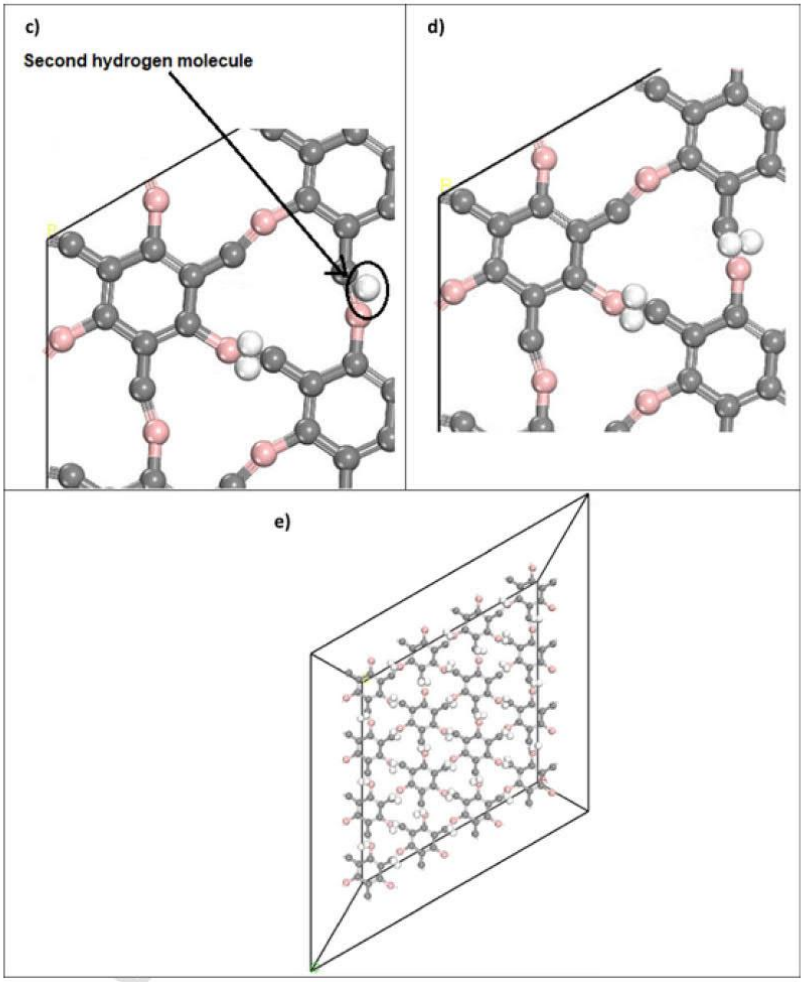

Fig. 5. Hydrogen adsorption process on γ-B-Graphyne structure. Inputs show the proposal hypothetical hydrogen adsorption systems, outputs show the geometry optimization process of the hydrogen adsorption hypothetical systems a, b) For the case γ-B-Graphyne adsorbing an H_2 molecule. c, d) For the case γ-B-Graphyne adsorbing two H_2 molecules. e) For the case γ-B-Graphyne adsorbing 33 H_2 molecules.

γ-B-Graphyne leads to large $E_b(Li)$ values. The average length between γ-B-Graphyne structure and Li atoms is 2.641 Å, all the lengths between γ-B-Graphyne structures are also summarized in Table 1.

3.2. Hydrogen storage

3.2.1. Hydrogen storage using γ-B-Graphyne decorated with Li atoms

In the previous section, the γ-B-Graphyne structure decorated with Li atoms is obtained, this structure will be called *nLi—γ-B-Graphyne*, where *n* takes values from 1 to 18, due to the number of Li atoms. To analyze hydrogen storage the geometry optimization technique is used.

To develop a hydrogen adsorption process, the molecular structure 18Li—γ-B-Graphyne (Fig. 2b) is used. Hydrogen molecules are placed molecule by molecule around Li atoms, this can be seen in Fig. 3 (inputs). After placing an H_2 molecule around the Li atom, a geometry optimization is carried out. The maximum number of H_2 molecules adsorbed for each Li atom is calculated using geometry optimization. According to calculations up to 5 H_2 molecules can be adsorbed in each Li atom, this is shown in Fig. 3. The first H_2 molecule is placed as shown in Fig. 3a (input), it is observed that the first hydrogen molecule leans towards to Li atom as a result of the geometry optimization process, this is illustrated in Fig. 3b (Output). The second H_2 molecule is added as shown in Fig. 3c (input), the result of the geometry optimization process is shown in Fig. 3d (output), so far these 2 H_2 molecules are adsorbed by a Li atom. The process of adding molecules is repeated until 5 hydrogen molecules are adsorbed per Li atom, this process is replicated in each Li atom until 90 H_2 molecules are adsorbed on the 18Li—γ-B-Graphyne structure. The 5 H_2 molecules adsorbed on the first Li atoms are shown in Fig. 3e and Fig. 3f. Fig. 3e shows the input of 5 H_2 molecules placed around the first Li atom, and Fig. 3f shows the geometry optimization process. Finally, the 18Li—γ-B-Graphyne structure which is adsorbing 90 H_2 molecules is shown in Fig. 3g (perspective view). Fig. 3f suggests that the H_2 adsorption is uniform around each Li atom.

In other words, each Li atom can adsorb up to 5 H_2 molecules in a very close distribution as is displayed in Fig. 3f.

Now it is well known that the 18Li—γ-B-Graphyne structure is a promising material for hydrogen storage. The next step is to calculate the gravimetric capacity for hydrogen storage (C_g), which is calculated following the next equation:

$$C_g = \frac{m_{H_2ads}}{m_{H_2ads} + m_{18Li-\!-\!-\gamma-B-graphyne}} \times 100\% \quad (3)$$

Where m_{H2ads} is the atomic mass of 90 H_2 molecules, and $m_{18Li—\gamma\text{-B-Graphyne}}$ is the atomic mass of 18Li—γ-B-Graphyne structure. The gravimetric capacity should achieve the DOE gravimetric targets, the ultimate gravimetric target proposed by DOE is 6.5 wt% The gravimetric capacity calculated for the 18Li—γ-B-Graphyne structure is 6.94 wt%, which is enough to reach DOE gravimetric targets.

Another important target for hydrogen storage is adsorption energy per H_2 molecule (E_{ads}) and the average binding energy per H_2 molecule (E_{ave}). Both energies should be between 0.2 and 0.4 eV/H_2 [42] to achieve reversible hydrogen storage at ambient conditions. The average binding energy of each H_2 molecule, adsorbed on the 18Li—γ-B-Graphyne structure is calculated following the next equation.

$$E_{ave} = \frac{E(18Li---\gamma-B-graphyne) + nE(H_2) - E(18Li---}{n}$$

Where *E[18Li—γ-B-Graphyne]* and *E[H_2]* are total energies of the 18Li—γ-B-Graphyne structure and an isolated H_2 molecule, respectively. *E[18Li—γ-B-Graphyne-nH_2]* is the total energy of the 18Li—γ-B-Graphyne structure with *n*H_2 molecules adsorbed on it, (*n* is the number of H_2 molecules adsorbed on the 18Li—γ-B-Graphyne and, *n* takes values from 1 to 90). In this case, the adsorption energy (E_{ads}) of each H_2 molecule is calculated. (E_{ads}) is calculated following the next equation.

$$E_{ads} = E\left(18Li---\gamma-B-graphyne + (n-1)H_2\right) + E\left(H_2\right) - E\left(18Li---\gamma-B-graphyne-nH_2\right) \quad (5)$$

Where *E[18Li—γ-B-Graphyne + (n-1) H_2]* is the total energy of the 18Li—γ-B-Graphyne structure with (n-1) H_2 molecules adsorbed on it. The calculated values of E_{ave} and E_{ads} for each H_2 molecule are shown in Fig. 4.

Average binding energy and adsorption energy, provide a clear idea to describe the hydrogen adsorption process. Fig. 4, summarizes the calculated values for average binding energy and adsorption energy, $E_{ave,}$ and E_{ads} values are between 0.331 and 0.338 eV/H_2 and between 0.321 and 0.353 eV/H_2 respectively. $E_{ave,}$ and E_{ads} values prove that the H_2 molecules are adsorbed on host material (18Li—γ-B-Graphyne), and all the adsorbed hydrogen molecules are in molecular form. $E_{ave,}$ and E_{ads} values are considered physisorption, due to typical values of physisorption being between 15 kJ/mol to 50 kJ/mol (0.155 to 0.518 eV) [49]. Besides, the Geometry parameters of the H_2 molecules adsorbed on the 18Li—γ-B-Graphyne structure are analyzed. The average H—H bond length is 0.7556 Å, this value is slightly bigger than the length value corresponding to an isolated H_2 molecule (0.750 Å), which means that the hydrogen adsorption process occurs in the non-dissociative form, in other words, the H_2 molecule will not dissociate to form clusters of hydrogen atoms. $E_{ave,}$ and E_{ads} values suggest that the boron substitution process leads to the enhancement of the hydrogen adsorption process. The results calculated in this work are compared to results obtained by Guo *et al.* [15] they develop the hydrogen storage on pristine γ-Graphyne decorated with Li atoms, their E_{ave} values are between 0.17 and 0.24 eV/H_2. The E_{ave} calculated in this work has an increase around of 55% concerning Guo values.

The geometry optimization process of hydrogen adsorption allows up to 5 H_2 molecules which suggests that the hydrogen adsorption is carried out through the Li atoms saturation. In this section, the hydrogen adsorption process is carried out. Besides, the results suggest that the hydrogen adsorption process at ambient temperatures is possible. Finally, the gravimetric capacity for hydrogen storage calculated is enough for reaching DOÉs gravimetric target.

3.2.2. Hydrogen storage using γ-B-Graphyne

To ensure that the Li atoms are fully responsible for the effective adsorption of the H_2 molecules, an additional study is carried out, mainly to evaluate the possible affinity of H_2 molecules with the carbon-boron bond of γ-B-Graphyne. To develop a hydrogen adsorption process, the molecular structure γ-B-Graphyne (Fig. 1e) is used. Hydrogen molecules are placed molecule by molecule on carbon-boron bonds, this can be seen in Fig. 5a, and 5c (inputs). After placing an H_2 molecule on a carbon-boron bond, a geometry optimization is carried out, this can be seen in Fig. 5b, 5d, and 5e (outputs). According to calculations up to 3 H_2 molecules can be adsorbed in each R2 ring, this is shown in Fig. 5. The geometry optimization calculations only permit the adsorption of H_2 on a single side of γ-B-Graphyne Finally, the γ-B-Graphyne structure is adsorbing 33 H_2 molecules this can be seen in Fig. 5e.

The gravimetric capacity for hydrogen storage (C_{g2}) for γ-B-Graphyne structure, is calculated following the next equation:

$$C_{g2} = \frac{m_{H_2ads}}{m_{H_2ads} + m_{\gamma-B-graphyne}} \times 100\% \quad (6)$$

Where m_{H2ads} is the atomic mass of 33 H_2 molecules, and $m_{\gamma\text{-B-Graphyne}}$ is the atomic mass of γ-B-Graphyne structure. The gravimetric capacity calculated for the γ-B-Graphyne structure is 1.45 wt%, which is not enough to reach DOE gravimetric targets.

To evaluate the reversible hydrogen storage at ambient conditions, the average binding energy (E_{ave2}) of each H_2 molecule, adsorbed on the γ-B-Graphyne structure is calculated following the next equation.

$$E_{ave2} = \frac{E(\gamma-B-graphyne) + nE(H_2) - E(\gamma-B-graphyne-nH}{n}$$

Where *E[γ-B-Graphyne]* and *E[H_2]* are total energies of the γ-B-Graphyne structure and an isolated H_2 molecule, respectively. *E[γ-B-Graphyne-nH_2]* is the total energy for the γ-B-Graphyne structure with *n*H_2 molecules adsorbed on it, (*n* is the number of H_2 molecules adsorbed on the γ-B-Graphyne, and *n* takes values from 1 to 33). In this case, the adsorption energy for the γ-B-Graphyne structure (E_{ads}) of each H_2 molecule is calculated following the next equation.

$$E_{ads2} = E\left(\gamma-B-graphyne + (n-1)H_2\right) + E\left(H_2\right) - E\left(\gamma-B-graphyne-nH_2\right) \quad (8)$$

Where *E[γ-B-Graphyne + (n-1) H_2]* is the total energy of the γ-B-Graphyne structure with (n-1) H_2 molecules adsorbed on it. The calculated values of E_{ave2} and E_{ads2} are between 0.107 and 0.112 eV/H_2 and between 0.109 and 0.120 eV/H_2 respectively. These values reveal that the hydrogen storage is not favorable on γ-B-Graphyne. In other words, is probable that the hydrogen storage on γ-B-Graphyne occurs at low temperatures, or high pressures (>60 Mpa). According to $C_{g2,}$ $E_{ave2,}$ and E_{ads2} values hydrogen storage on γ-B-Graphyne is not recommended. Besides $C_{g2,}$ $E_{ave2,}$ and E_{ads2} values ensure that the decoration of Li atoms on γ-B-Graphyne gives an enhancement of hydrogen storage conditions. The γ-B-Graphyne without Li decoration is not recommendable for hydrogen storage.

3.2.3. Adsorption isotherm

The hydrogen storage systems should reach targets according to temperature and pressure. For this reason, the equilibrium temperature and pressure for the 18Li—γ-B-Graphyne structure are calculated (The equilibrium temperature and pressure for the γ-B-Graphyne structure

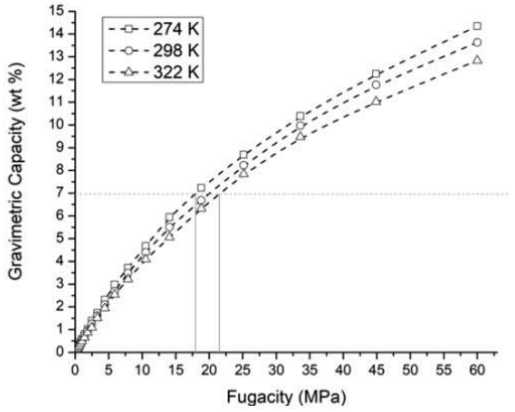

Fig. 6. Adsorption isotherm curves at 3 different temperatures (274 K, 298 K, 322 K) for the 18Li—γ-B-Graphyne.

are not calculated, due to this structure shows a low performance for hydrogen storage). Hydrogen adsorption on microporous materials at ambient temperatures and pressures up to 50 MPa has also been reported [50]. The adsorption isotherms at three different temperatures (274 K, 298 K, and 322 K) for the 18Li—γ-B-Graphyne structure is calculated in this section. For developing adsorption isotherms, the 18Li—γ-B-Graphyne solid system is proposed as an adsorbent. Also, 90 H_2 gas molecules are proposed as adsorbates. To calculate adsorption isotherms in this work is used Sorpion module (Biovia-Materials-Studio). Sorption module calculates adsorption isotherms for a sorbate in a sorbent framework from a series of simulations at different pressures and a fixed temperature. During the simulation, sorbate molecules within the framework are randomly rotated and translated, and, in addition, sorbates are randomly created and deleted from the framework to create the adsorption isotherms. The superposition of 4x4 unit cells (triclinic crystal parameters: a = 27.720 Å, b = 27.4729 Å, c = 30 Å, α = 90°, β = 90°, γ = 60°) is used to carry out the adsorption isotherms. The equilibrium pressure is obtained from the fitting curve displayed in Fig. 6.

In Fig. 6, is set a horizontal line at 6.94 wt%, drawing a vertical line in each intersection with adsorption isotherm curves the equilibrium pressure is obtained, which is between 18 and 22 MPa. According to other studies reported in Ref. [51], the equilibrium pressure calculated in this work exhibits an enhancement compared to the 3Ca—$C_{30}H_9$ system reported in Ref. [51]. And the equilibrium pressure values are very close to the results obtained in Ref. [44].

Finally, all the calculations developed in this work reveal that the 18Li—γ-B-Graphyne structure can be a good candidate for hydrogen storage, through hydrogen adsorption. Besides the 18Li—γ-B-Graphyne structure is theoretically capable of working at ambient temperatures, (274 K to 322 K) under pressures around 18 to 22 MPa.

4. Conclusions

This work summarizes the study of hydrogen storage, which is developed theoretically on γ-B-Graphyne using DFT calculations. First, the boron substitution on γ-Graphyne is carried out utilizing geometry optimization calculations. The boron substitution process is carried out by simply boron atoms substitution in specific sites (Fig. 1c). Boron substitution on γ-Graphyne is developed to create an active site. Second, a Li decoration is developed on γ-B-Graphyne. Li atoms are placed pyramidally on R2 sites. (Fig. 2a). As a result, the average value for $E_b(Li)$ is obtained which is equal to 3.006 eV. $E_b(Li)$ values indicate that Lithium clustering is not possible in this study. Besides boron substitution process leads to an increase in the $E_b(Li)$ values by around 55% concerning values reported in other works. For hydrogen storage, the gravimetric capacity to hydrogen storage is equal to 6.94 wt%, this result is enough to reach DOE gravimetric targets (6.5 wt%). The hydrogen gravimetric capacity storage value is obtained by adsorbing 90 H_2 molecules on 18Li—γ-B-Graphyne structure, each Li atom can adsorb up to 5 H_2 molecules. To measure the hydrogen bonding on the 18Li—γ-B-Graphyne structure E_{ave} and E_{ads} are calculated. E_{ave} and E_{ads} values are between 0.321 and 0.353 eV/H_2, all of the adsorbed hydrogen molecules are in molecular form. It is important to highlight that the boron substitution process leads to the enhancement of the hydrogen adsorption process. E_{ave} and E_{ads} values suggest H_2 adsorption at ambient temperatures. Finally, employing adsorption isotherms calculations, the equilibrium pressure is determined for the 18Li—γ-B-Graphyne structure, which is between 18 and 22 MPa.

CRediT authorship contribution statement

Frank J. Isidro-Ortega: Conceptualization, Methodology, Software, Validation, Formal analysis, Investigation, Resources, Data curation, Writing – original draft, Writing – review & editing, Supervision, Project administration. **J.S. Arellano:** Conceptualization, Validation, Supervision, Project administration. **Nayely Torres-Gómez:** Conceptualization, Validation, Supervision. **Abraham González-Ruíz:** Formal analysis, Investigation, Data curation, Writing – original draft. **Armando Vera-Garcia:** Formal analysis, Investigation, Data curation, Writing – original draft.

Declaration of Competing Interest

The authors declare the following financial interests/personal relationships which may be considered as potential competing interests: Frank Isidro reports financial support was provided by Technological Institute of Toluca.

Acknowledgments

We thank you to Consejo Nacional de Ciencia y Tecnología (CONACYT) No. CVU 635564, and Consejo Mexiquense de Ciencia y Tecnología (COMECyT), and for the grant awarded.

References

[1] G.S. Walker, *Solid-state hydrogen storage Materials and chemistry*, Woodhead Publishing, Cambridge England, 2008.
[2] Y. Zhao, Y. Kim, A.C. Dillon, M.J. Heben, S.B. Zhang, Hydrogen Storage in Novel Organometallic Buckyballs, Phys. Rev. Lett. 94 (2005) 1555041–1555044.
[3] "DOE Technical Targets for Onboard Hydrogen Storage for Light-Duty Vehicles | Department of Energy." [Online]. Available: https://www.energy.gov/eere/fuelcells/doe-technical-targets-onboard-hydrogen-storage-light-duty-vehicles [accessed: 11-Jan-2022].
[4] M. Mani-biswas, T. Cagin, Insights from theoretical calculations on structure, dynamics, phase behavior and hydrogen sorption in nanoporous metal organic frameworks, Comput. Theor. Chem. 987 (2012) 42–56.
[5] J. Liang, R. Zhang, Q. Zhao, J. Dong, B. Wang, J. Li, Molecular simulation of hydrogen storage in ion-exchanged Mazzite and Levyne zeolites, Comput. Theor. Chem. 980 (2012) 1–6.
[6] J.H. Cho, S.J. Yang, K. Lee, C.R. Park, Si-doping effect on the enhanced hydrogen storage of single walled carbon nanotubes and graphene, Int. J. Hydrogen Energy 36 (19) (2011) 12286–12295.
[7] W. Liu, Y.H. Zhao, Y. Li, Q. Jiang, E.J. Lavernia, Enhanced Hydrogen Storage on Li-Dispersed Carbon Nanotubes, J. Phys. Chem. C 113 (5) (2009) 2028–2033.
[8] M. Zhao, Y. Xia, L. Mei, Diffusion and condensation of lithium atoms in single-walled carbon nanotubes, Phys. Rev. B-Condens. Matter Mater. Phys. 71 (16) (2005) 1–6.
[9] C. Ataca, E. Aktürk, S. Ciraci, Hydrogen storage of calcium atoms adsorbed on graphene: First-principles plane wave calculations, Phys. Rev. B-Condens. Matter Mater. Phys. 79 (4) (2009) 1–4.
[10] A. Granja-delrío, J.A. Alonso, M.J. López, Steric and chemical effects on the hydrogen adsorption and dissociation on free and graphene – supported palladium

clusters, Comput. Theor. Chem. 1107 (2016) 23–29.
[11] J. Mao, P. Guo, T. Zhang, S. Zhang, C. Liu, A first-principle study on hydrogen storage of metal atoms (M = Li, Ca, Sc, and Ti) coated B 40 fullerene composites, Comput. Theor. Chem. 1181 (2020) 112823.
[12] M. Yoon, S. Yang, C. Hicke, E. Wang, D. Geohegan, Z. Zhang, Calcium as the superior coating metal in functionalization of carbon fullerenes for high-capacity hydrogen storage, Phys. Rev. Lett. 100 (20) (2008) 1–4.
[13] K. Suzuki, M. Kayanuma, M. Tachikawa, H. Ogawa, H. Nishihara, T. Kyotani, U. Nagashima, Path integral molecular dynamics for hydrogen adsorption site of zeolite-templated carbon with semi-empirical PM3 potential, Comput. Theor. Chem. 975 (1–3) (2011) 128–133.
[14] F.J. Isidro-Ortega, J.H. Pacheco-Sanchez, L.A. Desales-Guzman, Hydrogen storage on lithium decorated zeolite templated carbon, DFT study n, Int. J. Hydrogen Energy 42 (52) (2017) 30704–30717.
[15] Y. Guo, K. Jiang, B. Xu, Y. Xia, J. Yin, Z. Liu, Remarkable Hydrogen Storage Capacity In Li-Decorated Graphyne: Theoretical Predication, Phys. Chem. C 116 (2012) 13837–13841.
[16] G. Wu, et al., A comparative investigation of metal (Li, Ca and Sc)-decorated 6, 6, 12-graphyne monolayers and 6, 6, 12-graphyne nanotubes for hydrogen storage, Appl. Surf. Sci. 498 (2019) 143763.
[17] Y. Zhang, L. Zhang, H. Pan, H. Wang, Q. Li, Li-decorated porous hydrogen substituted graphyne: A new member of promising hydrogen storage medium, Appl. Surf. Sci. 535 (2021) 147683.
[18] L. Zhang, S. Zhang, P. Wang, C. Liu, S. Huang, H. Tian, The effect of electric field on Ti-decorated graphyne for hydrogen storage, Comput. Theor. Chem. 1035 (2014) 68–75.
[19] Q. Peng *et al.*, New materials graphyne, graphdiyne, graphone, and graphane: review of properties, synthesis, and application in nanotechnology, *Nanotechnol. Sci. Appl.* 10(7) (2014) 1–29.
[20] A. Ruiz, G. Alonso, P. Gamallo, First-principles study of structural, elastic and electronic properties of a-, b-and g-graphyne, Carbon N. Y. 96 (2016) 879–887.
[21] P.H. Jiang, H.J. Liu, L. Cheng, D.D. Fan, J. Zhang, J. Wei, J.H. Liang, J. Shi, Thermoelectric properties of γ-graphyne from first-principles calculations, Carbon N. Y. 113 (2017) 108–113.
[22] G. Li, Y. Li, H. Liu, Y. Guo, Y. Li, D. Zhu, Architecture of graphdiyne nanoscale fi lms, Chem. Commun. 46 (2010) 3256–3259.
[23] Q. Li, Y. Li, Y. Chen, L. Wu, C. Yang, X. Cui, Synthesis of γ-graphyne by mechanochemistry and its electronic structure, Carbon N. Y. 136 (2018) 248–254.
[24] M. Saito, K. Yamashita, T. Oda, Magic Numbers of Graphene Multivacancies, Jpn. J. Appl. Phys. 46 (No. 47) (2007) L1185–L1187.
[25] J.E. Padilha, R.G. Amorim, A.R. Rocha, A.J.R. Silva, A. Fazzio, Energetics and stability of vacancies in carbon nanotubes, Solid State Commun. 151 (6) (2011) 482–486.
[26] J.L. Li, Z.S. Hu, G.W. Yang, High-capacity hydrogen storage of magnesium-decorated boron fullerene, Chem. Phys. 392 (1) (2012) 16–20.
[27] Y. Zhou, W. Chu, F. Jing, J. Zheng, W. Sun, Y. Xue, Enhanced hydrogen storage on Li-doped defective graphene with B substitution: A DFT study, Appl. Surf. Sci. 410 (2017) 166–176.
[28] O. Faye, J.A. Szpunar, B. Szpunar, A. Chedikh, Hydrogen adsorption and storage on Palladium – functionalized graphene with NH-dopant: A first principles calculation, Appl. Surf. Sci. 392 (2017) 362–374.
[29] H. Liu, Y. Li, Modified carbon nanotubes for hydrogen storage at moderate pressure and room temperature, Fullerenes, Nanotub. Carbon Nanostruct. 28 (8) (2020) 663–670.
[30] J. Romanos, M. Beckner, M. Prosniewski, T. Rash, M. Lee, J.D. Robertson, L. Firlej, B. Kuchta, P. Pfeifer, Boron-neutron Capture on Activated Carbon for Hydrogen Storage, Sci. Rep. 9 (1) (2019).
[31] Z. Yan, et al., Lithium-decorated oxidized graphyne for hydrogen storage by first principles study Lithium-decorated oxidized graphyne for hydrogen storage by first principles study, J. Appl. Phys. 116 (2014) 174304.
[32] Y. Liu, W. Liu, R. Wang, L. Hao, W. Jiao, Hydrogen storage using Na-decorated graphyne and its boron nitride analog, Int. J. Hydrogen Energy 39 (2014) 12757–12764.
[33] J. Lu, Y. Guo, Y. Zhang, Y. Tang, J. Cao, A comparative study for hydrogen storage in metal decorated graphyne nanotubes and graphyne monolayers, J. Solid State Chem. 231 (2015) 53–57.
[34] R.Y. Sathe, S. Kumar, T.J. Dhilip Kumara, An ab initio study of reversible dihydrogen adsorption in metal decorated γ-graphyne, J. Appl. Phys. 126 (2019) 174301.
[35] J. Ren, N. Zhang, P. Liu, Li adsorption on nitrogen-substituted graphyne for hydrogen storage, Fullerenes, Nanotub. Carbon Nanostruct. 29 (3) (2020) 212–217.
[36] Y. Gao, H. Zhang, H. Pan, Q. Li, Ultrahigh hydrogen storage capacity of holey graphyne, Nanotechnology 32 (2021) 215402.
[37] B. Delley, From molecules to solids with the DMol3 approach, J. Chem. Phys. 113 (18) (2000) 7756–7764.
[38] B. Delley, An all-electron numerical method for solving the local density functional for polyatomic molecules, J. Chem. Phys. 92 (1) (1990) 508–517.
[39] Y. Gao, X. Wu, X.C. Zeng, Designs of fullerene-based frameworks for hydrogen storage, J. Mater. Chem. A 2 (16) (2014) 5910–5914.
[40] Y. Gao, X.C. Zeng, Ab initio study of hydrogen adsorption on benzenoid linkers in metal – organic framework materials, J. Phys. Condens. Matter 19 (38) (2007) 6220–6227.
[41] S. Grimme, Semiempirical GGA-Type Density Functional Constructed with a Long-Range Dispersion Correction, J. Comput. Chem. 27 (2006) 1787–1799.
[42] A.C. Dillon, K.M. Jones, T.A. Bekkedahl, C.H. Kiang, D.S. Bethune, M.J. Heben, Storage of hydrogen in single-walled carbon nanotubes, Nature 386 (6623) (1997) 377–379.
[43] Q. Peng, W. Jib, S. De, Mechanical properties of graphyne monolayers: a first-principles study, Phys. Chem. Chem. Phys. 14 (2012) 13385–13391.
[44] F.J. Isidro-Ortega, J.H. Pacheco-Sanchez, A. Gonzalez, DFT study of hydrogen storage on the metallic decoration of boron substitution on zeolite templated carbon vacancy, Int. J. Hydrogen Energy 45 (38) (2020) 19505–19515.
[45] H. Shin, et al., Cohesion energetics of carbon allotropes: Quantum Monte Carlo study, J. Chem. Phys. 140 (11) (2014) 114702.
[46] L.Z. Ouyang, et al., Enhanced high-rate discharge properties of graphene synthesized by plasma milling, Int. J. Hydrogen Energy 39 (2014) 12765–12772.
[47] L. Ouyang, Z. Cao, H. Wang, R. Hu, M. Zhu, Application of dielectric barrier discharge plasma-assisted milling in energy storage materials-A review, J. Alloys Compd. 691 (2017) 422–435.
[48] L. Yu-Ran, *Comprehensive Handbook of Chemical Bond Energies*, 1st ed. CRC Press, New York, 2007.
[49] D.P.J. Atkins Peter, *Physical Chemistry for the Life Sciences*. Oxford University, United States and Canada, 2006.
[50] T.G. Voskuilen, T.L. Pourpoint, A.M. Dailly, Hydrogen adsorption on microporous materials at ambient temperatures and pressures up to 50 MPa, Adsorption 18 (3–4) (2012) 239–249.
[51] F.J. Isidro-Ortega, J.H. Pacheco-Sánchez, R. Alejo, L.A. Desales-Guzmán, J.S. Arellano, Theoretical studies in the stability of vacancies in zeolite templated carbon for hydrogen storage, Int. J. Hydrogen Energy 44 (13) (2019) 6437–6447.